1973

An x-ray determination of the size distribution of wetting colloid particles

James M. Lamy
Lehigh University

AN X-RAY DETERMINATION OF THE SIZE DISTRIBUTION OF WETTING COLLOID PARTICLES

by

James M. Lamy

A Thesis

Presented to the Graduate Committee

of Lehigh University

in Candidacy for the Degree of

Master of Science

in

Metallurgy and Materials Science

Lehigh University

1973

CERTIFICATE OF APPROVAL

This thesis is accepted and approved in partial fulfillment of the requirements for the degree of Master of Science.

April 16, 1973
(Date)

Wayne Kraft
Professor in Charge

C. S. Carwile
Chairman of the Department
of Metallurgy and Materials Science

ACKNOWLEDGEMENTS

I express my gratitude to Professor R. W. Kraft of Lehigh University for his guidance throughout the course of this work. Due to the experience and wisdom of this direction, the work pursued a course which avoided potential pitfalls.

I thank Dr. J. A. Emerson of the Western Electric Engineering Research Center for introducing me to the challenge of research, for his encouragement and aid during the more frustrating times in this work, and for his contagious enthusiasm throughout this project.

To Dr. J. T. Kenney, of the Western Electric Engineering Research Center, I express my thanks for expressing a need for this study, and his confidence and patience during the project.

I also express my gratitude to Drs. J. F. D'Amico and W. P. Townsend of the Engineering Research Center for the fruits of many discussions.

The patience, encouragement, and help given me by my wife, Susie, are most deeply appreciated, and to her I owe perhaps the greatest thanks.

TABLE OF CONTENTS

LIST OF TABLES

LIST OF FIGURES

FIGURES

FIGURES

ABSTRACT

A means for colloidal solution characterization was sought in order to describe changes in the wetting properties of metal hydrosols with solution age and concentration. The size of the hydrosol particles was selected as a parameter which would depict the changes in the age and constituent concentration of the solutions. The technique of small angle x-ray scattering was applied to determining the in sol particle size distributions. The experimental and analytical details of the technique were verified by determining size distributions of colloidal particles which had been previously determined elsewhere.

Three hydrosols were studied. A series of chromium hydrosols was prepared with different concentrations of the constituents. No data were obtained due to insufficient scattered intensity. A stannous-stannic hydrosol was studied as a function of solution age. The results of this study show that a large number of very small particles (<40Å) are present in the hydrosol along with a smaller number of larger particles (>45Å). As the solution ages, the size of the larger particles is enhanced. A cerium hydrosol was studied as a function of the concentration of the constituents. This study shows that the particle size decreases as the solution concentrations are increased, and that the distribution of sizes tends to separate into two distinct distributions as the concentration is increased.

I. INTRODUCTION

During the past few years, a metallization process has been developed at the Western Electric Engineering Research Center.[1-4] This process, known as Photoselective Metal Deposition, or PSMD, is one in which metal is deposited onto a dielectric substrate, such as a circuit board, only in those regions for which a conducting path is required. This process, called an additive process, has the advantage over previous subtractive processes in that there is no copper path build up where no circuit path is desired. Thus, no wasteful subtractive process is required to remove the copper from regions where no path is desired.

This selective deposition is accomplished, in part, through the use of colloidal solutions which have an interesting property. When a substrate is immersed in one of the colloidal solutions for a period of time, the colloidal particles adhere to, or sensitize, the surface of the substrate.[2,5] When this occurs, the nature of the surface changes from non-wettable to wettable. That is, before sensitization, water forms beads on the surface of the substrate, but covers the surface of a sensitized substrate uniformly, or wets the surface. Colloids having this property are known as wetting colloids, and are used in a surface pretreatment step in the PSMD process.

The colloidal solutions are subject to certain instabilities, though. As the solutions age, there is a tendency for the particles to flocculate and precipitate out of solution. Also, as the solution ages, there is a gradual change in the immersion time necessary to sensitize a substrate. It is for these reasons that a technique for solution characterization is sought. It is hoped that with suitable characterization of the solutions, predictivemodels for the behavior of the solutions may be formulated.

The problem of finding a means for solution characterization then arises. One approach is to examine the particles of the colloidal solution since it is the particles that render a surface wettable. It is recognized that examination of the particles themselves eliminates from consideration those properties which arise from the interaction between the particles and the suspending medium (such as rheological effects) but no single characterization can fully describe all aspects of a colloidal solution.

The particles of the solution may be defined by knowing their chemical composition, size, and zeta potential (electrophoretic mobility). For any specific colloidal solution, both the chemical composition and zeta potential are independent of the solution concentration and age. The particle size, though, must be changing as the solution ages since particles eventually become large enough to precipitate

from solution. Also, the time required for precipitation depends on the concentration of the solution constituents[6], so that the size depends on the solution concentration. Thus the particle size is a parameter which will reflect changes in the solution concentration and age. The objective of this work, then, is to determine the particle size of the wetting colloidal particles with it understood that the sizes of the particles of the solution represent one characterization of the solution.

Table 1[7,8] lists various techniques for determining particle sizes and the range of sizes suited to the technique. Also, the techniques which may be applied to determining particle sizes in solution are designated. Immediately eliminated from consideration are those techniques which can not be used to determine the dimensions of particles in solution. Of the remaining techniques, the method of small angle x-ray scattering is the only technique capable of satisfying the range of sizes of interest (20A-1500A) Ultracentrifugation approaches the lower size limit, but the time required for an experiment increases as the particle size decreases, so that this technique is rejected. The technique of ultrafiltration also approaches the lower size limit, but this technique must be used in conjunction with an absorbtion technique, and loses accuracy as the particle size decreases. Thus, the technique of small angle x-ray

scattering is selected.

The remainder of this thesis presents the analytical and experimental details of the method of small angle x-ray scattering, that is, how the size information is actually obtained. The experimental and analytical methods developed here are tested by measuring particle sizes of colloids previously studied elsewhere. Finally, several wetting colloids are characterized by this technique, the object of this work.

II. THEORY OF SMALL ANGLE X-RAY SCATTERING*

Small angle x-ray scattering is a technique whereby the sample (in this case, the colloidal solution) is irradiated by a collimated x-ray beam and the intensity scattered by the sample is measured in the solid angle very near to the direct beam. The scattering of radiation is caused by the difference in electron density between the colloidal particles and the suspending medium.

It is instructive to draw an analogy between traditional x-ray diffraction and small angle x-ray scattering.[9] Traditional x-ray diffraction predicts a peak in an intensity vs scattering angle curve for an angle which satisfies Bragg's law. That is, $I = KI_o$ if $n\lambda = 2d \sin\theta$

where I = scattered intensity

I_o = incident intensity

K = attenuation factor

λ = wavelength of the radiation

2θ = scattering angle

d = dimension over which the electron density fluctuates periodically (lattice spacing)

n = order of the diffraction, assumes integer values

Typical values for a crystallographic examination are: $\lambda = 1.5\text{Å}$, $2d = 3\text{Å}$, $n = 1$. Thus, $\theta = \sin^{-1}(1/2) = 30°$. If d

is replaced by the dimensions of a colloidal particle, for example, 100Å, the angle for the peak is changed and is given by:

$$\theta \simeq \sin^{-1}(n\lambda/2d) = \sin^{-1}(1.5/200)$$

$$\theta = 0.43°$$

Thus, for particles of dimensions 10 to several hundred times the wavelength of the radiation, the diffraction pattern of interest lies within a few degrees of the incident beam.

Unfortunately, the analogy to x-ray diffraction may not be extended to determination of particle sizes since not all small angle scattering curves exhibit peaks. For this reason, an expression for the intensity of scattered radiation in terms of the particle size is developed.

General Theory of Small Angle X-Ray Scattering

In the following development, several assumptions will be made. First, the atomic scattering factors of the atoms of the particles are assumed independent of the angle of scattering, and are given by the number of electrons of the atom. This assumption is valid for small angles. Second, the effects of crystal structure are neglected, and the electron density is assumed to be continuous. This assumption is also valid for small angles since the lattice effects are important only for larger angles. The third assumption is that no inelastic scattering is to be considered. That is, the wavelength of the scattered radiation is assumed

to be identical to the wavelength of the incident radiation

The amplitude of radiation scattered by an atom of a particle (Figure 1) in a direction defined by the unit vector, $\overline{S}$, is given by:

$$A_j = A_o f_j e^{-i(\delta)}$$

A_j is the scattered amplitude, A_o is the incident amplitude f_j is the atomic scattering factor of the jth atom, and δ is the phase difference between the radiation scattered from point O and the atom j. From Figure 1, the phase difference is given as:

$$\delta = 2\pi/\lambda \left[(\overline{S}-\overline{S}_o)\cdot\overline{OM}_j\right] \qquad (1)$$

If $\overline{h}$ is defined as $(2\pi/\lambda)(\overline{S}-\overline{S}_o)$, then the expression for the scattered amplitude becomes:

$$A_j = A_o f_j \exp(-i\overline{h}\cdot\overline{OM}_j) \qquad (2)$$

The magnitude of $\overline{h}$ is equal to $(4\pi/\lambda)\sin\theta$.

The amplitude of the radiation scattered by the entire particle is determined by summing the amplitudes scattered by each atom of the particle. However, the intensity, rather than the amplitude of the scattered radiation, is the experimentally measurable quantity. The intensity of the scattered radiation is given by the product of the amplitude

and the complex conjugate of the amplitude. The vectorial notation may be dropped if the average intensity from randomly oriented particles is considered. The expression for scattered intensity as a function of the angle parameter, h, then becomes:

$$I(h) = I_o \sum_K \sum_j f_K f_j \frac{\sin hr}{hr} \qquad (3)$$

I(h) is the magnitude of the intensity scattered through the angle parameter h. The term r is the magnitude of the vector $\overline{OM}_j$. The terms f_j and f_K are the scattering factors of the jth and Kth atoms. If the assumptions of continuous electron density and constant scattering factors are applied, the double summation may be replaced with a double integral as:

$$I(h) = \int_{Vol} \int \rho_K \rho_j \frac{\sin hr}{hr} d\nu_K d\nu_j \qquad (4)$$

In the above, f_K and f_j are replaced with $\rho_K d\nu_k$ and $\rho_j d\nu_j$ respectively, with ρ_K, ρ_j being the average electron density in the volume elements $d\nu_K$, $d\nu_j$.

The expression for intensity may be simplified by introducing a function which relates the size of the particle to the product $\rho_j \rho_K$. This function is known as the single particle characteristic function, $\gamma_o(r)$. The product $\rho_K \rho_j$ is replaced by $\bar{\rho}^2 \gamma_o(r)$, with an accompanying change in the limits of integration. $\gamma_o(r)$ is formally defined as

the probability that a point located a distance r from another point in the particle will itself lie in the particle. The substitution of $\bar{\rho}^2\gamma_o(r)$ for $\rho_j\rho_k$ then allows integration over all space. The attendant changes in the form of the expression yield the following:

$$I(h) = \bar{\rho}^2 V \int_0^\infty 4\pi r^2 \gamma_o(r) \frac{\sin hr}{hr} dr \qquad (5)$$

The form of the function $\gamma_o(r)$ for various particle sizes and shapes has been determined.[9] The function may most easily be determined by considering two identical particles whose centers are separated by a distance, r, as in Figure 2. The single particle characteristic function is then given as the fraction of the particle volume which is common to both particles. For spheres of radius R,

$$\gamma_o(r) = 1 - 3/4\ (r/R) + 1/16\ (r/R)^3, r \leq 2R \qquad (6)$$

$$\gamma_o(r) = 0 \qquad , r > 2R$$

Thus the expression for scattered intensity from any particle shape or size may be determined by inserting the correct particle characteristic function into equation (5).

Particle size information may be determined directly from a measured curve of scattered intensity. Different size dependent parameters can be extracted from experimental I(h) vs h curves as follows:[9]

1. Electronic radius of gyration:

As $h \to o$, $I(h) = K \exp(-h^2 Rg^2/3)$

$$Rg^2 = -3 \frac{d(\ln(I(h)))}{d(h^2)} \tag{7}$$

2. Average surface to volume ratio; S/V:

$$S/V = \pi \lim_{h\to\infty} h^4 I(h) / \int_o^\infty h^2 I(h)\,dh \tag{8}$$

3. Average volume, <V>

$$\langle V\rangle = 2\pi^2 I(o) / \int_o^\infty h^2 I(h)\,dh \tag{9}$$

Each of these three size dependent parameters may be manipulated to yield a particle diameter. That is, the radius of gyration of a sphere is $\sqrt{3/5}$ of the actual particle radius. The volume of a sphere is given as $1/6\pi d^3$, so that the diameter, d, may be extracted from the average volume. Similarly, a particle diameter may be extracted from the surface to volume ratio.

In order to evaluate the size dependent parameters of equation (7)-(9), it is necessary to make use of several general properties of the scattering curves. First, the curve in the low angle region is completely described by the exponential approximation, $I(h) \simeq K \exp(-h^2 Rg^2/3)$. Thus, if the intensity is measured at angles small enough for this

approximation to be valid, then the values of intensity at smaller angles may be extrapolated to evaluate the intensity at h= o, and the low angle contribution to the two integrals (equations 8 and 9). This approximation is valid up to angles for which $hr \leq 1.8$, with r taken as the particle radius. Second, the high angle portion of the curve also approaches an asymptote, $I(h) \simeq Kh^{-4}$. Thus, to evaluate the high angle contributions to the integrals of equations (8) and (9), and the numerator of equation (8), it is necessary only to obtain data into the region where this approximation is valid. This approximation is generally valid for $hr \geq 8$. The last point which should be mentioned is that the size dependent parameters depend on the ratios of quantities obtainable from the scattering curve. For this reason, it is the shape of the scattering curve, rather than the absolute intensity, that is of interest in obtaining size parameters.

Of the three methods for obtaining size parameters (equations 7-9), the most direct method is to use equation 7. A plot of $\ln I(h)$ vs h^2 will yield a straight line as h approaches zero, and the particle size may be quickly obtained from the slope of this line. The other two techniques, although useful, involve measurements of two quantities with the size dependent parameter taken as the ratio of these quantities.

Unfortunately, there is one problem associated with using any one of the three equations (equations 7-9) to obtain particle sizes. For all but a very few colloids, the average diameters which result from the manipulations of the three size dependent parameters will not be consistent. This inconsistency arises since the expression for intensity is based on a single particle or a group of identical particles as the scatterer. If a system of identical particles is studied, the diameters will be consistent. If the particles are of different sizes, then the size parameters measured will represent differently weighted averages[10] over the range of sizes.

The most useful size information is the distribution of particle diameters, rather than single, weighted parameters. It is with this in mind that the theory is applied to polydisperse systems, systems comprised of particles of a range of sizes.

Theory For Polydispersed Systems

In this discussion, the shape of the particles will be assumed spherical. This will allow substitution of the particle characteristic function, $\gamma_o(r)$, for spheres into equation (5) to yield a direct expression for scattered intensity. This limitation is necessary since without some assumptions, regarding the shape of the particles, the distribution of sizes is not accessible by small angle

x-ray scattering.[9] By substituting the characteristic tion for spheres into equation (5) and integrating, an expression for the intensity scattered by a monodisperse system of spheres of radius R is given as.[9]

$$I_R(h) = \frac{9\pi}{2}\left[\frac{J_{3/2}(hR)}{(hR)^{3/2}}\right]^2 \qquad (10)$$

$$= 9\left[\frac{\sin hR - hR\cos hR}{(hR)^3}\right]^2$$

In the expression, $J_{3/2}(hR)$ is the Bessel function of the first kind of order 3/2, and reduces to the trigonometric functions given. A plot of this function for spheres of radius 50Å is shown in curve (a) of Figure 3. It should again be mentioned that, to determine particle sizes, the shape of the scattering curve is important rather than the intensity values. The intensity values depend linearly on the number of particles and on the square of the electron density difference between the particle and the suspending medium, but the shape of the curve depends only on the particle size.

For a group of particles of a distribution of sizes, the intensity recorded at an angle h will be given by,[11]

$$I(h) = K\int_0^\infty I_R(h)\rho(R)dR \qquad (11)$$

since the dependence on intensity is linear with respect to the number of particles. Here, $I_R(h)$ is given by equation (10), and $\rho(R)$ is the distribution of radii. A typical curve is presented in curve (b) of Figure 3 for the distribution of particle sizes shown in the insert of Figure 3. The qualitative differences between the two curves ((a) and (b) of Figure 3) are the disappearance of peaks and the sharper drop in intensity of the polydispersed system.

The problem of determining the distribution of diameters from a scattering curve such as in curve (b) of Figure 3 is hopelessly ambiguous without imposing the shape assumption, as has been mentioned. The reason for this is that the form of an intensity vs scattering angle curve for a monodispersed sol of ellipsoids, for example, can be shown to be almost identical to a polydispersed system of spheres. The validity of any size distribution determination is the immediately limited to the validity of the shape assumption. However, by making the assumption of spherical particles, the particle size distribution is, in principle, accessible by the technique of small angle x-ray scattering.

There are a variety of techniques which have been developed to perform the deconvolution of the scattering curve to yield the particle size distribution. The general methods will only be enumerated here, but are described in more detail in Appendix I. Also presented in this appendix is a comparison of the results of each technique on a series

of theoretical scattering curves representing various distributions for the purpose of selecting the most applicable technique.

1. An integral transform of the expression for scattered intensity may be manipulated to yield a direct expression for the size distribution such as is in the insert of Figure 3.[11-14]

2. The experimental scattering curve is compared to various theoretical curves representing different distributions, and the distribution of sizes is deduced from the theoretical curve of best fit.[15]

3. The shape of the distribution is assumed to fit to a Maxwellian distribution (see the appendix for the mathematical expression of this distribution).[15] With the additional assumption that the intensity is expressible by the low angle approximation (equation 7), the integration of an equation such as equation (11) may be performed directly. This yields an intensity expression in terms of variables which define the distribution and suitable graphical manipulation of the data will yield the distribution variables.

4. The data is plotted as ln(I) vs h^2, as is suggested by equation (7). A plot such as this is known as a Guinier plot, and the slope of this plot is

shown to depend on the particle size. The technique for determining the size distribution performs a reconstruction of the plot by successive straight lines. The slopes of the straight lines determine particle sizes and the number of particles of a given size depends on the intercept of the corresponding line.

On the basis of the comparison of the techniques in the appendix, several conclusions were made. The best technique is the method of integral transforms method 1. The accuracy of the results and the time required to analyze a curve are better than any other technique. However, this technique is valid only if data is accessible well into the high angle asymptotic region, which is not always the case in an experiment. In the event that the data does not extend into the asymptotic region, a graphical technique must be used with attendant loss in precision. Of the graphical techniques, the third technique is the most accurate.

In summary, then, the size distribution may be determined from the experimental scattering curve. The problem of determining the sizes of particles is then reduced to obtaining the intensity of scattered radiation as a function of the scattering angle.

III. EXPERIMENTAL ASPECTS

A. Apparatus

The requirements imposed on the apparatus to measure the small angle scattering curve are somewhat similar to the requirements for any diffraction experiment. However, the degree to which these requirements are satisfied is more critical to the outcome of the experiment and, eventually, to the information obtained about the sample than in normal diffraction studies.

The general requirements which should be attended to in a small angle x-ray scattering study are a beam of high but constant intensity, monochromatic radiation, a non-divergent beam, and uniform intensity across the beam. The high intensity is required since for most samples the intensity must be measured over several orders of magnitude of intensity. If the incident intensity is not high, then the tail of the scattering curve (the high angle asymptotic region) may lie below the noise level of the system and be inaccessible to experiment. The requirement of monochromatic radiation is imposed since all the equations derived have been based upon having a single wavelength of radiation. If the effects of white radiation are considered, the equations will become much more complex and unwieldly. The divergence of the beam is important since the range of angles of a typical experiment is much smaller than the range for a diffraction

pattern. Hence the beam must be of dimensions and resolution to differentiate between scattering angles on this reduced scale. The uniformity of the beam is required to simplify the technique of removing the effects of collimation smearing. Collimation smearing arises since, for any beam of finite dimensions, the intensity recorded at an apparent scattering angle is actually the sum of intensities scattered through a range of angles. This effect will be discussed in more detail later in this section.

Apparatus

The experimental apparatus consists of an x-ray generation system, a collimation system and goniometer, and a detector system. A schematic of the equipment is presented in Figure 4.

The x-ray generating system consists of a GE XRD 700 system, and a Siemens x-ray tube and tube stand. The GE XRD 700 system is comprised of a high voltage transformer, a voltage stabilizer, and a closed loop heat exchanger for cooling the x-ray tube anode. The collimation system and goniometer used is a Kratky small angle x-ray camera. The goniometer is controlled by means of a Digital Automatic Model 500 controller. During experiments, the collimation system is evacuated with an Extractor HV-6 vacuum pump. The detector system consists of a GE SPG 8 counter tube, a DAC Model 210 preamplifier, and a DAC Model 200 Spectrometer. The spectrometer consists of an amplifier, scaler, ratemeter,

and pulse height analyzer. The output of both the spectrometer scaler and the goniometer controller is registered through a connected teletype.

Operation of The Apparatus

The Kratky camera is pictured in Figure 5 and is shown schematically in Figure 6. The principles of operation of the camera may be described by enumerating the paths a beam of radiation may take as it passes through the camera, with reference to Figure 6.

A beam emanating from the focal spot of the x-ray tube may strike the edge of the entrance slit, E. In this case, it does not enter the camera and is not of interest. A beam could enter E and strike the block, B, or the bridge, Br. If the beam strikes the edge of the block, the beam may be scattered due to the electron density difference between the steel and air, and could conceivably be registered at the detector. Any radiation which follows this path is labelled as parasitic scattering and could overshadow the actual sample scattering. The radiation scattered by the block in this manner may not pass above horizontal, since it will be absorbed by the bridge which is coplanar with the block (±.2μ). Thus, no parasitic scattering may be registered above the axis of the camera due to parasitic scattering from the block. Alternately, parasitic scattering could

have an origin due to the edge of the bridge. However, this radiation also is prevented from rising above the vertical camera axis, and all parasitic scattering is, in principle, eliminated.[17]

A beam may strike an air molecule at any point in the system and be scattered above the camera axis. This radiation could also overshadow the actual sample scattering. For this reason, the collimator and region between sample and detector are evacuated. At a pressure of 2-3 torr, the air scattering is negligible.

A beam could pass through the sample and strike the detector plane directly. The radiation which follows this path then defines the position of unscattered ($2\theta=0°$) radiation. The intensity of unscattered radiation, the direct beam, varies with the vertical position in the detector plane, and describes a trace as is pictured in Figure 6. The centroid of this trace is taken as the definition of $2\theta=0°$.

Finally, the beam may strike a particle at the sample plane and be scattered through an angle, 2θ. The radiation strikes the detector plane at a position above the camera axis given by: $m = a \tan(2\theta)$, where a is the sample to detector distance (214.5 mm). In other words, at the detector slit position, the scattering angle is given as $2\theta = \tan^{-1}(m/a)$. For the range of angles normally encountered, $\tan(2\theta) \simeq 2\theta$, so that $2\theta \simeq m/a$. The intensity recorded at 2θ is then due entirely to the sample with no parasitic scattering or air

scattering, in principle, being registered. In practice, there is always some background level which is impossible to eliminate. The background intensity is also measured as a function of the scattering angle with no sample present and is subtracted from the sample scattering curve.

The width of the intensity profile of the direct beam at the detector plane is increased as the width of the entrance slit is increased. For a given slit width, the minimum angle at which scattered intensity may be recorded is given by the ratio m*/a. m* is the height above the centroid of the direct beam at which the direct intensity is zero, and increases as the slit width increases. The angular resolution is then decreased as the entrance slits are increased, so that to maximize the angular resolution, the smallest slits should be used.

The intensity of the scattered radiation is often only a small fraction of the intensity of the direct beam. It is for this reason that the intensity which strikes the sample should be as high as possible. In the Kratky camera, the shape of the beam is rectangular, with dimensions depending on the entrance slit width and the dimensions of the length delimiter slit (Figure 7). The length delimiter slit is set at 25mm, and for a typical entrance slit of 100μ, the beam dimensions, at the entrance slit will be 12.5x.100mm, or effectively line shaped. The effective focal spot dimensions for the x-ray tube used, (Siemens AG Cu 40/2) at a take-off

angle of -6° are 7.5x.25mm. Thus, the shapes of the collimated beam and the focal spot are similar, which makes possible utilization of a greater portion of the total of all radiation emitted from the x-ray tube.

As the width of the entrance slit is decreased, the intensity which strikes the sample is also decreased. Thus there is a trade-off between intensity and angular resolution. The angular resolution requirement is relaxed for smaller particles. so that larger entrance slits may be used as the particle size decreases.

The shape of the beam causes an effect known as collimation smearing, as has been mentioned. This effect arises, as shown in Figure 8, due to the finite dimensions of the beam. The intensity which is recorded at an apparent angle, 2θ, is actually the sum of intensities scattered through a range of angles between $2\theta_{min}$ and $2\theta_{max}$. The intensity recorded is then the average over this range. Due to this effect, the experimentally obtained scattering curve is different than the real scattering curve of the sample, and must be corrected, or desmeared, to yield the actual scattering curve. Schmidt and various coworkers [18,19] have examined this problem and have derived techniques for desmearing experimental curves. The collimation smearing effect and the techniques for desmearing are presented in Appendix II.

The development of the desmearing technique in the appendix contains an assumption that the beam is of uniform

intensity across its length. This assumption is made valid by assuring that all collimation edges are parallel to, and pointing at the focal spot of the x-ray tube. If the edges are not parallel, there will be a non-uniform beam, a loss in angular resolution, and a decreased intensity. There are several techniques for aligning the edges.[20-22] However, the most precise is that developed by Anderegg, Mardon, and Hendricks,[20] which is used to check and make periodic adjustments to the alignment.

Operation of the Kratky Camera Goniometer

The scattering angle, 2θ, is given by the height of the detector slit above the centroid of the direct beam divided by the sample to detector distance (214.5mm). The position of the detector is controlled by the goniometer screw, G, of Figure 5, which is, in turn, controlled by the DAC 500 controller. The DAC 500 is a unit which is capable of automatic operation, and drives a motor (SLO SYN HS 25) which, drives the goniometer screw. The position of the detector is monitored by a shaft encoder motor (ACCU-CODER MODEL 715) which generates pulses as the motor shaft rotates. The pulses are recorded in the DAC 500 unit and define the angle. The conversion between the number of pulses and the scattering angle is: 862 counts= 1 milliradian.

Operation of the X-Ray Tube

The x-ray tube is powered by a GE XRD 700 generator operated at 40kV and 25mA. The generator supplies full wave

rectified, stabilized voltage to the tube. The anode is water cooled by a closed loop heat exchanger which maintains a constant anode temperature. The CuK_β radiation is eliminated with a Ni foil inserted in the collimator of the Kratky camera.

Operation of the Spectrometer and Counter Tube

The counter tube used is a GE SPG 8 gas proportional counter. Its plateau curve is shown in Figure 9. An operating voltage of 1480 volts is selected since, at this voltage, the count rate is insensitive to voltage fluctuations.

The pulses generated in the counter tube are amplified by the DAC 210 preamplifier and are transmitted to the DAC 200 spectrometer. The pulses are further amplified by the spectrometer and are sent to the scaler circuit to be counted. The ratemeter is not used to record intensities due to lack of precision.

The amplitude of the current pulses depends on the energy of the x-ray photons[23] which generate the pulses. The effects of radiation other than the CuKα may be eliminated by counting only those pulses whose amplitude corresponds to the energy of the CuKα radiation. This is accomplished by the pulse height analyzer which passes to the scaler circuit only the pulses within a range of amplitudes centered about the CuKα height, so that the effects of white radiation are removed. For the amplifier setting and counter tube voltage used, the pulse height analyzer is set to pass only those pulses whose heights are between 1.15 volts and 2.00 volts (a baseline of

1.15 volts with a window of 0.85 volts).

Small angle scattering curves are obtained by placing the sample (in liquid form) in a capillary tube and placing the capillary tube in the sample holder of the camera. After alignment of the capillary parallel to the beam, the scattering curve is obtained by stepping the goniometer through the angles desired, and by counting the number of pulses per unit time at each angle. There is an error associated with establishing an intensity on the basis of a given number of counts. This expected error decreases as the number of counts increases. For all data points taken, the minimum number of counts to specify an intensity was 4,500 corresponding to an error of 1%.

The data points are then plotted and smoothed graphically, and are then collimation error desmeared. The curve which is yielded by the collimation desmearing program is then the actual sample scattering curve which is analyzed. A typical curve is shown in Figure (10).

B. Sample Preparation

Four different colloids were prepared for analysis. This section presents the method of preparation of these samples.

1. Gold Colloid

This colloid is prepared by the technique of Turkevitch et al.[24] The size distribution of the particles of this colloid is highly reproducible,[24]

so this colloid is suited as a standard. Preparation consisted of dissolving 10mg $HAuCl_4 \cdot 3H_2O$ in 95ml of water and heating the solution to the boiling point. 5ml of a 1/2% sodium citrate solution (25mg citrate) was added to the boiling solution. After approximately five minutes of boiling with vigorous agitation, the solution changed colors from a faint pink to a deep wine red. This solution was then concentrated approximately 20 to 1 by heating in a partial vacuum and was then mounted in a glass capillary tube.

2. Chromium Hydrosol

A series of chromium hydrosols was prepared by the technique of Demchak and Matijevik.[25-26] A typical sample was prepared by adding NaOH to a solution of 10^{-3}M $CrK(SO_4)_2$ and aging at 75°C for 21 hours. In actual preparation, the concentration of $CrK(SO_4)_2$ and the amount of NaOH added to the solutions were varied so that a series of solutions could be examined.

3. Stannous-Stannic Hydrosol

Two similar stannous-stannic hydrosols were prepared for examination. The first was made by dissolving 1g $SnCl_4 \cdot 5H_2O$ in 100ml of H_2O. Immediately after dissolution of the $SnCl_4$, a second addition of 2.0g of $SnCl_2 \cdot 2H_2O$ was dissolved in the solution followed immediately by a third addition, 1.5g of $SnCl_2 \cdot 2H_2O$. The additions were all made at room temperature under mild agitation.

The solution thus prepared was stored, and samples were withdrawn periodically.

The second solution, called the special solution, was prepared essentially the same. 1g $SnCl_4 \cdot 5H_2O$ was dissolved in 100ml H_2O. However, after dissolution of the $SnCl_4$, the solution was aged twenty minutes before the secondary and tertiary additions were made. The sample thus prepared was stored in a bottle and samples were withdrawn periodically.

4. Cerium Hydrosol

Three cerium hydrosols were prepared by dissolution of $Ce(NH_4)(NO_3)_2 \cdot xH_2O$ in deionized water. Only the solution concentration was varied, with concentrations of 1/2%, 1%, and 4% by weight being selected. Each solution was allowed to stabilize one half hour before being mounted in the Kratky camera.

IV. VERIFICATION OF THE TECHNIQUE

As a test of the analytical procedures developed in Section II and the experimental methods of Section III, three colloidal solutions whose size distributions had been determined elsewhere were analyzed here. It is the purpose of this section to present the results of the analysis made here and compare them with the previously determined data to check the validity of the procedures developed here.

The colloids examined are two different colloidal silica solutions and a colloidal gold solution . The colloidal silica solutions are available commercially from E. I. DuPont de Nemours Co., Inc. under the trade name Ludox®. The two different Ludox samples used were type TM and type HS, each having a different particle size distribution. The colloidal gold was prepared by the technique of Turkevitch, Stevenson, and Hillier[24] outlined in Section III.

Results

The scattering curves for Ludox HS and TM and for the colloidal gold sol are shown, plotted as log I vs log2θ in Figures 10, 11, and 12 respectively. These curves are corrected for collimation error and are thus ready for analysis. Since all curves extend into the asymptotic region (the curves extend into straight lines whose slope is -4 so that the intensity is proportional to h^{-4}), the method of integral transforms is suitable for determining the particle

sizes. The distributions of diameters for the three samples are presented in Figures 13, 14, and 15. Also shown in Figure 13 is the distribution of diameters deduced by Brill[14] by the technique of x-ray scattering and electron microscopy. The distribution of the diameters of the gold particles as deduced by Turkevitch[24] is superimposed on Figure 15. Turkevitch used the technique of electron microscopy to determine this distribution. Unfortunately, no published distribution of diameters for Ludox TM exists. The approximate range of the mean size of the particles, as determined by the supplier,[29] is superimposed on Figure 14.

Discussion and Conclusions

A comparison of these results with the results in the literature indicate that the agreement is remarkably good. This agreement is taken as a verification of both the technique for analysis and the calibration of the experimental apparatus.

V. RESULTS AND ANALYSIS OF RESULTS

Three hydrosols (colloids suspended in water) were examined, a chromium sol, a stannous-stannic sol, and a cerium sol. The techniques of preparation have been presented in Section III of this thesis. Each hydrosol is similar in the sense that the growth of the particles occurs through hydrolysis to yield the colloid. These solutions, then, undergo a drop in pH as the particles grow. This section presents the results and analysis of the results of the examinations of each hydrosol.

Chromium Sol

The chromium sols investigated here had been previously characterized elsewhere.[25-28] The size distributions of the hydrosols had been determined by other techniques for various solution concentrations and pH's. It was hoped that, by using the previous characterizations as a starting point, the range of solution concentrations could be extended to model the wetting hydrosols of use in the PSMD process.

Results

No particle size data could be obtained for any of the chromium hydrosols prepared. For each sample, the scattered intensity was indistinguishable from the background so no analysis could be made. There are two possible explanations. One possibility is that the electron density difference between the particles and the suspending medium is too low

for any appreciable scattering to be recorded. The magnitude of the scattered intensity depends on the square of the electron density difference. This explanation seems unjustifiable since the particles are comprised of metal atoms and the suspending medium is water. The most likely explanation is that there are too few particles in solution for any appreciable scattering. The scattered intensity depends on the number of particles irradiated, so that a low intensity is expected from a solution with few particles. This explanation is confirmed by the fact that, for the size of the particles determined by Demchak and Matijevik[25] and the amount of chromium in solution, few particles were present in the solution.

Stannous-Stannic Hydrosol

This hydrosol is one of the wetting colloids used to sensitize substrates for the PSMD process. As this solution ages, there is a gradual change in the rate of substrate sensitization as well as an increased tendency for the particles to flocculate and precipitate. For these reasons, the particle size distribution of this solution was measured as a function of solution age at room temperature to determine the nature of the particle growth.

Six samples were analyzed. The first five samples were withdrawn from a solution prepared by the standard technique presented in Section III. These five samples were withdrawn

at various solution ages. The sixth sample was taken from a solution prepared by the special formulation presented in Section III. The difference between the two solutions is that the time between additions of the components is varied. Table (2) lists the sample numbers assigned, the solution age when samples were withdrawn, and the solution age represented by the scattering curves obtained. The difference between the two solution ages is due to the time necessary to obtain a scattering curve in the Kratky camera, approximately five hours. For all but the fresh samples (samples 1 and 6), this time is negligible as compared to the solution age. For the fresh samples, though, the effect of the time to obtain a scattering curve was taken into account by obtaining scattering curves from two identical fresh samples. The first scattering curve was obtained by measuring the intensity first at small angles and incrementing to higher angles, and the second, by starting at the largest angle and incrementing downwards. The resultant scattering curves are taken as the average of the two curves.

The scattering curves for samples 1 through 6 are shown in Figure (16), plotted as log I - log(2θ). As is evident from these plots, none of the curves extends into the high angle asymptotic region ($I = Kh^{-4}$). For each curve the scattered intensity was not sufficient to make the asymptotic region accessible. For this reason, the graphical technique

for determining the size distribution was selected. The scattering curves are replotted as $\log(I) - \log(h^2)$ and are shown in Figure (17).

Analysis

The plots of the data on these samples do not resemble the theoretical plots for any polydisperse system discussed in Appendix I. (See Appendix I, Figures 26 & 28). However, it is possible to envision two scattering curves whose sum yields a plot similar to the actual data. Shown in Figure (18) are two theoretical scattering curves, a and b, whose sum, c, represents the scattering curve of a distribution of particle sizes given as the sum of the distribution of curves a and b. The resultant intensity curve does resemble actual data in form. Further, in the development of this technique for determining size distributions, Shull and Roess[15] suggest that some scattering curves must be separated into two distinct curves.

In light of Figure (18) and the suggestion of Shull and Roess, each of the scattering curves of Figure (17) are separated into two separate scattering curves, each of which is analyzed independently. A typical separation process and analysis is shown in Figure (19) for the curve of sample 5. For samples 2 through 6, analysis is similar to that of the example and will not be shown. The curve of sample 1, though, creates problems. No two curves were found which, on trans-

lation, form a straight line. Fortunately, after separation of the curve into two components (Figure (20)) the first component (large h^2) does satisfy the technique. The remaining curve contains a number of peaks characteristic of a monodispersed sol, and, for a monodispersed sol, the positions of the peaks may be used to determine sizes. The peak positions may be determined from the equation for scattering from monodispersed sols.

$$I(h) \alpha \left[\frac{\sin(hR) - hR \cos(hR)}{(hR)^3} \right]^2 \qquad (10)$$

This equation predicts periodic peaks and zeroes in the scattering curve with a period given by:

$$I(h) = 0 \Rightarrow \sin(hR) = hR \cos(hR)$$

$$\tan hR = hR \text{ at peak (or zero) positions}$$

Also, $\tan hR = hR$ for $hR = n\pi$ so that the separation of the zeroes of the scattering curve satisfies the following: $\Delta(hR) = \pi$. From Figure (20), the positions at which the peaks occur are separated by an average h of .070 so that the diameter of the particles is given as 45Å.

For each sample, then, the distribution of diameters is given as the sum of two distributions, whose parameters are listed in Table 3. The number of particles represented by each distribution may be determined by a method analogous to technique 4 for determining size distributions. As men-

tioned in the development of this technique (Guinier plot deconvolution), the intensity at $2\theta = 0°$ is given as:

$$I(0) = nCR^3 \tag{12}$$

with n being the number of particles of radius R, and c a constant. The same logic used to determine the relative numbers of one specific size is used to determine the number of particles represented by one distribution, with the replacement of R^3 with $E(R^3)$, the expected value of R^3. This quantity is given as the weighted average below:

$$E(R^3) = \int_0^\infty R^3 \rho(r)\, dr \tag{13}$$

In Table 4 are listed the intensity at 0° obtained by extrapolating each separated curve, the expected value of d^3, and the relative numbers of particles represented by each distribution of each curve. The resultant particle diameter distributions for samples 1-5 are shown in Figure (21) and for samples 1 and 6, in Figure (22).

As has been mentioned, only qualitative conclusions may be drawn from distributions derived by this graphical technique. There are trends which appear consistent throughout the six samples, though. By comparing the distributions the following observations can be made:

1. Each distribution has a large number of small particles whose distribution follows a curve of rapid

decline. The distributions are not normalized and the scales of each distribution are adjusted to reflect the presence of the larger particles. For this reason, and since the distributions of the smaller particles may be derived from the region of the scattering curve of lowest intensity, the distribution of smaller particles may be considered qualitatively the same.

2. The distribution of larger particles broadens with age in reference to Figure (21).

3. The ratio of the number of smaller particles to larger particles remains essentially constant as a function of solution age (Table 4), with the exception of sample 5. For this sample there is a decrease in the number of larger particles.

4. The difference due to changing the time between additions (sample 1 compared to sample 6, Figure (22) is that the distribution of larger particles is more polydisperse and represents bigger particles for the special formulation.

One additional piece of information was obtained as another characterization of the difference between the solutions of samples 1 and 6. This information is the difference in the rate at which the solution pH changes as the solutions are formulated. Since the growth of particles is caused by hydrolysis, there is a decrease in pH as the solution ages.

Figure (23) presents a plot of the solution pH as a function of time for the first one half hour of solution age. On the basis of this figure, there is a difference in the pH of the solutions of samples 1 and 6, the pH of sample 1 being substantially lower than for sample 6 due to the earlier additions of $SnCl_2 \cdot 2H_2O$.

Cerium Hydrosol

The cerium system, a wetting colloid, was studied for three reasons. First, the effect of the solution concentration may be studied in a more direct manner than in the multicomponent Stannous-Stannic system. Second, the growth of the particles depends on hydrolysis, so that observations made in examining this system may suggest further studies in a multicomponent system. Third, this system is more stable than the stannous-stannic system. The pH of these solutions reaches a stable value so that the effect of aging while the scattering curves are being measured is neglected.

The scattering curves for the three solutions, prepared as mentioned in Section III, are shown in Figure (24). As with the stannous-stannic system, data were not accessible in the large angle asymptotic region so that the graphical technique was applied to determine size distributions. Analysis was essentially the same as for the stannous-stannic system, two distributions being present for each sample, and will not be elaborated. Table 5 lists the distribution parameters for each sample, and Table 6 lists the deter-

mination of the relative number of particles of each distribution. The resultant distributions for these samples are shown in Figure (25).

As before the distributions presented in Figure (25) may be only qualitatively interpreted, due to the technique used. The trends, though, can be enumerated.

1. The largest particle size present in solutions decreases as the solution concentration increases.
2. There is an increasing tendency for the distribution to separate into two distributions as the concentration increases. (Note: The apparent bimodal distribution of the 1/2% solution combined to form the distribution shown).
3. The relative number of large particles decreases as the concentration increases.

VI. DISCUSSION OF RESULTS

Stannous-Stannic Hydrosol

On the basis of the observed trends in the particle size distributions of the stannous-stannic hydrosol, it is possible to postulate a mechanism for the behavior of this system. It should again be mentioned that this hydrosol is prepared by three separate additions, namely, a primary addition of $SnCl_4$ followed by secondary and tertiary additions of $SnCl_2$.

The postulated mechanism for the colloid growth is as follows. First, the primary addition of Sn^{4+} ($SnCl_4$ dissociates into Sn^{4+} and Cl^- ions) immediately begins to form nuclei and particle growth occurs. This is suggested by the work of Johnson and Kraus[30] who studied the growth of particles from $SnCl_4$ solutions of the approximate concentration used here. However, the growth of these particles is interrupted by the additions of $SnCl_2$. As the second and third additions are made ($SnCl_2$), part of the Sn^{2+} ions are oxidized to form Sn^{4+} ions[31], and these ions form nuclei and begin to grow with the Sn^{2+}, driving the pH of the solution lower. The hydrolysis reaction is pH dependent[31] and slows due to the decrease in pH (see Figure 23, curve (a)). The particle size distribution of sample 1 (Figure 22) suggests this mechanism. The almost monodispersed distribution of larger particles represents the extent of growth of Sn^{+4} particles due to the primary addition. The growth was interrupted after a very

short period of time leaving the monodispersed sol. The large number of small particles is due to the new nuclei formed on addition of the $SnCl_2$.

The size distribution of sample 6, prepared by the special formulation, supports this mechanism. In this case, the Sn^{+4} particles were allowed to grow undisturbed by the $SnCl_2$ additions for twenty minutes. (See Figure (23)). The size distribution of this sample (Figure 22) shows a more polydispersed distribution of larger particles which seems to reflect the additional growth time.

As the solution ages (Figure 21) the hydrolysis reaction proceeds very slowly and causes growth of the larger particles by one of two mechanisms. First, the larger particles could combine and thus grow. This should be accompanied by a decrease in the relative number of large particles. Second, the smallest particles could combine with the larger particles to reduce their surface energy, and thus cause growth of the larger particles. This would cause an increase in the relative number of larger particles. With the exception of sample 5, the relative number of larger particles remains essentially constant, so either mechanism could occur (see Table 4). For sample 5, the decrease in the number of larger particles can be attributed to precipitation of the largest particles, which occurs in solutions of this approximate age.

Cerium Hydrosol

It is again possible to postulate a particle growth mechanism which conforms to the observed trends (Figure 25) in the particle size distributions for the cerium hydrosols. For the 1/2% solution, the number of nucleation sights is relatively small. The cerium in solution then associates with the first nuclei to form and results in relatively large particles. As the solution concentration is increased, there is an increased rate of nuclei formation which slows the hydrolysis reaction. The first nuclei to form grow rapidly initially, but then stop growing when additional nuclei form, The distribution of larger sizes then represents the first nuclei to form. The increasing number of small particles (Table 6) is due to the increasing likelihood for nuclei formation at higher concentrations.

CONCLUDING REMARKS

The main purpose of this work was to establish a technique for characterizing colloidal solutions. It was hoped that the characterization would lead to an understanding of the effects of solution age, concentration and formulation on solution properties. The sizes of the colloidal particles was selected as a parameter which would reflect changes in the system. On the basis of the cerium and the wetting tin data, this parameter appears to be sensitive to solution changes, and is thus a suitable characterization.

The method of small angle x-ray scattering was selected as a technique to determine particle sizes of colloidal particles. Since the parameters which result directly from experiment represent weighted averages of the particle size distributions, the distribution of sizes was sought. Two techniques were found applicable from a theoretical standpoint. The amount and accuracy of the information deduced from a scattering curve depends on many factors. In some cases, such as the chromium hydrosol system, no information was obtained. Generally, the technique is useful for at least qualitative portrayal of the distribution of sizes of the particles which may be used to predict the behavior of some systems. Thus, the technique of small angle x-ray scattering is a suitable technique for characterizing the colloidal solutions.

Two systems examined yield information which suggests further studies. The wetting tin system shows a marked sensitivity to the sequence of formulation, and it is likely that this system is somewhat sensitive to the concentration of the constituents (on the basis of the cerium study). A more detailed examination would involve variations of the concentrations and times between dissolutions of the constituents in an attempt to determine the degree of changes in the system, and to support or reject the mechanisms which have been postulated.

TABLE 1

SIZE RANGE FOR VARIOUS

TECHNIQUES OF PARTICLE SIZE DETERMINATION

METHOD	PARTICLE DIAMETER (Å)	IN SOLUTION
Coulter Counter	$2x10^4 - 10^6$	Yes
Transmission Electron Microscopy	$10 - 10^8$	No
BET Nitrogen Adsorbtion	$10^2 - 10^6$	No
Centrifugation	$10^2 - 10^8$	Yes
Ultrafiltration	$50 - 10^4$	Yes
Light Scattering	$10^3 - 3x10^5$	Yes
X-ray Scattering	$10 - 10^4$	Yes

TABLE 2

SOLUTION AGES OF THE STANNOUS-STANNIC SAMPLES

SAMPLE	SOLUTION AGE WHEN SAMPLE WITHDRAWN (hrs)	SOLUTION AGE REPRESENTED BY SCATTERING CURVE (hrs)
1	0	2.5
2	142	144
3	188	190
4	558	560
5	1250	1252
6	0*	2.5*

*SPECIAL PREPARATION

TABLE 3

DISTRIBUTION PARAMETERS FOR THE

STANNOUS - STANNIC HYDROSOL SAMPLES

SAMPLE	SMALL PARTICLES		LARGE PARTICLES	
	n	d_o	n	d_o
1	0.7	15.6	*	45.0
2	-0.66	28.2	1.27	54.5
3	-0.93	38.6	0.10	96.0
4	-0.84	34.5	0.0	89.0
5	0.1	33.2	2.0	109
6	-0.60	44.5	4.0	58.5

* monodispersed

TABLE 4

DETERMINATION OF THE RELATIVE NUMBERS OF EACH DISTRIBUTION FOR THE STANNOUS - STANNIC HYDROSOL

SAMPLE	SMALL PARTICLES			LARGE PARTICLES			RELATIVE NUMBER**
	I(o)	$E(d^3)$	NUMBER*	I(o)	$E(d^3)$	NUMBER*	
1	11	2.2×10^3	.005	77	9.1×10^5	8.4×10^{-4}	6.0
2	11	3.7×10^3	.003	63	$13. \times 10^5$	5.0×10^{-4}	6.0
3	15	6.0×10^3	.0025	100	29×10^5	3.5×10^{-4}	7.1
4	7.8	5.0×10^3	.0015	90	21×10^5	4.4×10^{-4}	3.6
5	89	13.0×10^3	.0071	100	140×10^5	$.71 \times 10^{-4}$	101.4
6	26	14.0×10^3	.0019	55	45×10^5	1.2×10^{-4}	15.8

* This number is only meaningful in comparison with similar numbers derived from the same curve.

** The ratio of the number of small particles to large particles.

TABLE 5

DISTRIBUTION PARAMETERS FOR THE CERIUM HYDROSOLS

CONCENTRATION	SMALL PARTICLES		LARGE PARTICLES	
	n	d_o	n	d_o
1/2 %	1.27	28.2	2.25	42.0
1 %	-.9	34.5	9.5	24.5
4 %	.4	16.3	10.0	23.8

TABLE 6

DETERMINATION OF THE RELATIVE NUMBERS OF EACH DISTRIBUTION OF THE CERIUM HYDROSOL

CONCENTRATION	SMALL PARTICLES			LARGE PARTICLES			RELATIVE NUMBER**
	I(o)	$E(d^3)$	NUMBER*	I(o)	$E(d^3)$	NUMBER*	
1/2	9.6	1.8×10^{4}	5.4×10^{-4}	54	9.3×10^{4}	5.8×10^{-4}	0.93
1	16	$.47 \times 10^{4}$	34×10^{-4}	70	9.5×10^{4}	7.4×10^{-4}	4.59
4	16	$.21 \times 10^{4}$	78×10^{-4}	100	9.3×10^{4}	10.7×10^{-4}	7.30

* This number is only meaningful in comparison with similar numbers derived from the same curve

** Ratio of the number of smaller particles to larger particles

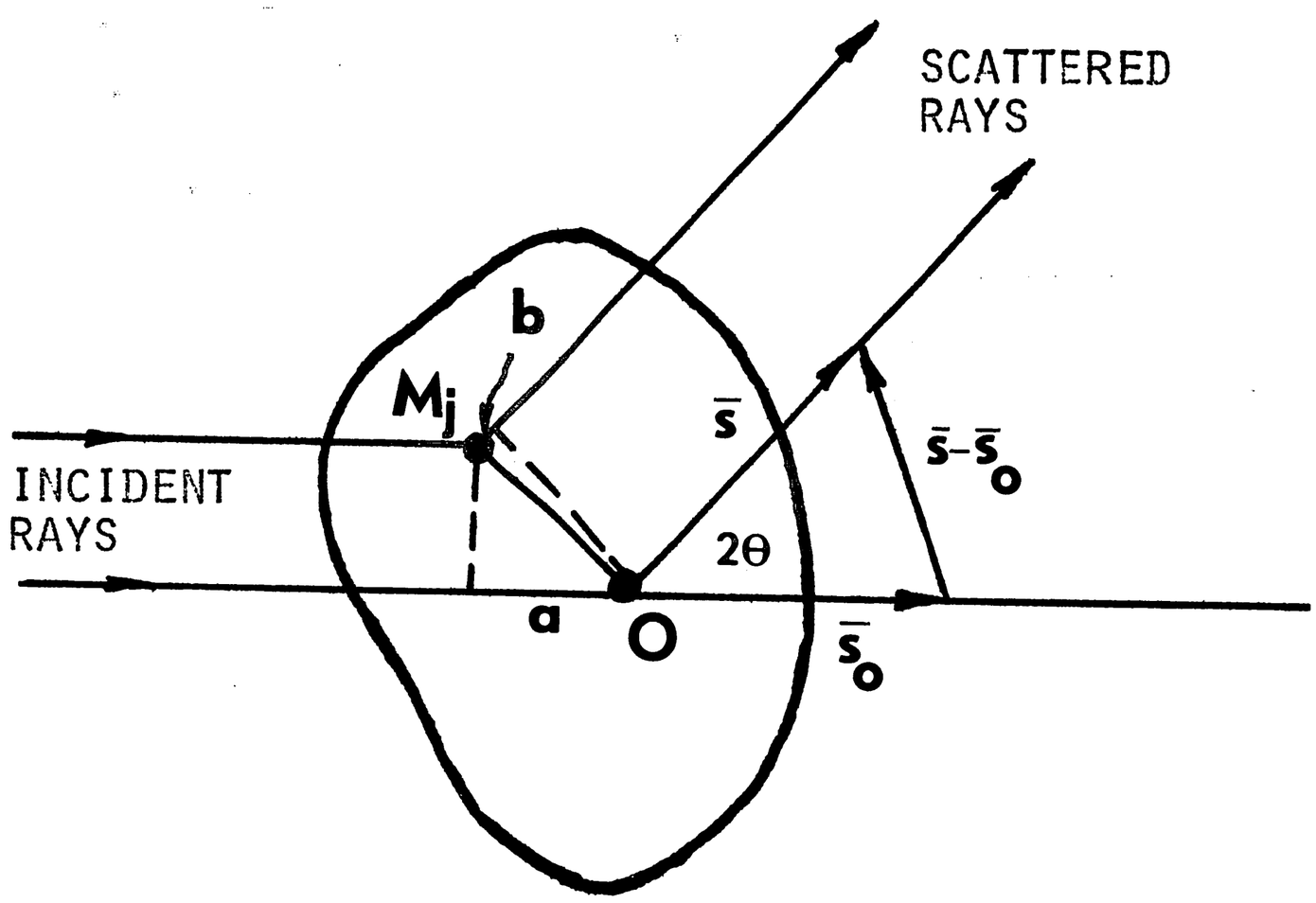

INCIDENT AMPLITUDE = A_o

PHASE FACTOR = $a-b = 2\pi/\lambda\left\{[\bar{S}_o\cdot\overline{OM_j}] - [\bar{S}\cdot\overline{OM_j}]\right\}$

$$= 2\pi/\lambda\left\{[\overline{S-S_o}]\cdot\overline{OM_j}\right\}$$

$$\bar{h} \equiv 2\pi/\lambda[\overline{S-S_o}] \quad , \quad |\bar{h}| = 4\pi/\lambda \sin\theta$$

SCATTERED AMPLITUDE = $A = A_o \exp[-i\,\bar{h}\cdot\overline{OM_j}]$

FIGURE 1 ORIGIN OF SCATTERING BY A PARTICLE

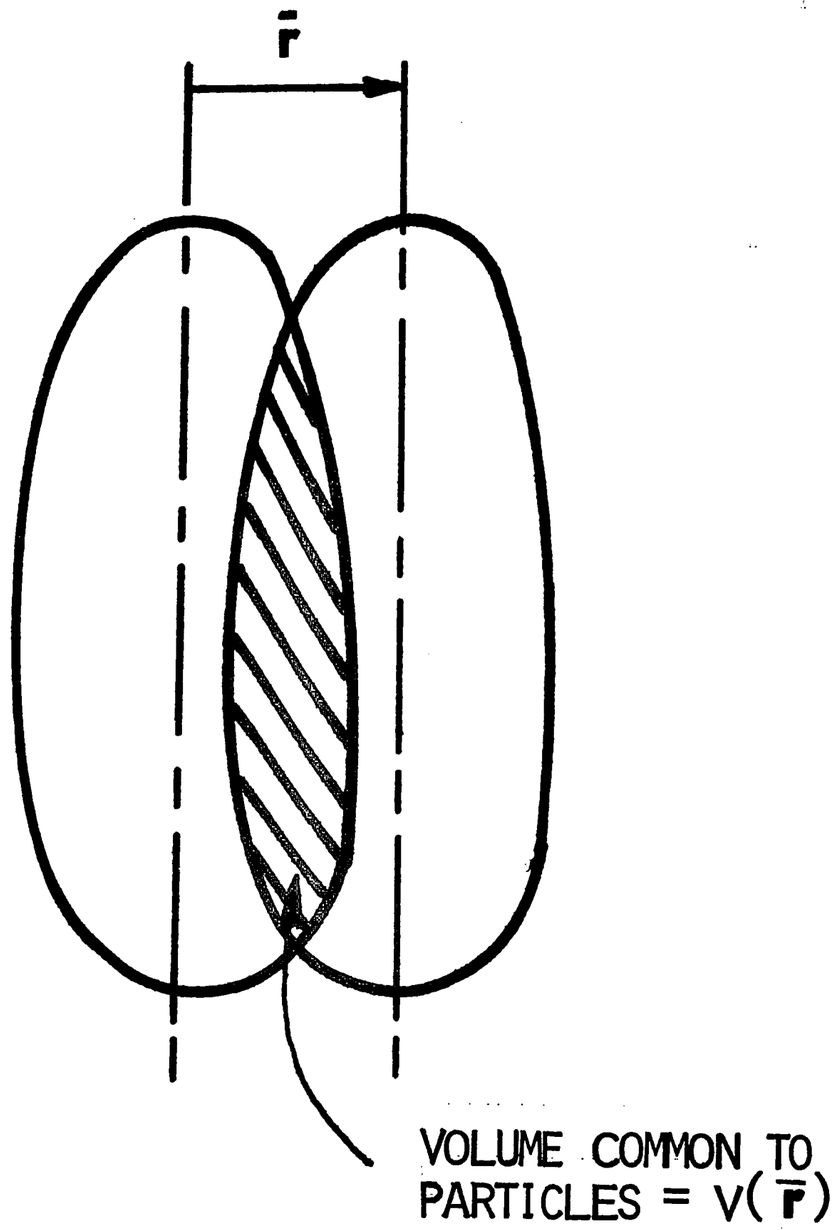

PROBABILITY TERM = $\frac{V(\bar{r})}{V(o)} = \frac{V(\bar{r})}{V}$

AVERAGE OVER ALL ORIENTATIONS OF $\bar{r}$ YIELDS:

$$\frac{\overline{V(r)}}{V(o)} \equiv \gamma_o(r)$$

FIGURE 2 DETERMINATION OF THE SINGLE PARTICLE CHARACTERISTIC FUNCTION. $\gamma_o(r)$.

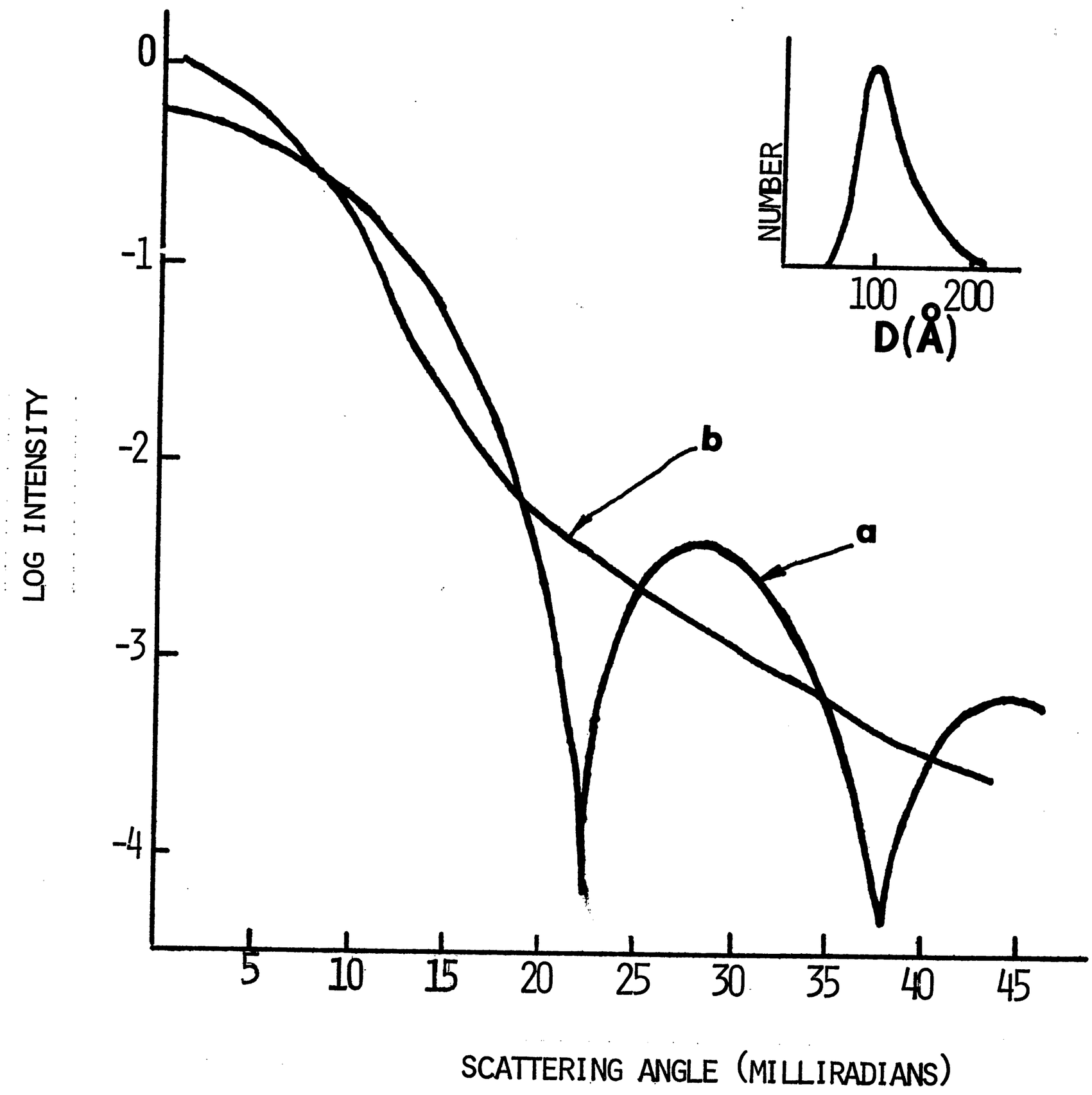

FIGURE 3 THEORETICAL SMALL ANGLE X-RAY SCATTERING CURVES FOR (a) A MONODISPERSED SOL OF DIAMETER 100Å, AND (b) A POLYDISPERSE SOL WITH A DISTRIBUTION AS IN THE INSERT

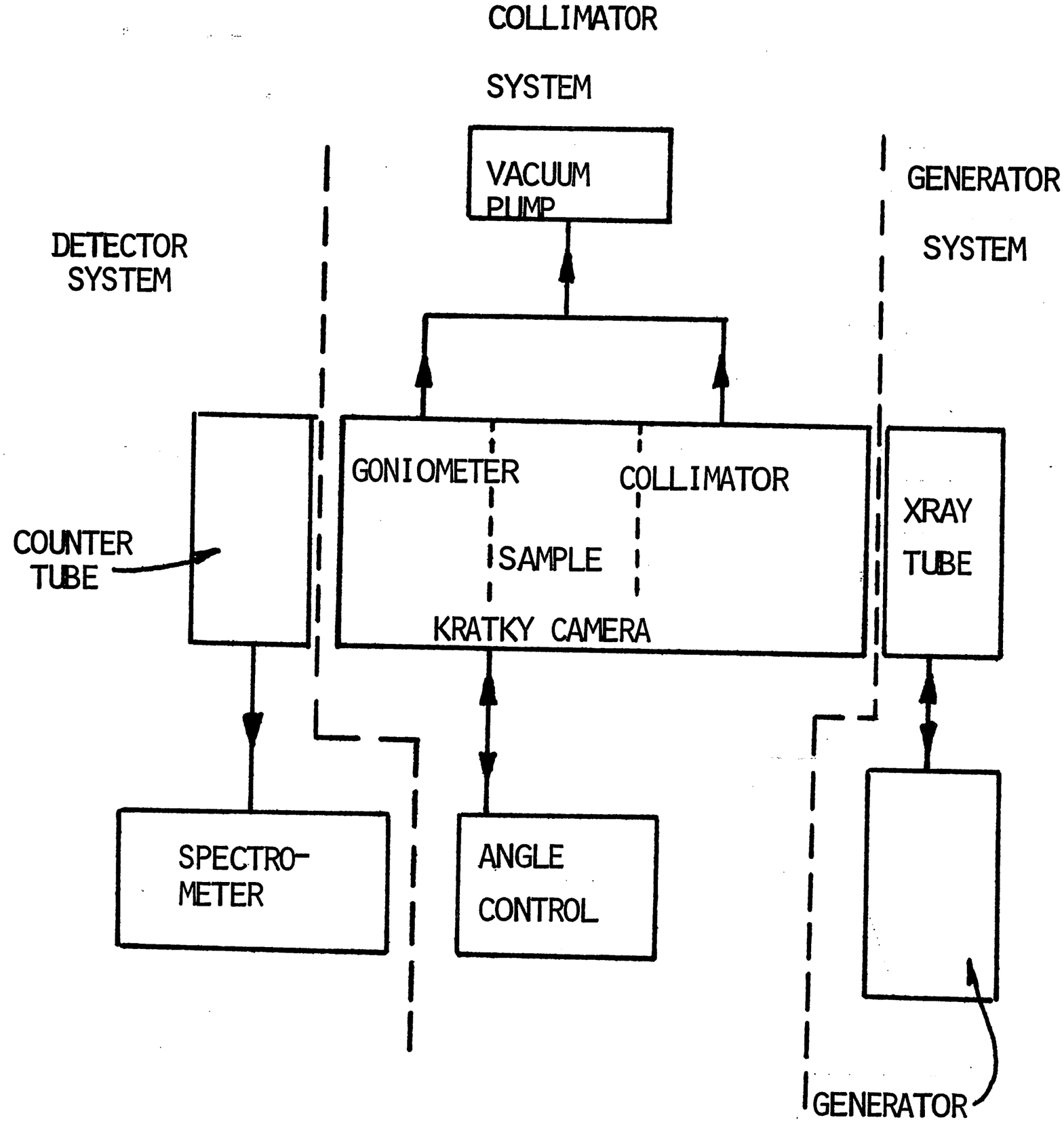

FIGURE 4 SCHEMATIC OF X-RAY SCATTERING APPARATUS

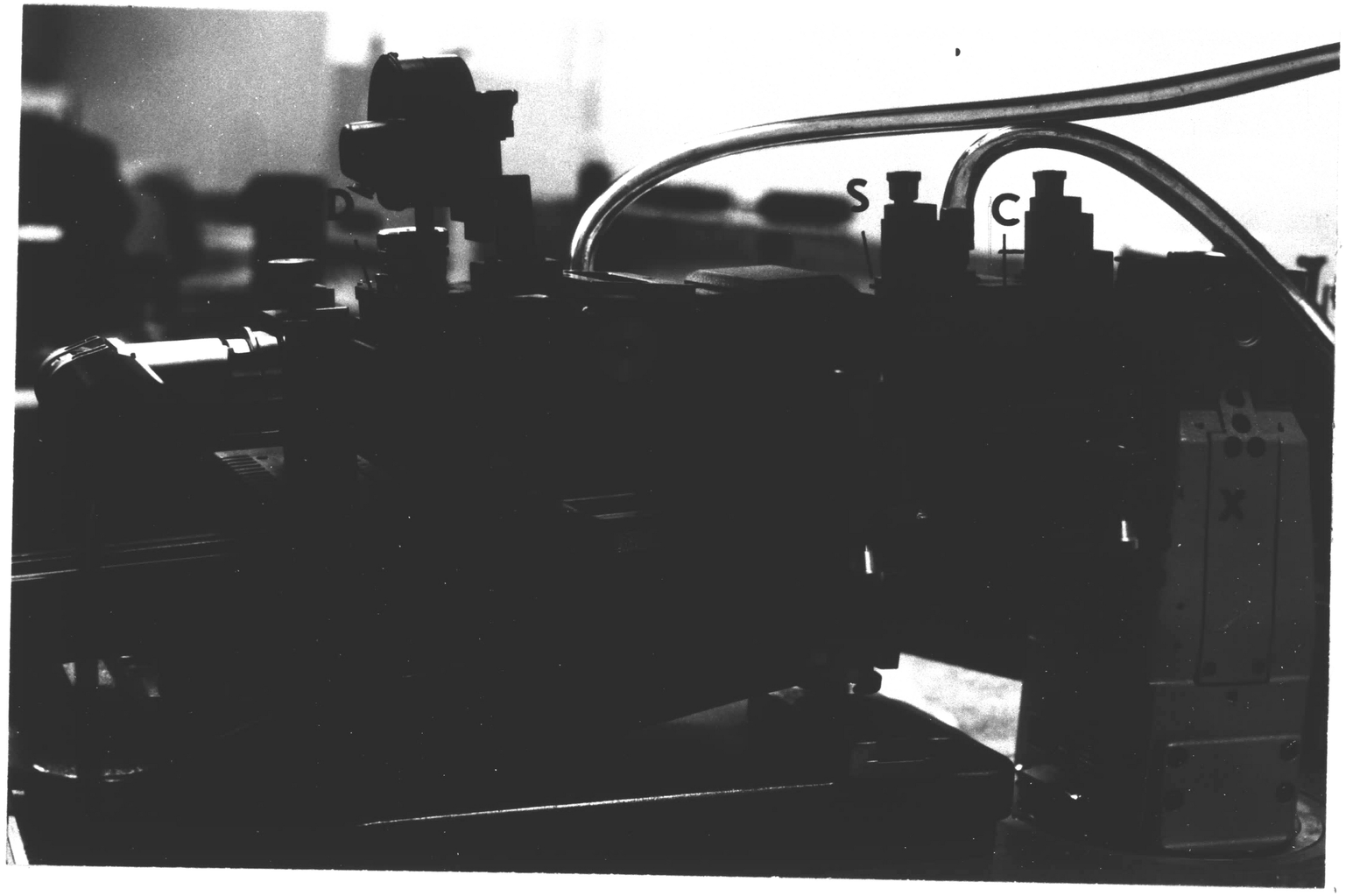

FIGURE 5 PHOTOGRAPH OF KRATKY CAMERA SHOWING: GONIOMETER SCREW, G; DETECTOR PLANE, D; SAMPLE PLANE, S; COLLIMATOR, C; AND X-RAY TUBE, X.

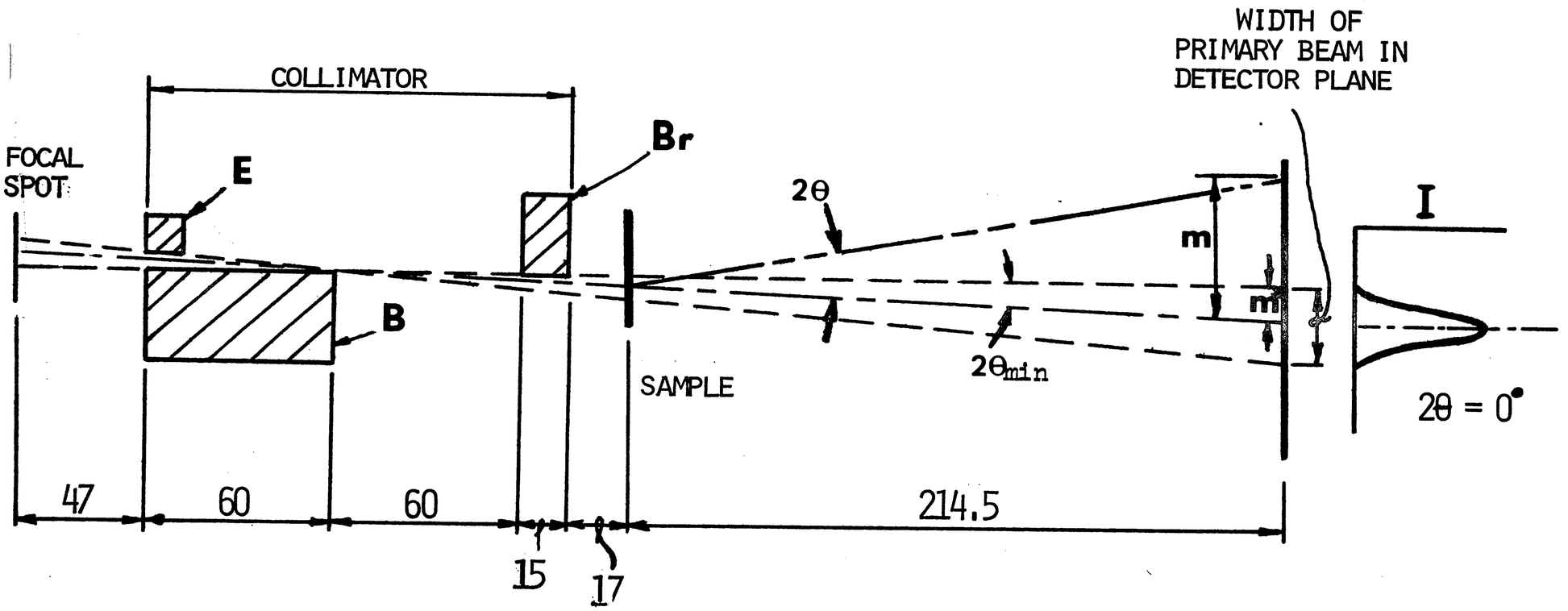

FIGURE 6 VERTICAL CROSS SECTION OF KRATKY CAMERA SHOWING INTENSITY DISTRIBUTION ALONG THE BEAM WIDTH (ALL DIMENSIONS ARE IN MILLIMETERS)

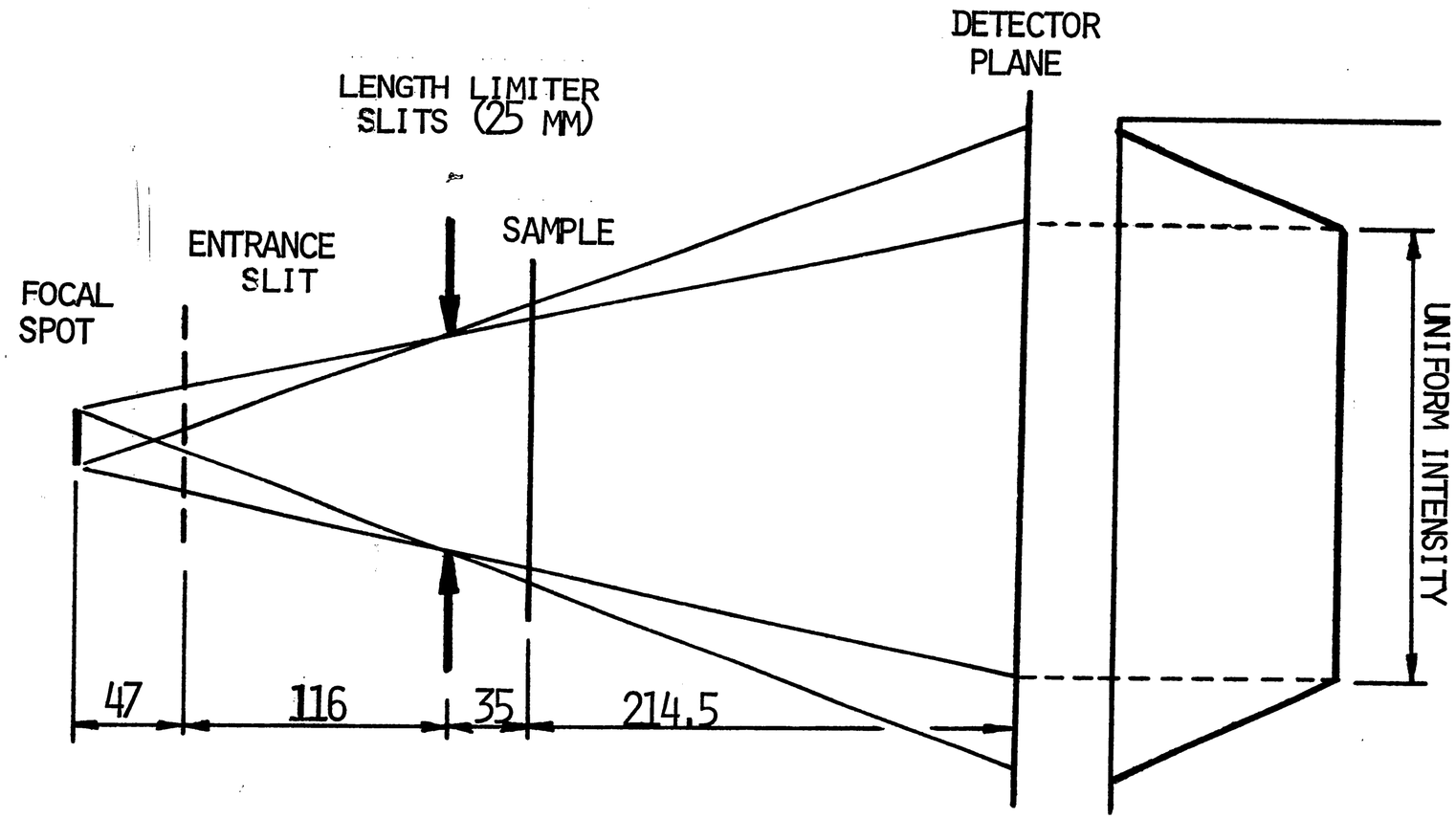

FIGURE 7 HORIZONTAL CROSS SECTION OF KRATKY CAMERA SHOWING THE INTENSITY DISTRIBUTION ALONG THE BEAM LENGTH (ALL DIMENSIONS ARE IN MILLIMETERS)

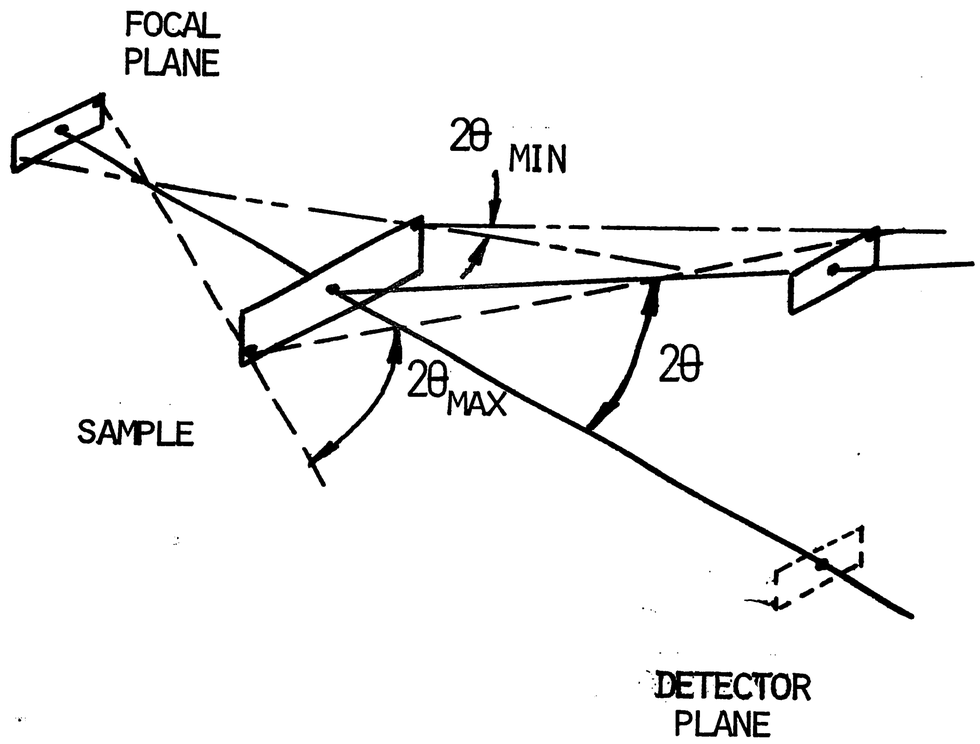

FIGURE 8 ORIGIN OF THE COLLIMATION SMEARING EFFECT. AT THE NOMINAL ANGLE, 2θ, SCATTERED INTENSITY IS RECORDED IN THE ANGULAR RANGE ($2\theta_{MIN}$, $2\theta_{MAX}$)

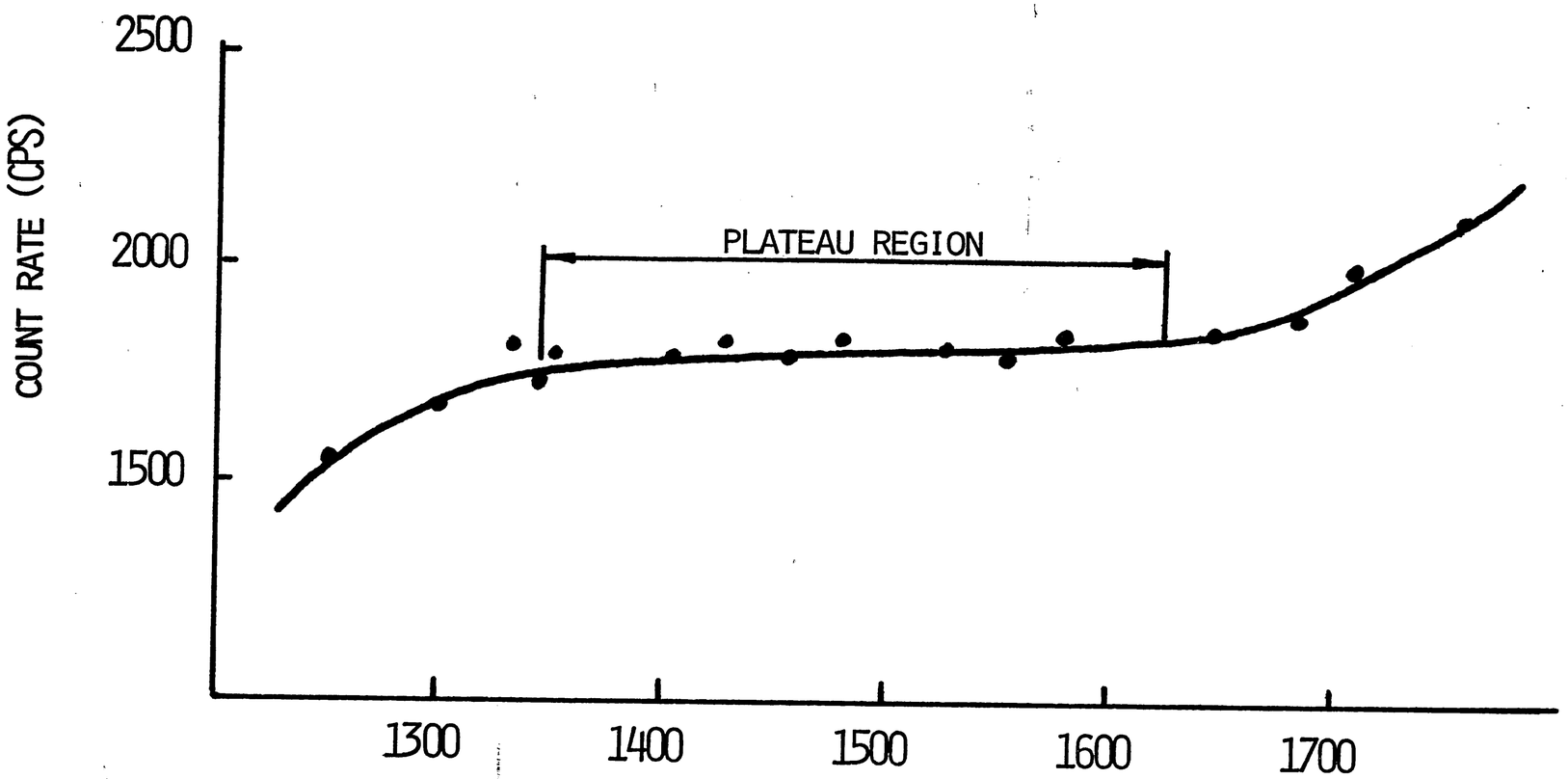

FIGURE 9 PLATEAU CURVE OF SPG-8 COUNTER TUBE. THE OPERATING VOLTAGE IS 1480 VOLTS.

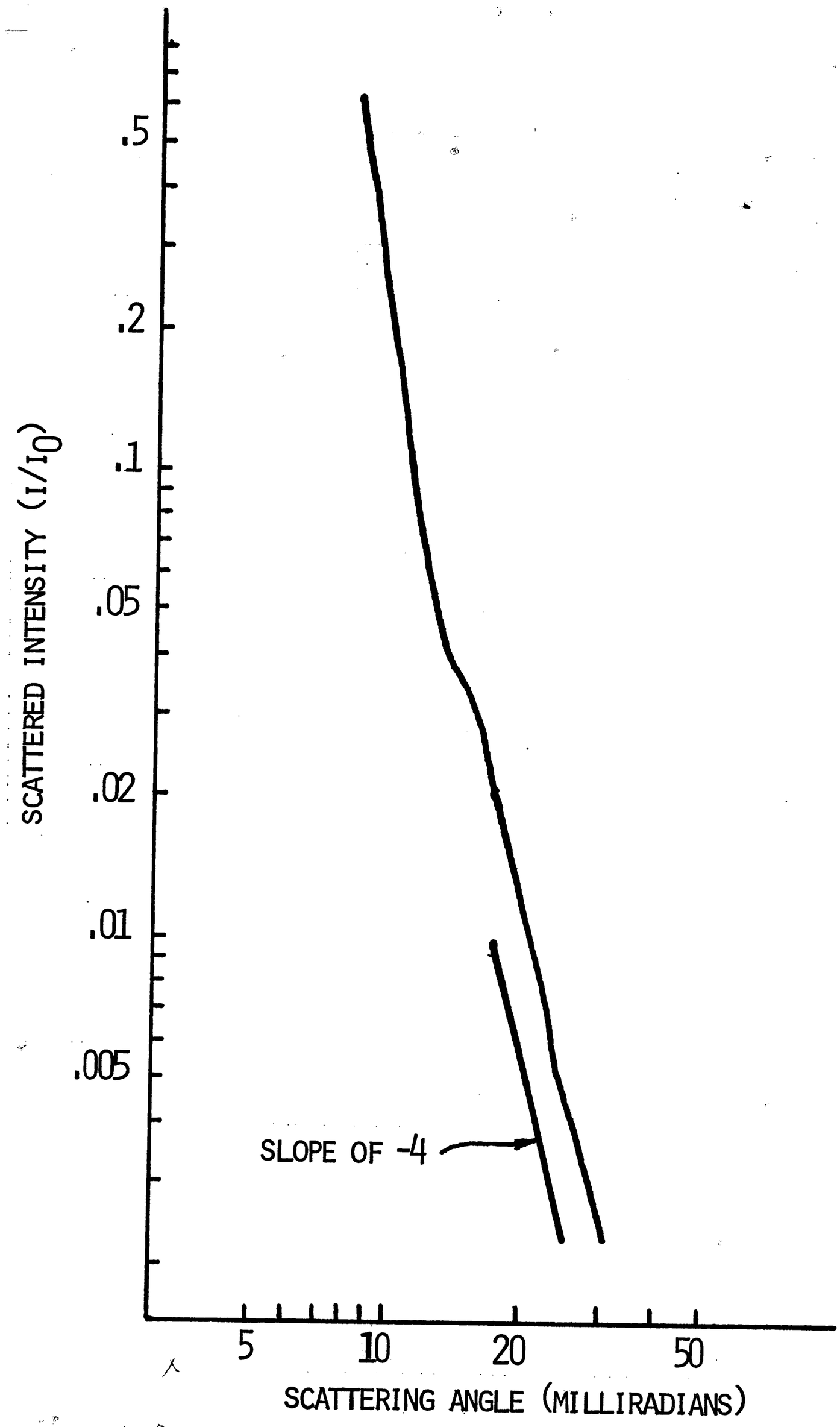

FIGURE 10 PLOT OF SCATTERED INTENSITY AS A FUNCTION OF ANGLE FOR LUDOX HS

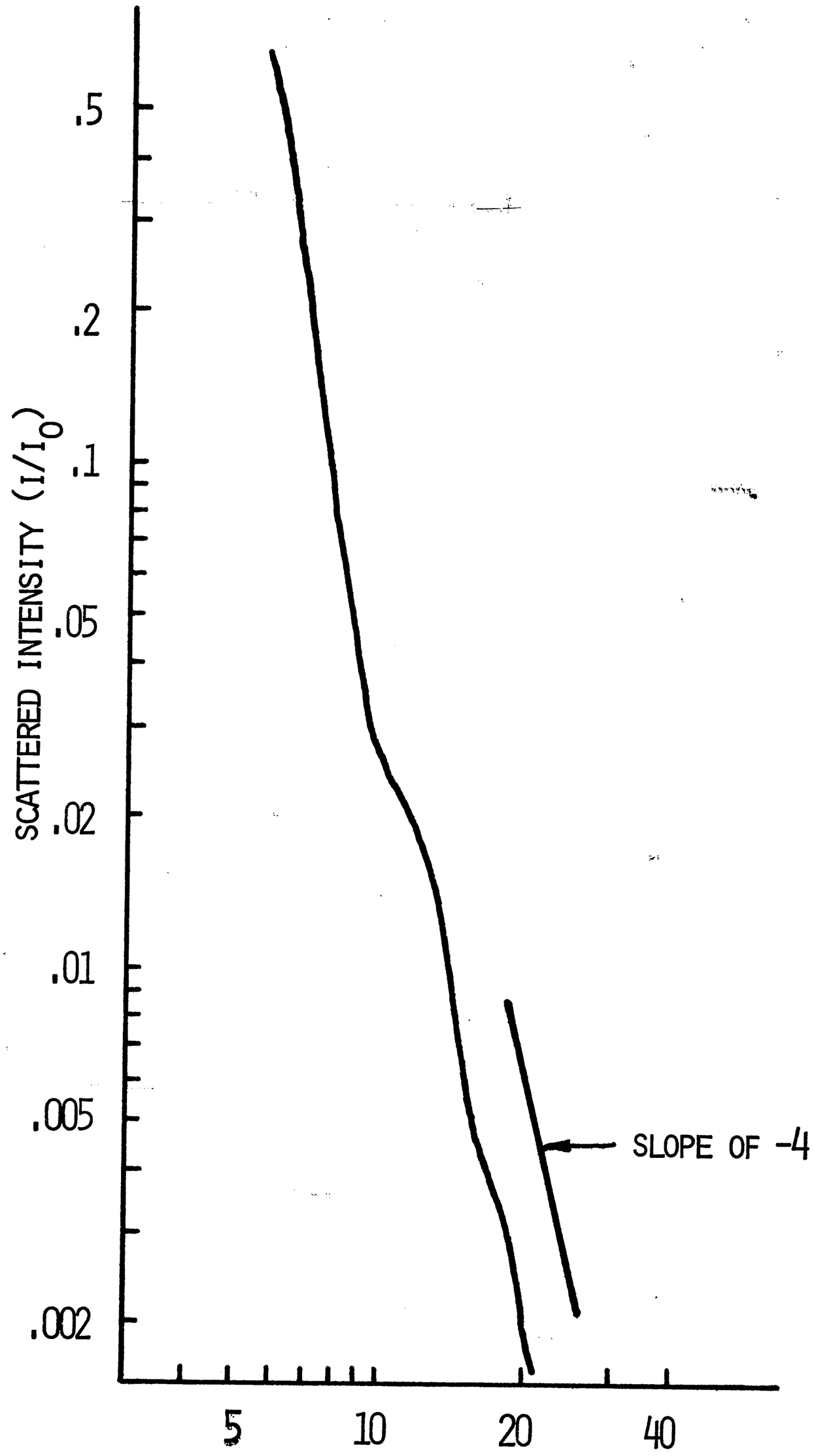

FIGURE 11 PLOT OF SCATTERED INTENSITY AS A FUNCTION OF ANGLE FOR LUDOX TM

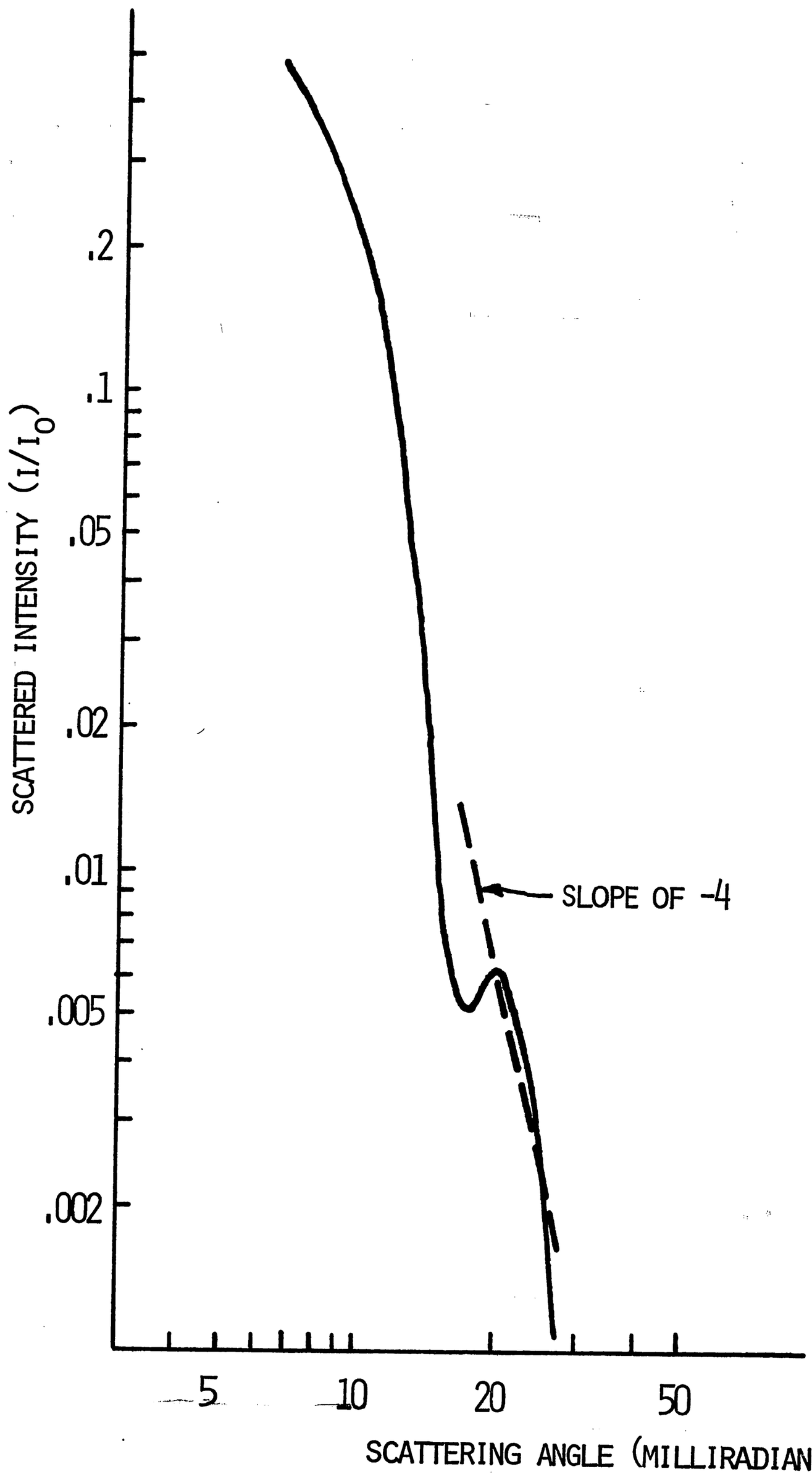

FIGURE 12 PLOT OF SCATTERED INTENSITY AS A FUNCTION OF ANGLE FOR COLLOIDAL GOLD

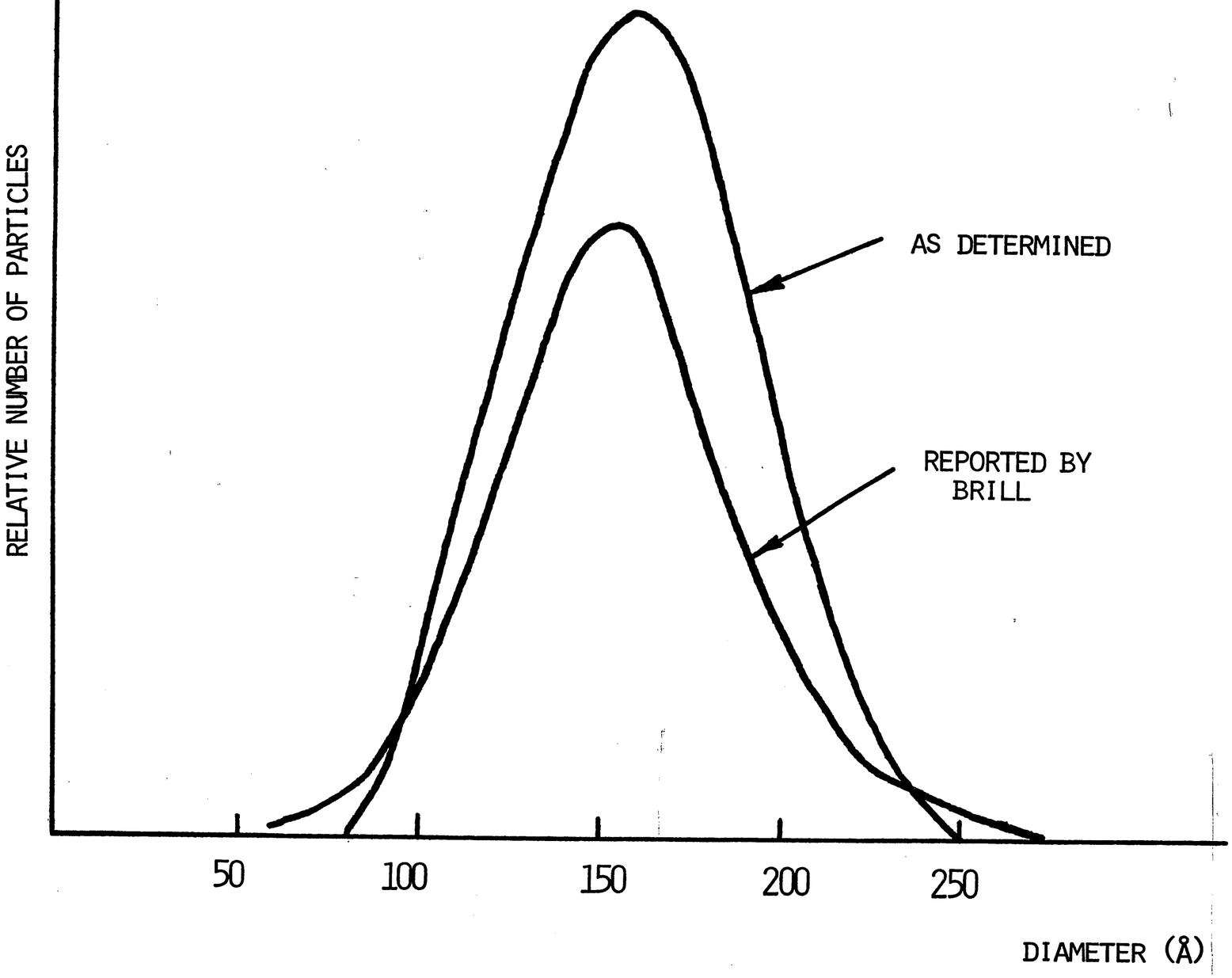

FIGURE 13 DISTRIBUTION OF DIAMETERS FOR LUDOX HS

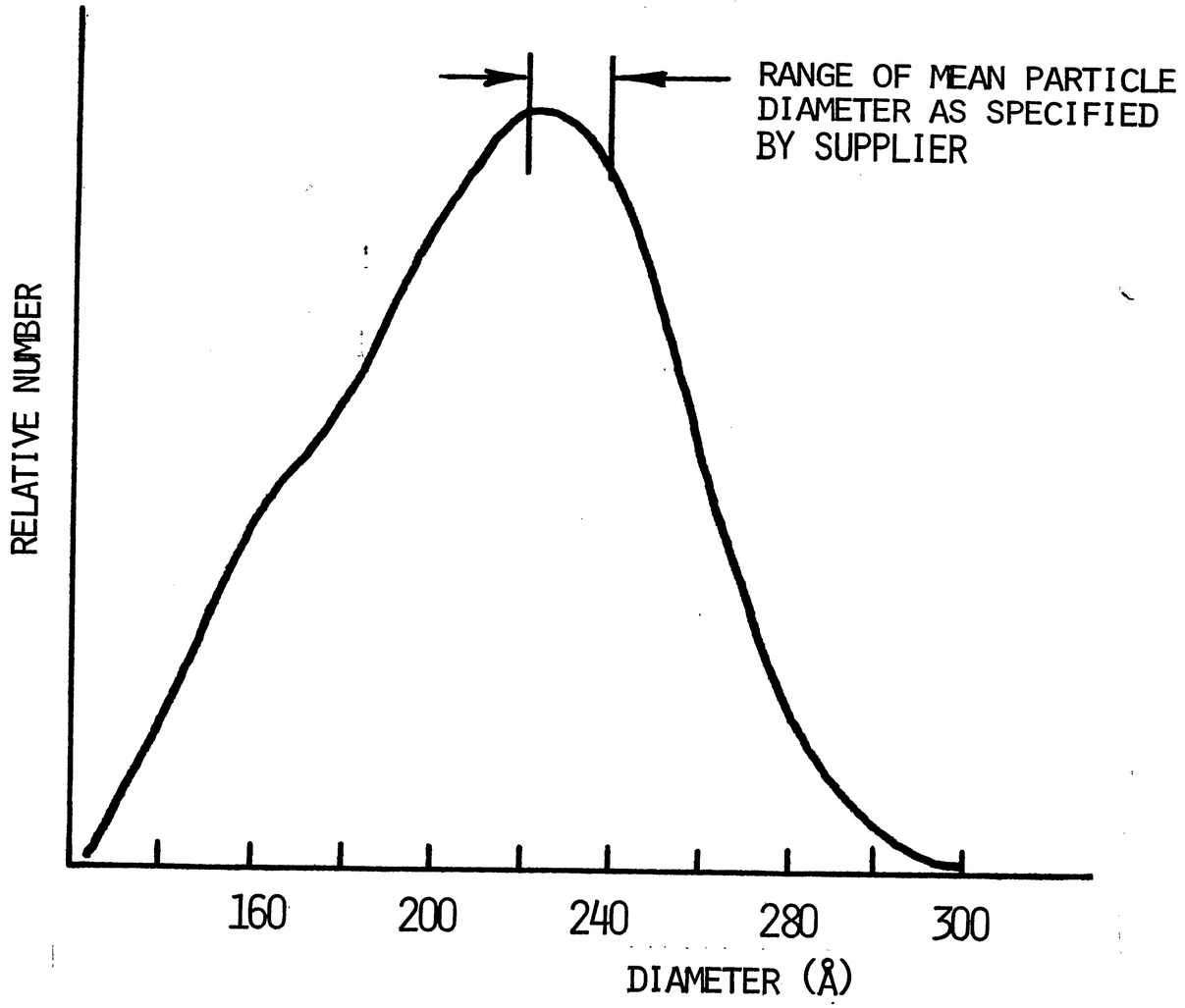

FIGURE 14 DISTRIBUTION OF DIAMETERS FOR LUDOX TM

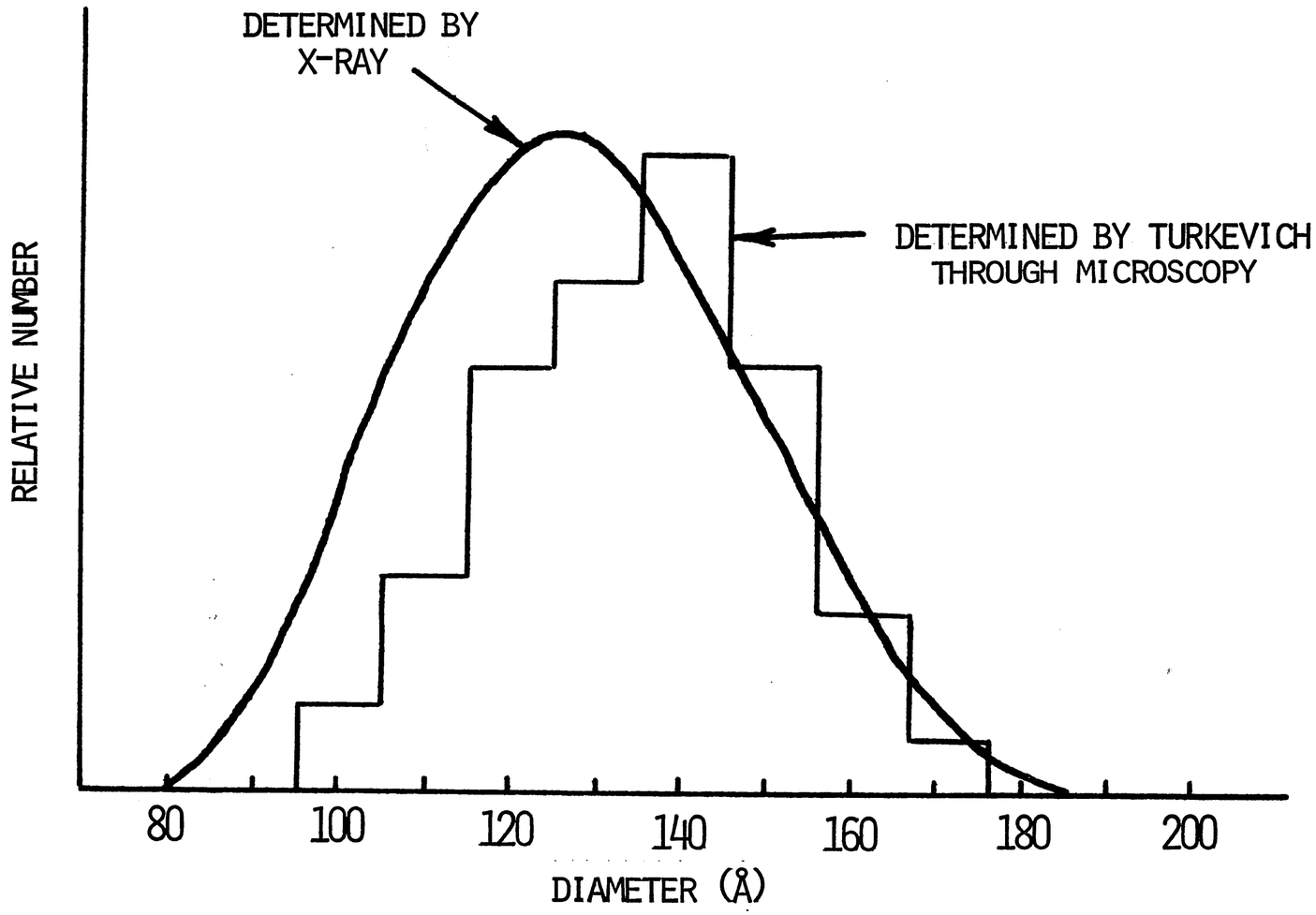

FIGURE 15 DISTRIBUTION OF DIAMETERS FOR COLLODIAL GOLD

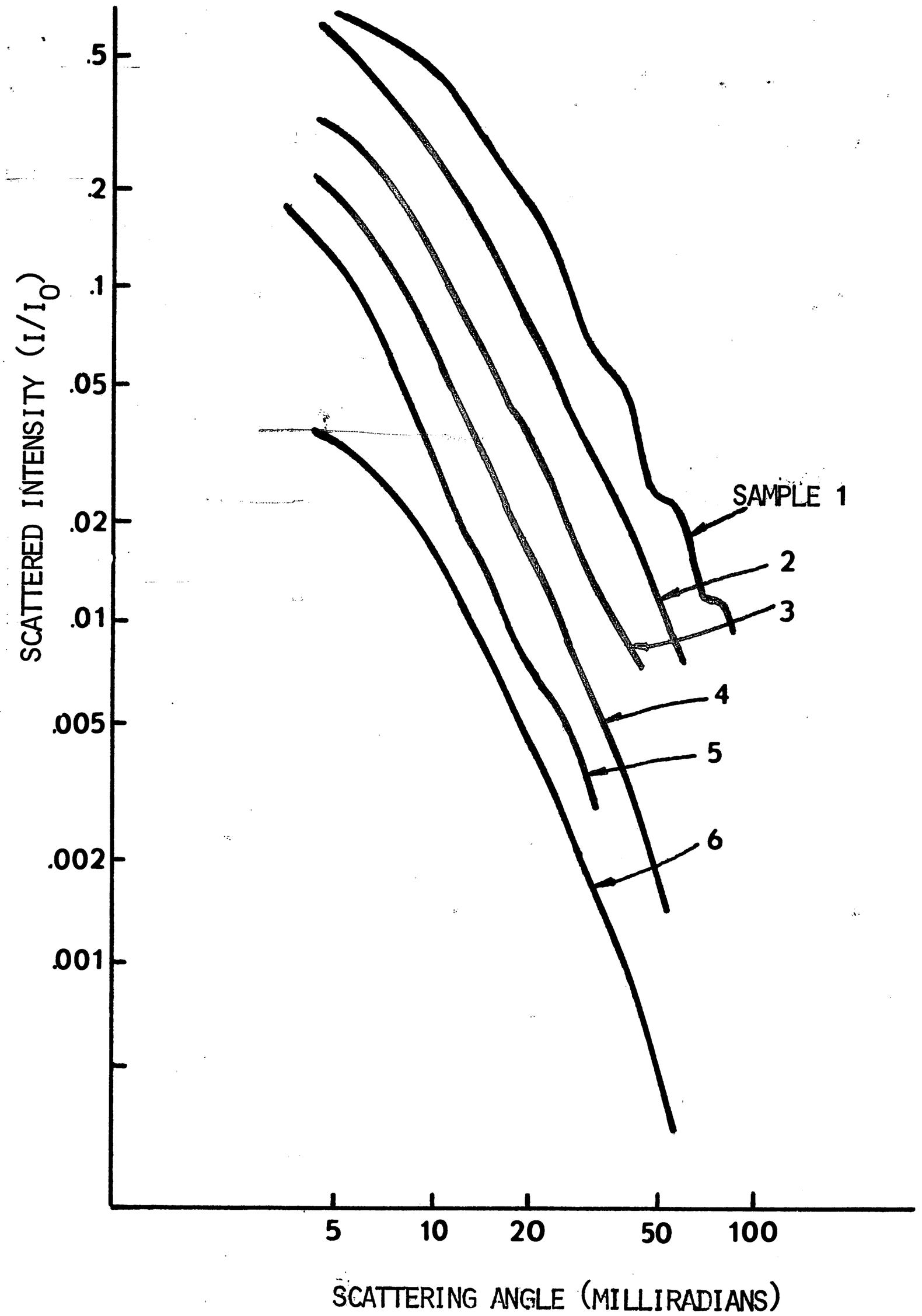

FIGURE 16 PLOT OF SCATTERED INTENSITY AS A FUNCTION OF ANGLE FOR STANNOUS-STANNIC HYDROSOLS

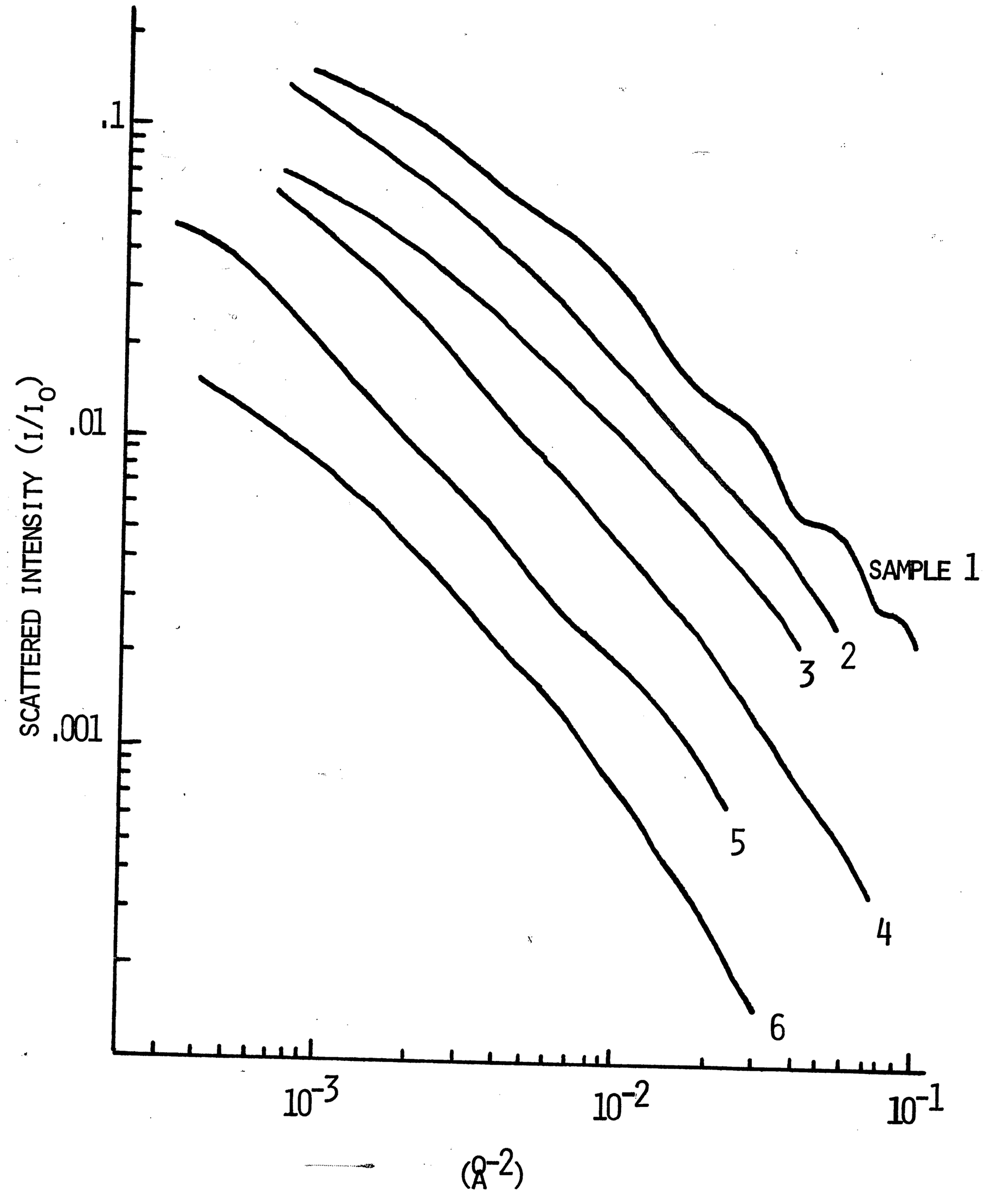

FIGURE 17 A PLOT OF SCATTERED INTENSITY AS A FUNCTION OF FOR THE STANNOUS-STANNIC HYDROSOLS

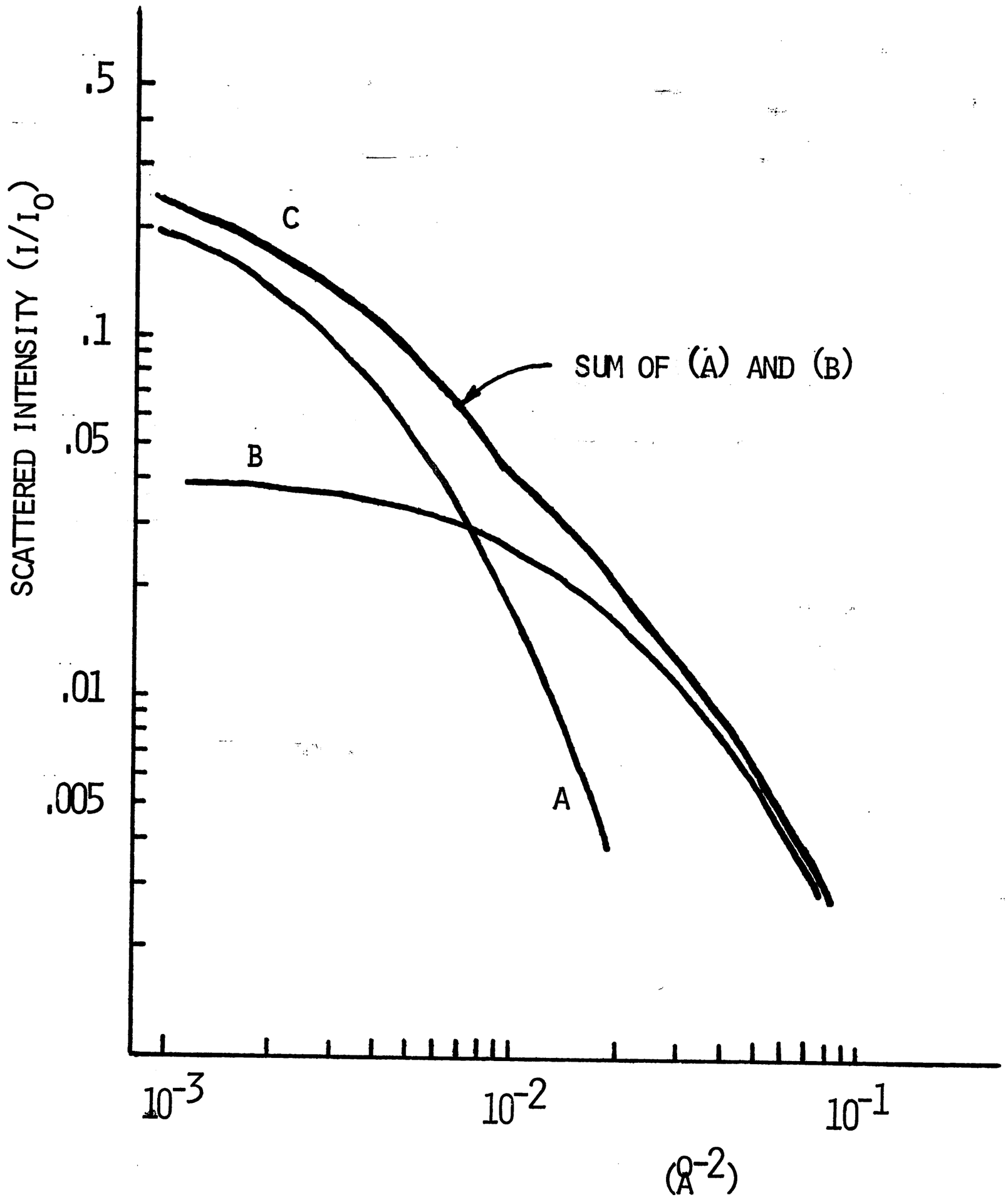

FIGURE 18 A THEORETICAL SCATTERING CURVE FROM A BIMODAL DISTRIBUTION

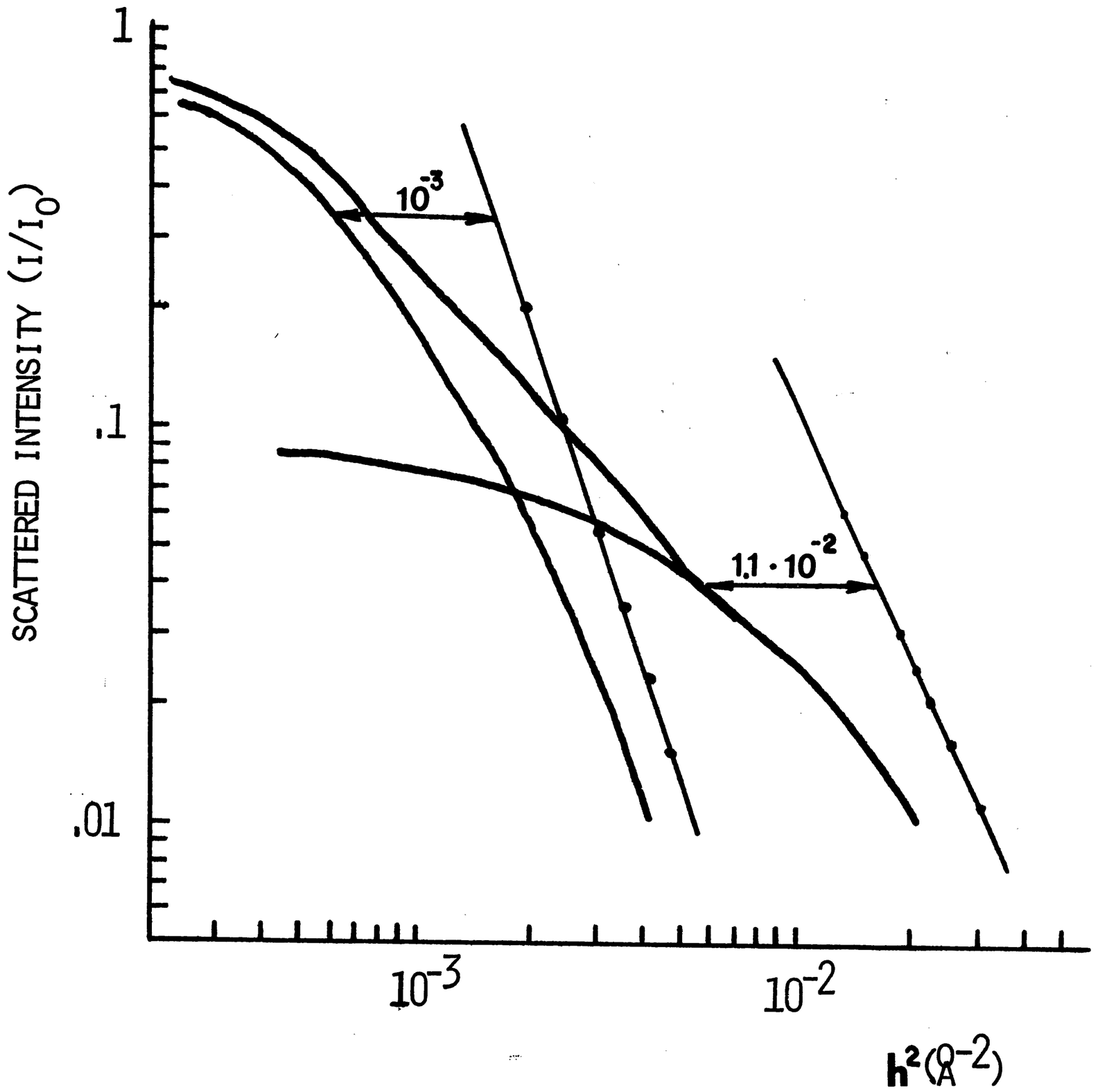

FIGURE 19 DETERMINATION OF DIAMETER DISTRIBUTION OF SAMPLE 5

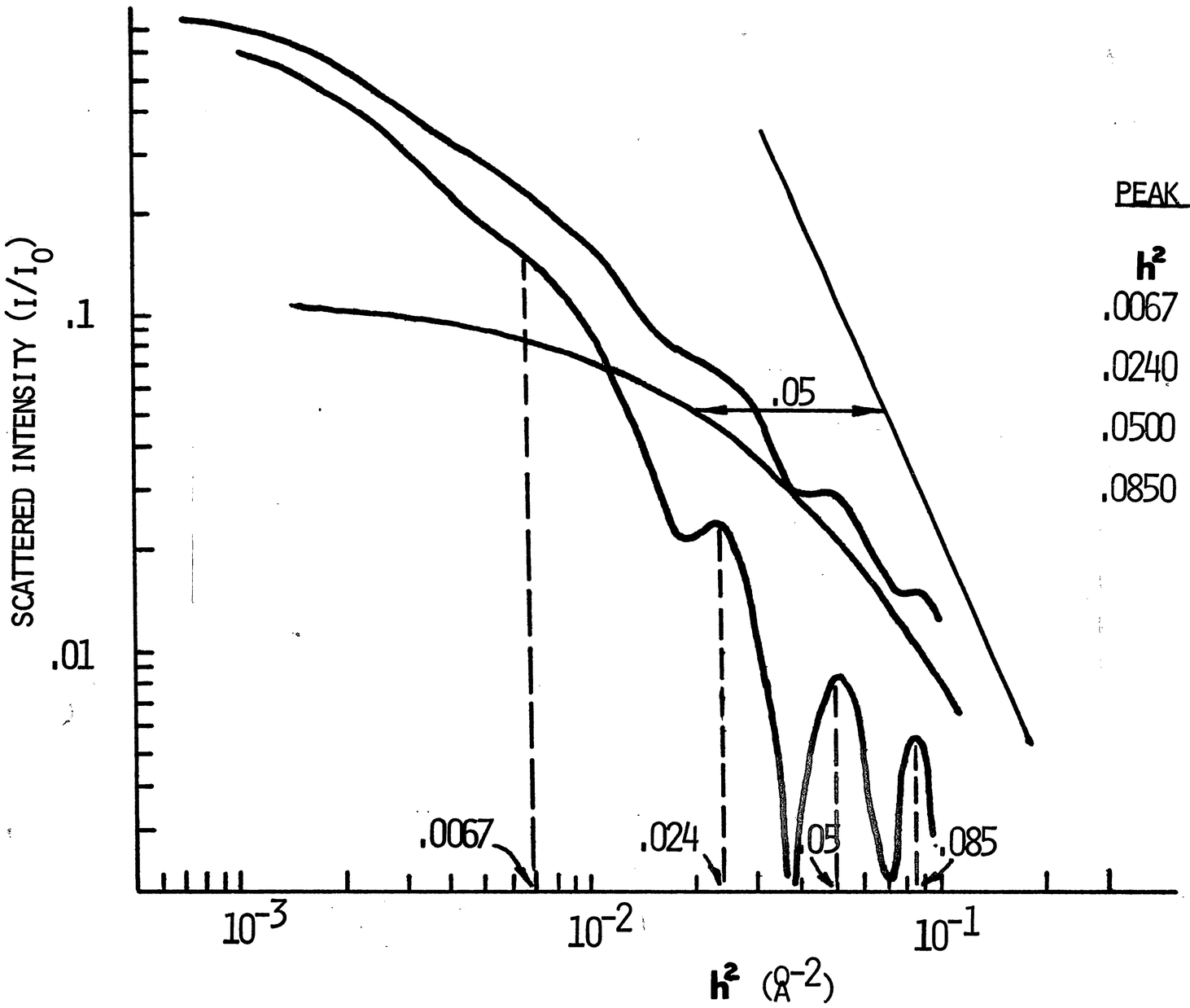

PEAK POSITIONS

h^2	h	Δh
.0067	.083	
		.071
.0240	.154	
		.070
.0500	.224	
		.068
.0850	.292	

FIGURE 20 DETERMINATION OF DIAMETER DISTRIBUTION OF SAMPLE 1

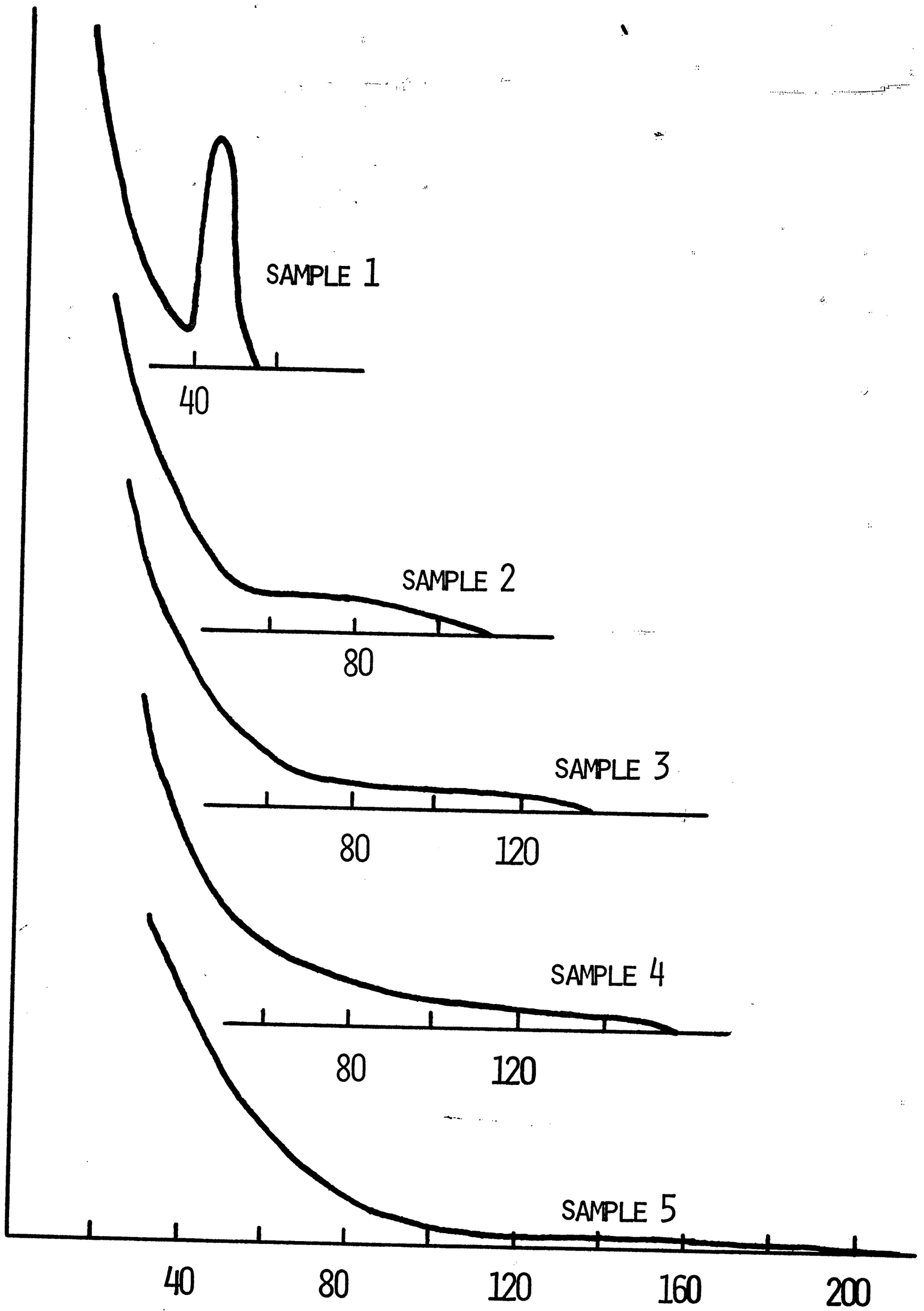

FIGURE 21 DISTRIBUTION OF PARTICLE DIAMETERS FOR STANNOUS-STANNIC HYDROSOLS

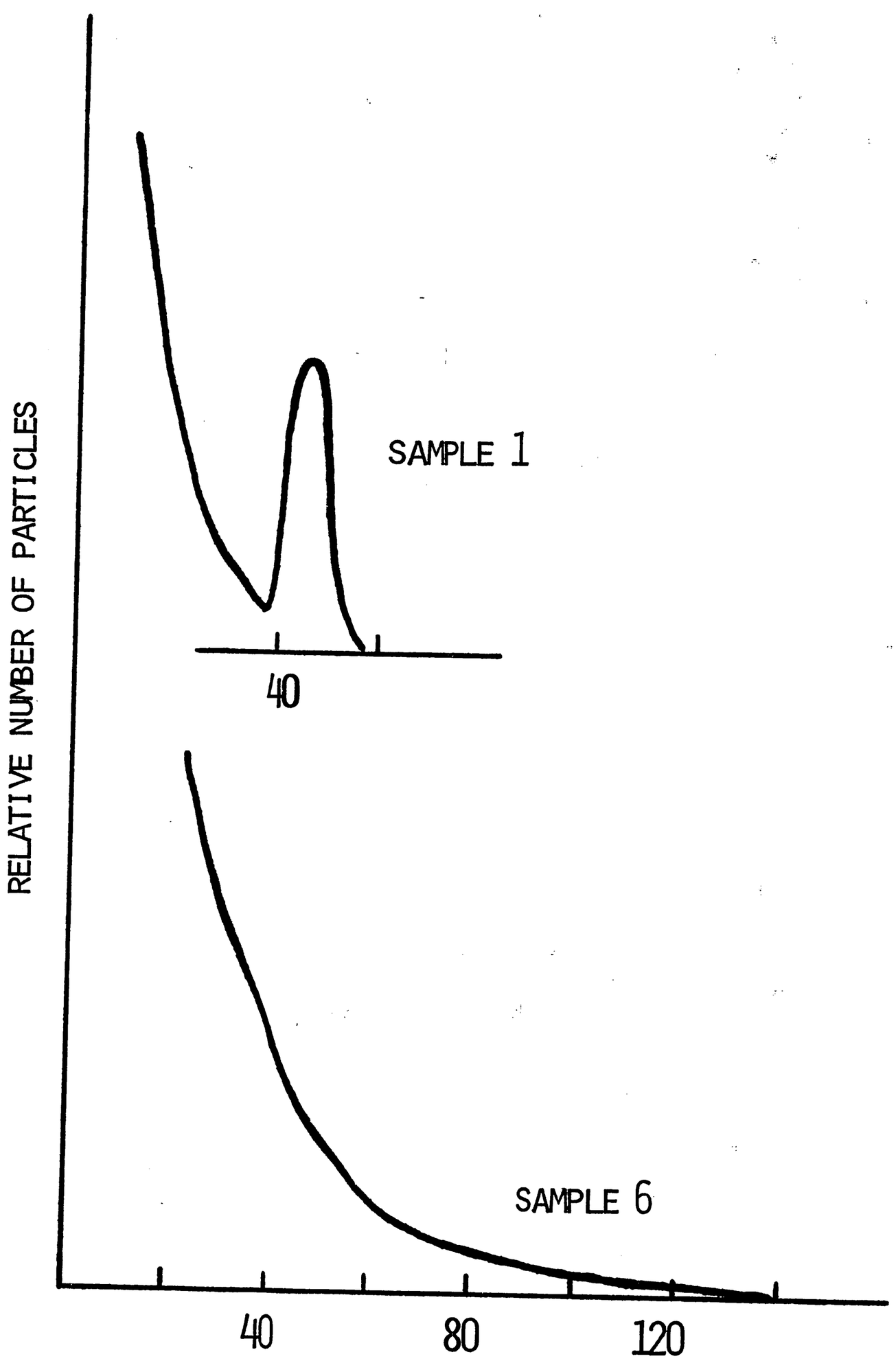

FIGURE 22 DISTRIBUTION OF PARTICLE DIAMETERS FOR STANNOUS-STANNIC HYDROSOLS

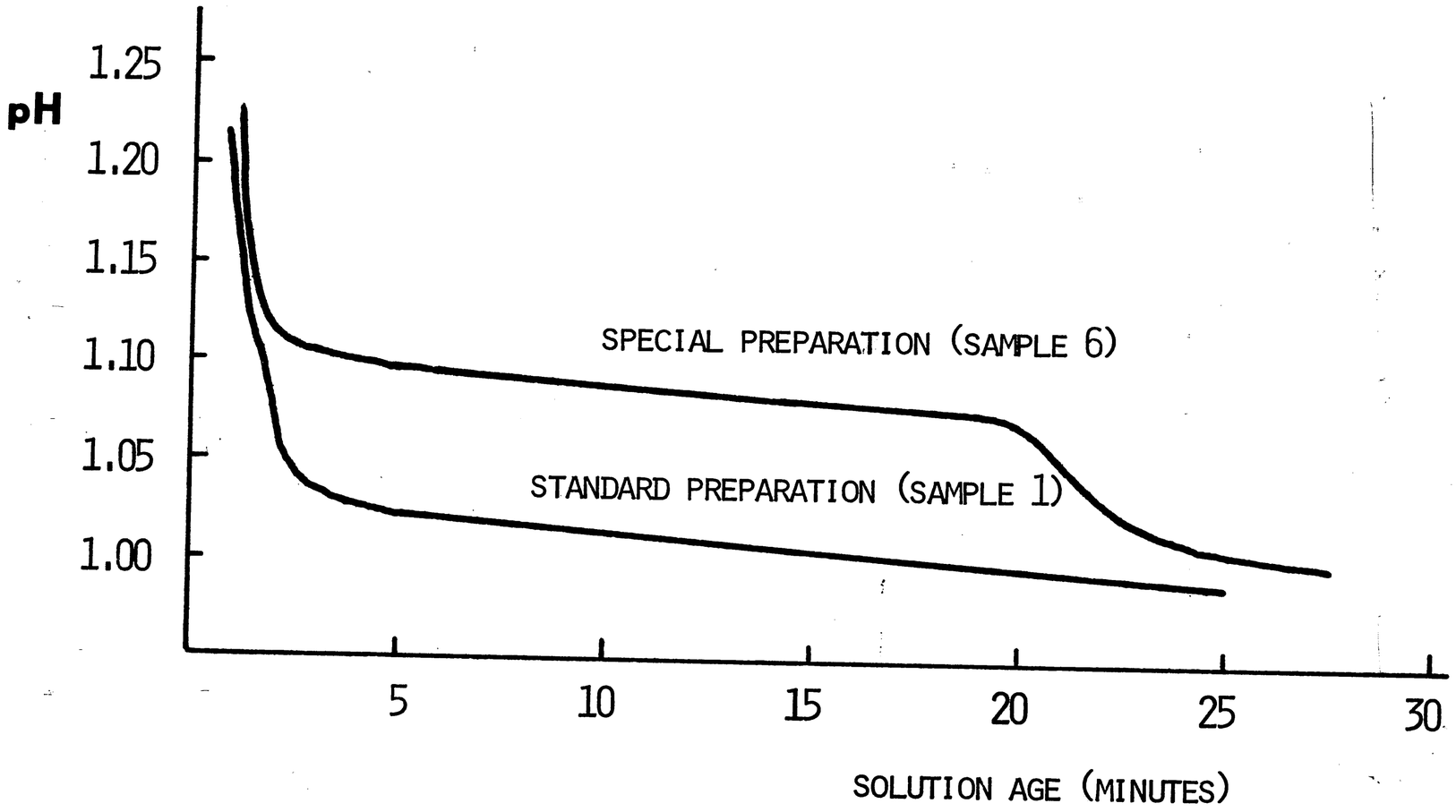

FIGURE 23 A PLOT OF pH VS SOLUTION AGE SHOWING THE DIFFERENCE BETWEEN THE STANDARD AND SPECIAL FORMULATIONS OF STANNOUS-STANNIC HYDROSOL

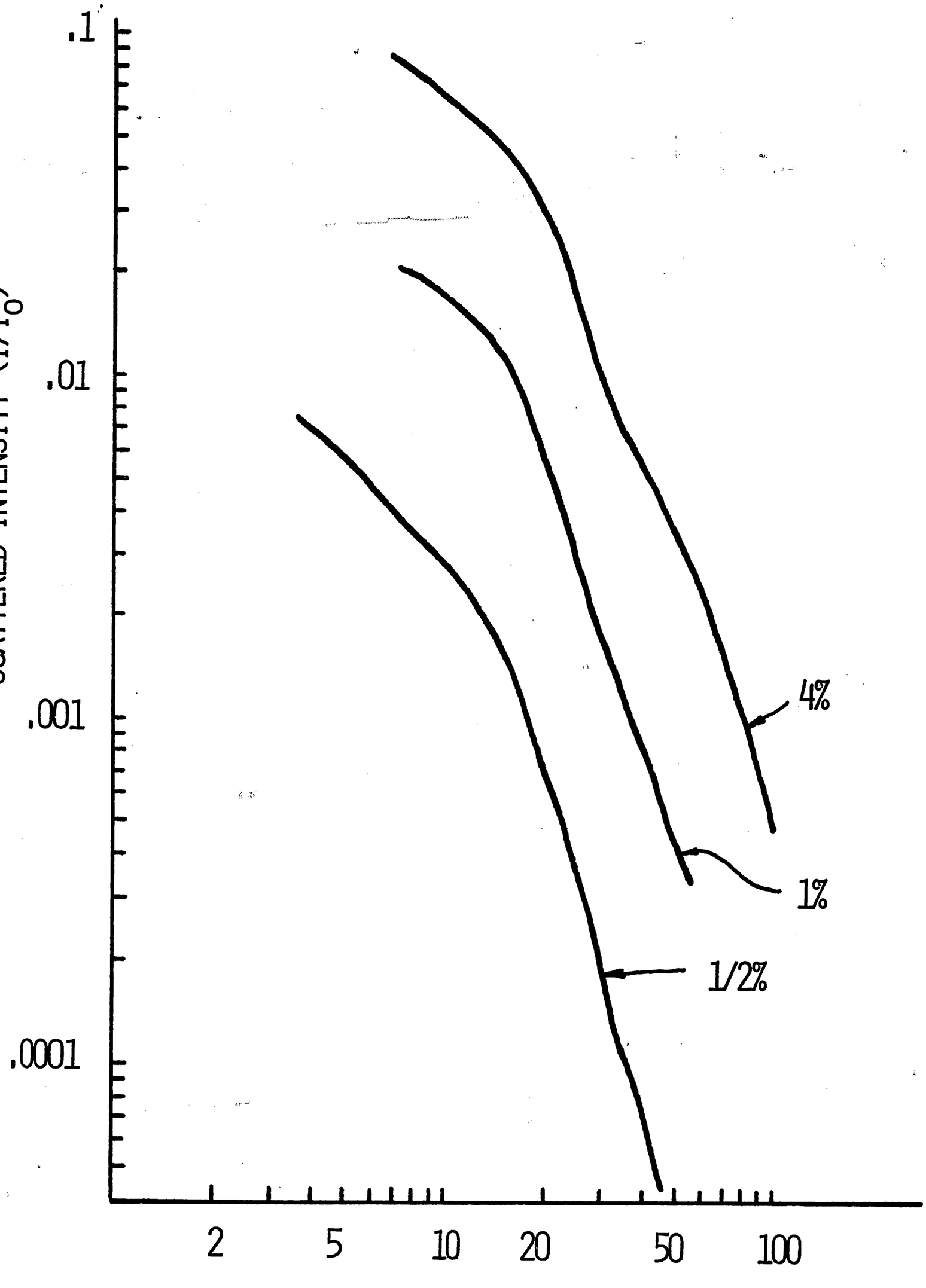

FIGURE 24 PLOT OF SCATTERED INTENSITY AS A FUNCTION OF ANGLE FOR CERIUM HYDROSOLS

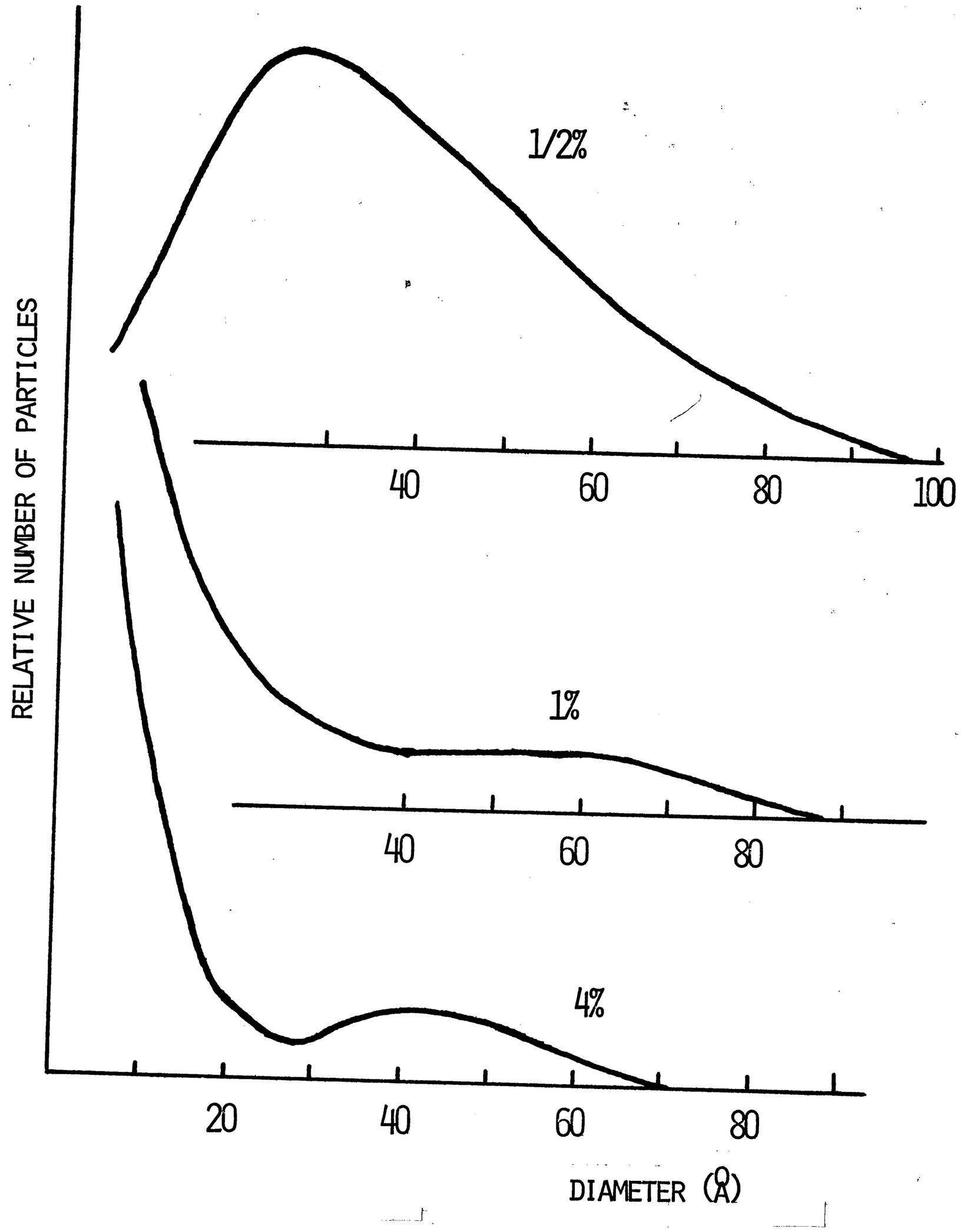

FIGURE 25 DISTRIBUTION OF PARTICLE DIAMETERS FOR CERIUM HYDROSOLS

APPENDIX I

TECHNIQUES FOR DETERMINING PARTICLE SIZE DISTRIBUTIONS BY SMALL ANGLE X-RAY SCATTERING

This appendix presents the development of the various techniques used to determine size distributions from measurements of small angle x-ray scattering curves. The various techniques will be described and a comparison of the various techniques made. On the basis of the comparison, the most applicable technique will be selected.

Techniques

1. Integral Transform Method [11-14]

This technique involves rather extensive mathematical manipulation of the expressions for scattered intensity. The details of the manipulations are discussed in depth by Brill,[14] but will be briefly reviewed here.

The expression for scattered intensity (equation 5) for a monodispersed system may be extended to a polydispersed system by redefining the particle characteristic function to reflect the polydispersity.

$$\gamma(r) = \int_0^\infty a^3 \rho(a)\, \gamma_o(r/a)\, da \Big/ \int_0^\infty a^3 \rho(a)\, da \qquad (14)$$

In the above, $\gamma(r)$ is the system characteristic function, $\gamma_o(r/a)$ is the single particle characteristic function,

and $\rho(a)$ is the distribution of diameters. This expression is inserted into equation (5) to reflect the polydispersity. The form of equation (5) lends itself to a fourier sine transform. The results of such a transform yield another expression for $\gamma(r)$.

$$\gamma(r) = \frac{1}{2\pi^3 \bar{\rho}^2 V} \int_0^\infty h^2 I(h) \frac{\sin hr}{hr} dh \qquad (15)$$

By differentiating equation (14) twice, and with some manipulation, the size distribution may be expressed in terms of the characteristic function as:

$$\rho(a) = - \frac{2\bar{V}}{\pi} \frac{d}{dr} \left(\frac{\gamma''(r)}{r}\right) \qquad (16)$$

By substitution of equation (15) into equation (16) an expression is yielded in which $\rho(a)$ is expressed in terms of intensity parameters.

$$\rho(r) = \frac{1}{\pi^3 \bar{\rho}^2 \gamma} \int_0^\infty (h^4 I(h) - A) \alpha(hr) dh \qquad (17)$$

In the above, A represents $\lim_{h \to \infty} h^4 I(h)$, or the constant of proportionality in the high angle asymptotic region, and $\alpha(x)$ is given as:

$$\alpha(x) = (1 - 8/x^2) \cos(x) + (8/x^3 - 4/x) \sin(x)$$

Brill[14] has devised numerical techniques for performing the integration of equation (17) and has incorporated

these techniques in a computer program. This program was obtained and has been adapted for use in this work.

2. Curve Matching Technique[15]

This technique involves the straightforward comparison of the experimental scattering curve with various theoretical scattering curves for different size distributions. The size distribution is taken to be the distribution for the theoretical curve which best fits the experimental curve.

In practice, several distribution shapes are used to generate the theoretical curves:

1. log normal: $\rho(r) \alpha \exp-[(\log r_o - \log r)^2/2\sigma^2]$ (18)

2. Maxwellian: $\rho(r) \alpha \frac{2r^n}{r_o^{n+1}\,\Gamma(\frac{n+1}{2})} \exp(-r_o^2/r^2)$ (19)

3. Gaussian: $\rho(r) \alpha \exp-(\frac{r-r_o}{2\sigma^2})^2$ (20)

In the above expressions, r_o is a diameter which specifies the approximate mid-range size of the distribution and the terms σ and n specify the range of sizes of the distribution.

Various families of theoretical curve which best fits One family contains the theoretical curves for distributions of each of the shapes, but whose range and mean values are approximately the same. This family of

curves will allow selection of the distribution shape to be used. Each other family contains curves for one of the distribution shapes, but for different values of n or σ.

In practice, the theoretical curves are plotted as log I-log($h^2 r_o^2$). When the experimental curve, plotted as log I-log(h^2), has been fit to one of the theoretical curves, a comparison of axes will yield r_o^2. An example of the form of the theoretical curves is presented in Figure 26. Also shown (Figure 27) are the distributions represented in Figure 26.

3. Graphical manipulation of the scattering curve to yield distribution parameters.[15]

Shull and Roess show that for a Maxwellian distribution of particle sizes, an expression for intensity may be directly integrated. The intensity scattered from a polydisperse system has been shown to be:

$$I(h) = \int_0^\infty \rho(r)\ I_r(h)\,dr \qquad (11)$$

By inserting for $\rho(r)$ the mathematical form of a Maxwellian distribution (equation (19)) and for $I_r(h)$ the low angle asymptotic approximation for intensity, $I(h) \simeq Kr^3 \exp(-h^2 r^2/3)$, equation 11 then becomes:

$$I(h) = K \frac{2}{r_o^{n+1}\ \left(\frac{n+1}{2}\right)} \int_0^\infty r^{n+3} \exp(-(1/3h^2 + r_o^{-2})r^2)\,dr \qquad (21)$$

Shull and Roess[15] show that this may be integrated directly to yield:

$$I(h) = 2K \frac{\Gamma(\frac{n+4}{2})}{\Gamma(\frac{n+1}{2})} r_o^3 \left[1/3h^2 r_o^2 + 1\right]^{-(n+4)/2} \quad (22)$$

Taking the logarithm of both sides yields:

$$\log I = \log C - \frac{n+4}{2}\left(\log h^2 + 3/r_o^2\right) \quad (23)$$

This suggests plotting the data in the form log I- $\log(h^2 + \alpha^2)$, and varying α^2 until the scattering curve lies on a straight line. The quantities n and r_o will result from the slope of the line and the magnitude of the translation, α^2, respectively. Once n and r_o have been determined, the distribution has been completely specified. An example of this technique is shown in Figure 28.

4. Graphical deconvolution of a Guinier Plot:[16]

The low angle approximation for scattered intensity, $I(h) \simeq Kr^3 \exp(-h^2 r^2/3)$, is used to determine particle sizes through a Guinier plot, a plot of $\ln(I) - h^2$. In a plot of this type, the scattering curve approaches a straight line whose slope is a measure of the particle size. This technique for determining the size distribution performs a deconvolution of the experimental curve, or a separation of the intensities due to particles

of different sizes. The deconvolution begins by constructing a tangent to the experimental curve at the point of last slope and extending the tangent to intersect the intensity axis. The slope of this tangent corresponds to the smallest particles of the system, whose size may be determined through equation (7). The effect of the smallest particles is then removed from the original curve by subtracting the intensity due to these particles. In other words, the tangent constructed is subtracted from the original curve, and the process is continued on the new curve, one which does not reflect the presence of the small particles. The process continues until only a single straight line remains whose slope corresponds to the largest particles of the solution.

The intensity scattered by n particles of radius R is given as:

$$I(h) = nCR^3 \exp(-h^2R^2/5) \qquad (24)$$

At h=0, the intensity is then given by:

$$I(o) = nCR^3 \qquad (25)$$

Thus, to evaluate the relative number of particles of each size, the intercepts of the tangents constructed are divided by the cube of the particle radii corresponding to the slope of the tangent. An example of this technique is shown in Figure 29.

Comparison of the Techniques

Each technique presented approaches the problem of determining the distribution of sizes in a different manner. It is to be expected that some techniques will be more applicable to some situations than others. It is for this reason that the techniques are to be compared by examining the results of the techniques for distributions of various shapes. The techniques are to be evaluated qualitatively by visual comparison of the distributions derived from various theoretical curves with the actual distribution of the theoretical curve. In this comparison, five theoretical intensity curves are to be analyzed, each corresponding to a differently shaped distribution of particle sizes. The distributions considered are shown in Figures 30 through 34. Each of the techniques was used to analyze each of the curves. The analysis is not presented here since it is not of primary interest, but the results of the techniques are shown in Figures 35 through 39.

Discussion of Results

The observations made in qualitatively examining the results are enumerated.

1. Technique 1 is by far the most accurate technique, and the easiest to apply (it is performed by computer). Unfortunately, the data must extend well into the asymptotic region in order to apply this technique. If

the data do not extend into the asymptotic region, this technique should not be used.

2. Technique 2 is very easily applied and yields consistent results. One severe limitation, though, is the inflexibility of the technique. The distribution derived must be present in one of the families of curves. If this is not the case, as happened in the rectangular distribution, no fit may be made.

3. Technique 3 has the advantage of being insensitive to random fluctuations in data. The technique forces data to fit a straight line and essentially causes a smoothing process. The results are reasonably accurate, except for the rectangular distribution, and the technique is easy to apply.

4. Technique 4 provides few data points. For many of the curves, very few points were obtained, and those that were corresponded to the smallest and largest dimensions of the distribution. This technique might be useful, then, if only the range of sizes present is desired.

Conclusions

On the basis of the observations presented, the technique of integral transforms is selected to determine the size distributions from experimental data. However, if data is not accessible in the asymptotic region, the graph-

ical technique 3 will be used since the results are seemingly accurate. If the graphical technique is used, the distribution of sizes derived will be considered to be qualitatively valid only.

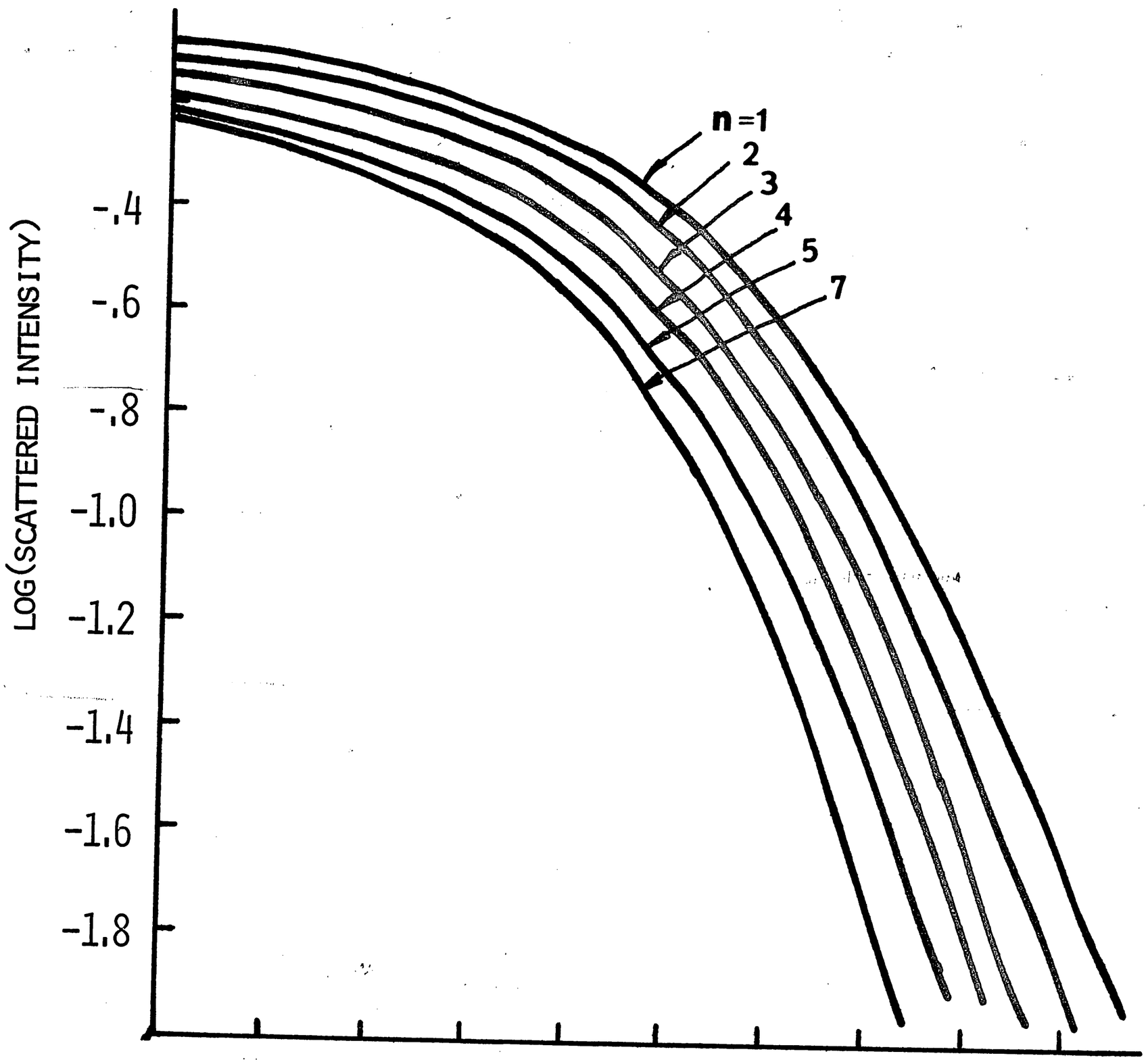

FIGURE 26 A FAMILY OF THEORETICAL SCATTERING CURVES FOR MAXWELLIAN DISTRIBUTIONS OF PARTICLE DIAMETERS OF VARIOUS SHAPES

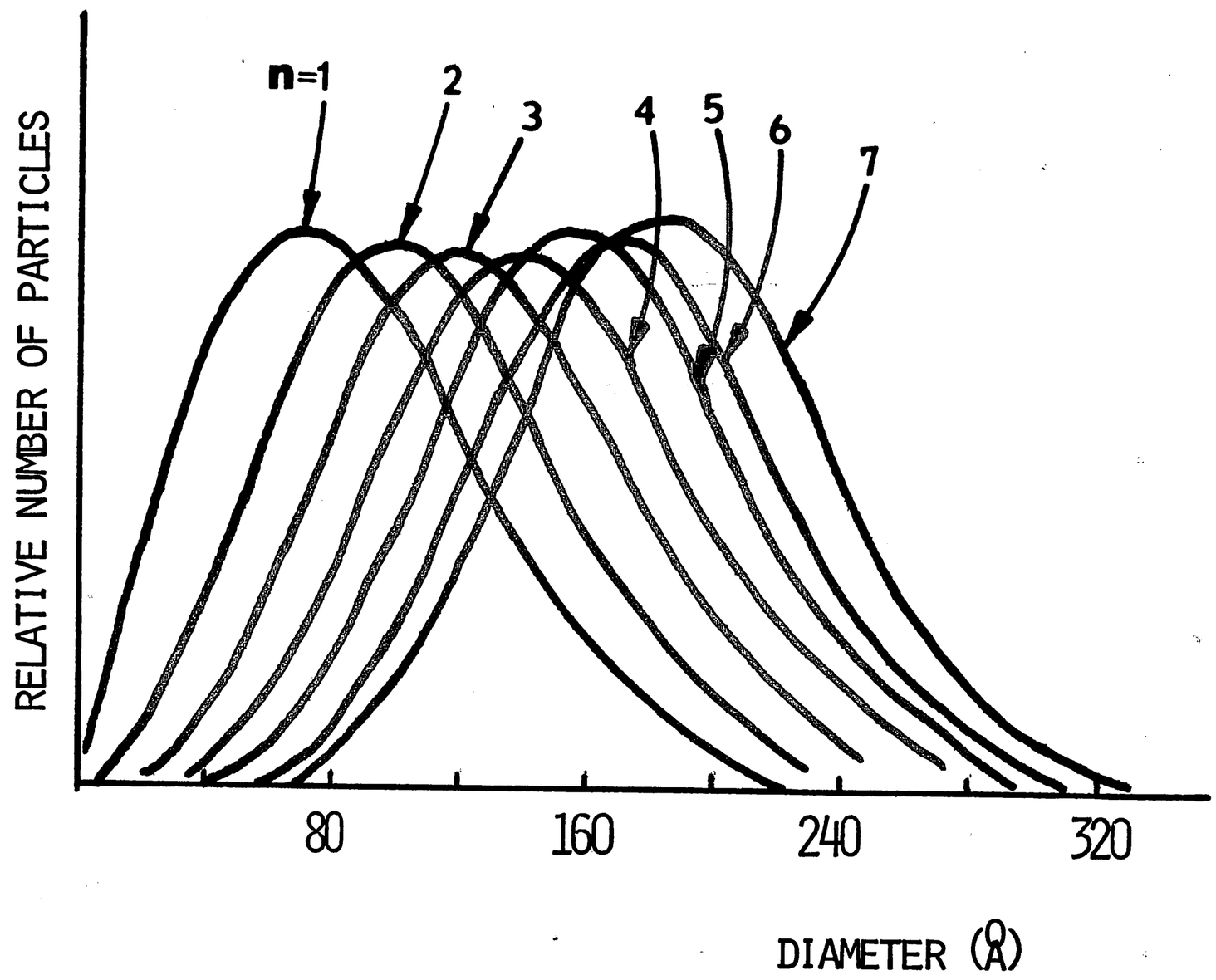

FIGURE 27 THE FAMILY OF MAXWELLIAN DISTRIBUTIONS REPRESENTED IN THE THEORETICAL SCATTERING CURVES OF FIGURE 26

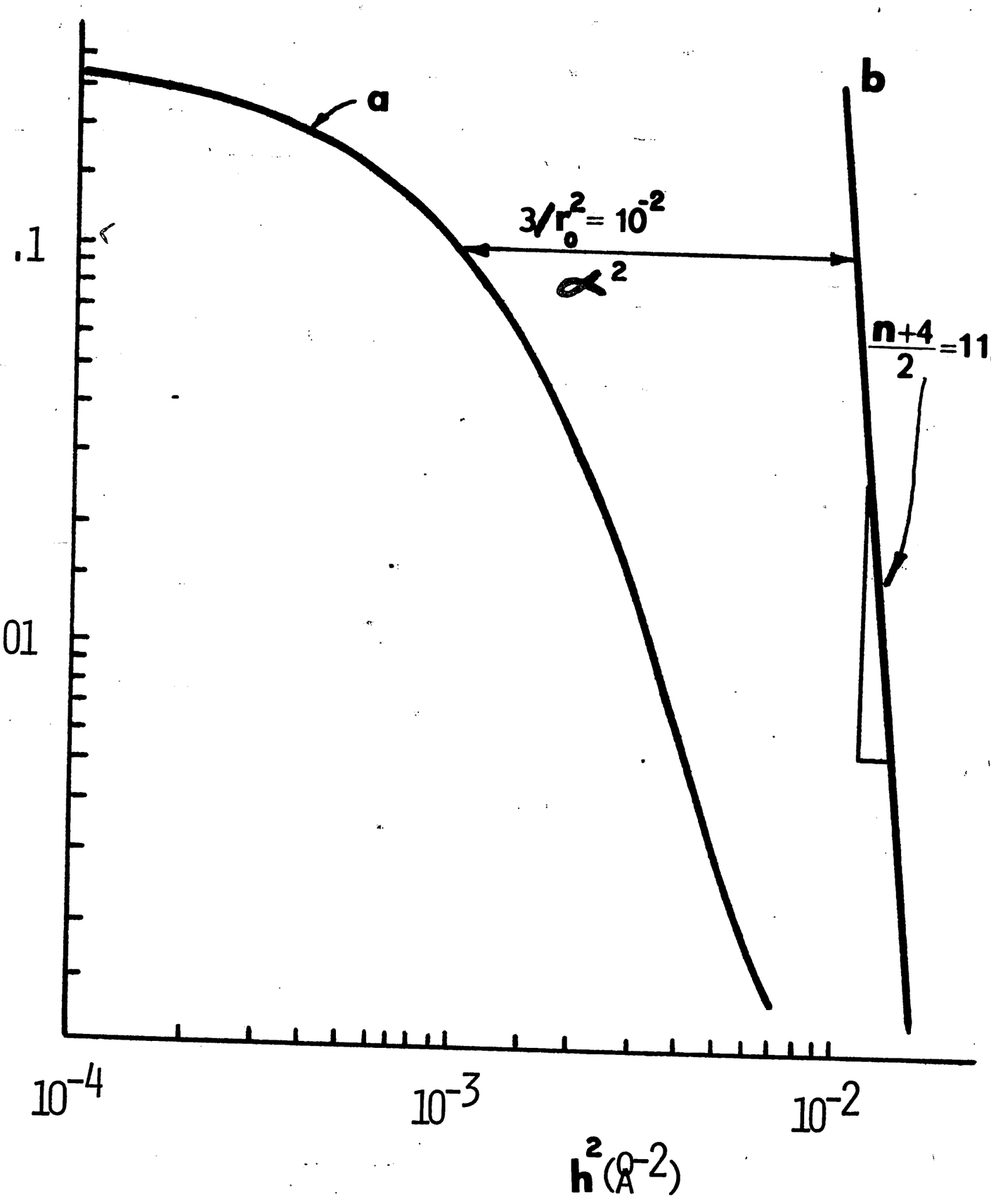

FIGURE 28 AN EXAMPLE OF TECHNIQUE 3 FOR DETERMINING THE DISTRIBUTION OF DIAMETERS. A TRANSLATION FACTOR, α^2, IS SOUGHT FOR WHICH THE MEASURED CURVE (a) BECOMES A STRAIGHT LINE (b). THE SLOPE OF THE STRAIGHT LINE DEPENDS ON n AND α^2 ON r_0^2.

ILLUSTRATION OF GRAPHICAL DECONVOLUTION OF GUINIER PLOT

STEP	r^2	d	k INTERCEPT	k/d^3
1	900	60	0.6	44.5
2	3120	112	53	37.8
3	7700	174	500	106
4	14,500	240	1300	94

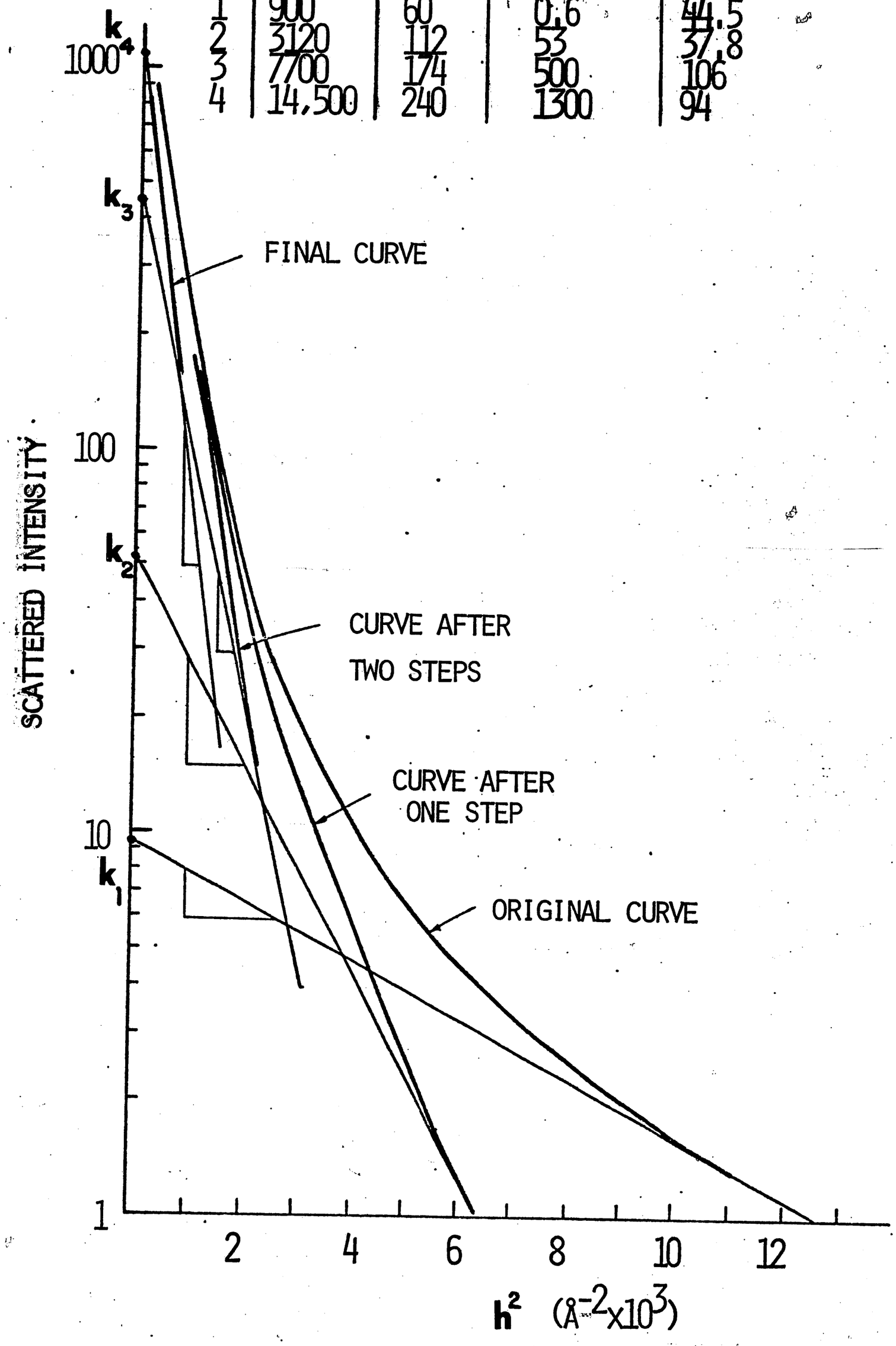

FIGURE 29 AN ILLUSTRATION OF TECHNIQUE 4 FOR DETERMINING THE PARTICLE SIZE DISTRIBUTION

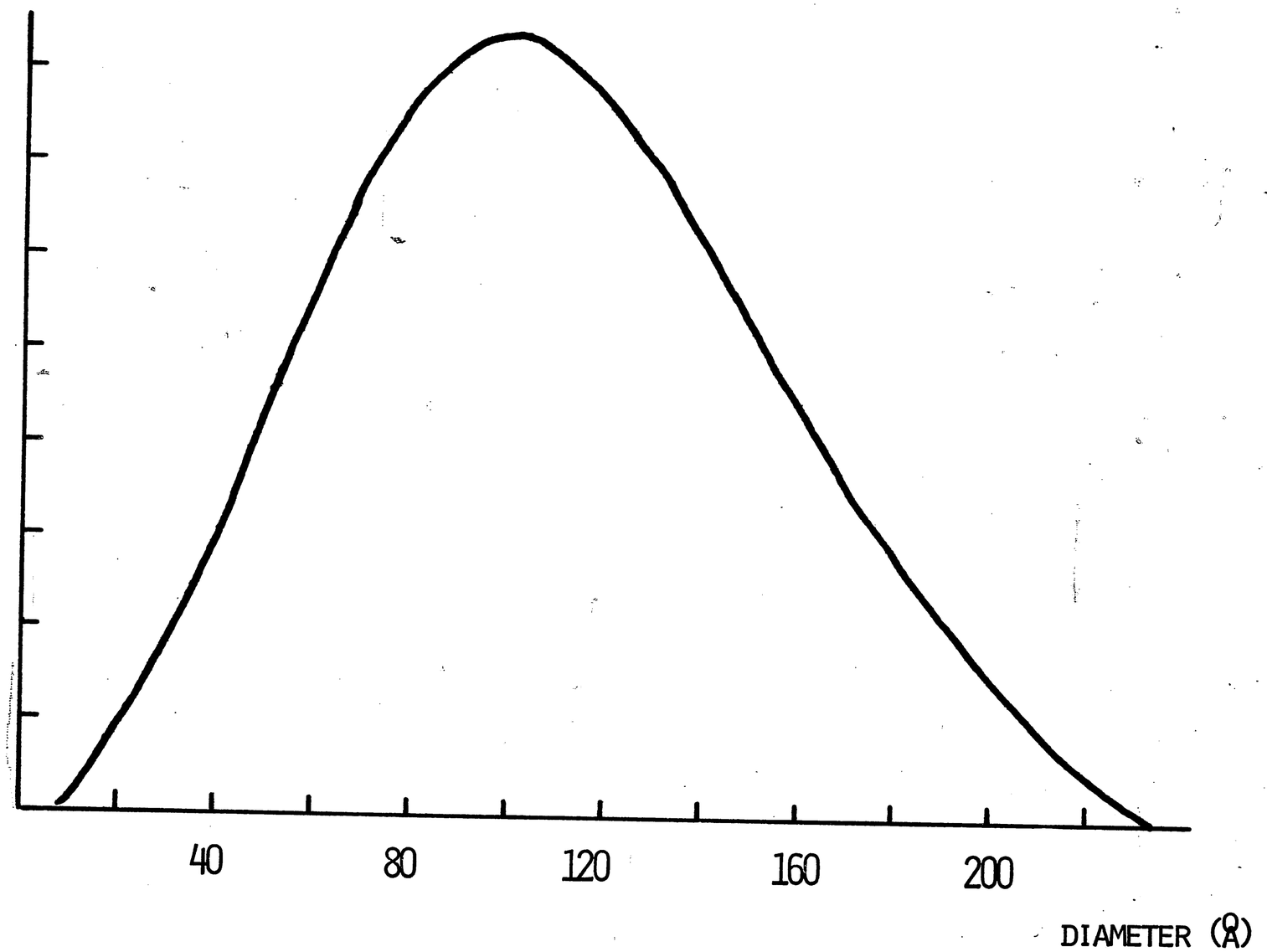

FIGURE 30 MAXWELLIAN DISTRIBUTION USED TO TEST THE VARIOUS TECHNIQUES FOR DETERMINING SIZE DISTRIBUTIONS

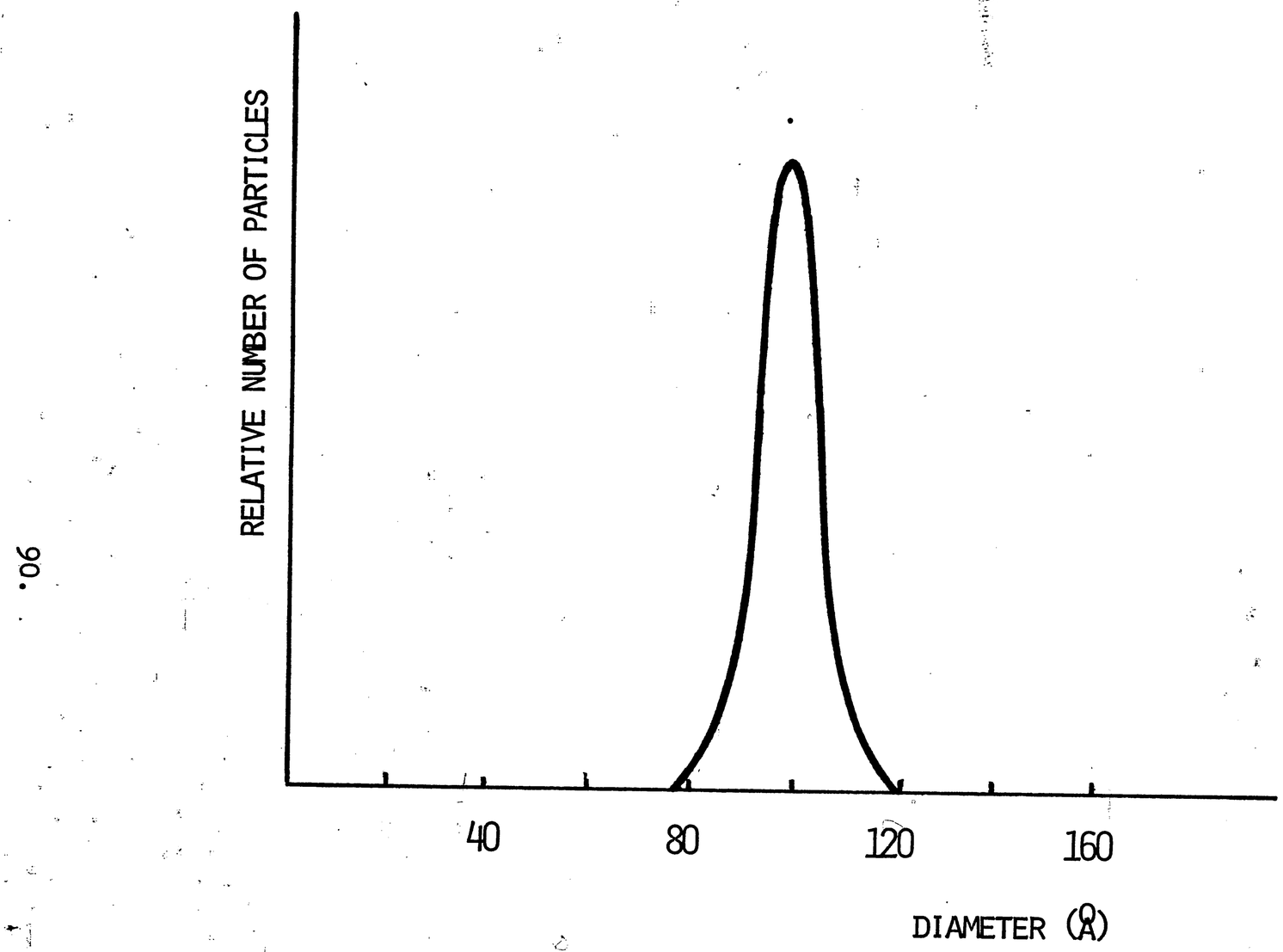

FIGURE 31 LOGNORMAL DISTRIBUTION USED TO TEST THE VARIOUS TECHNIQUES FOR DETERMINING SIZE DISTRIBUTIONS

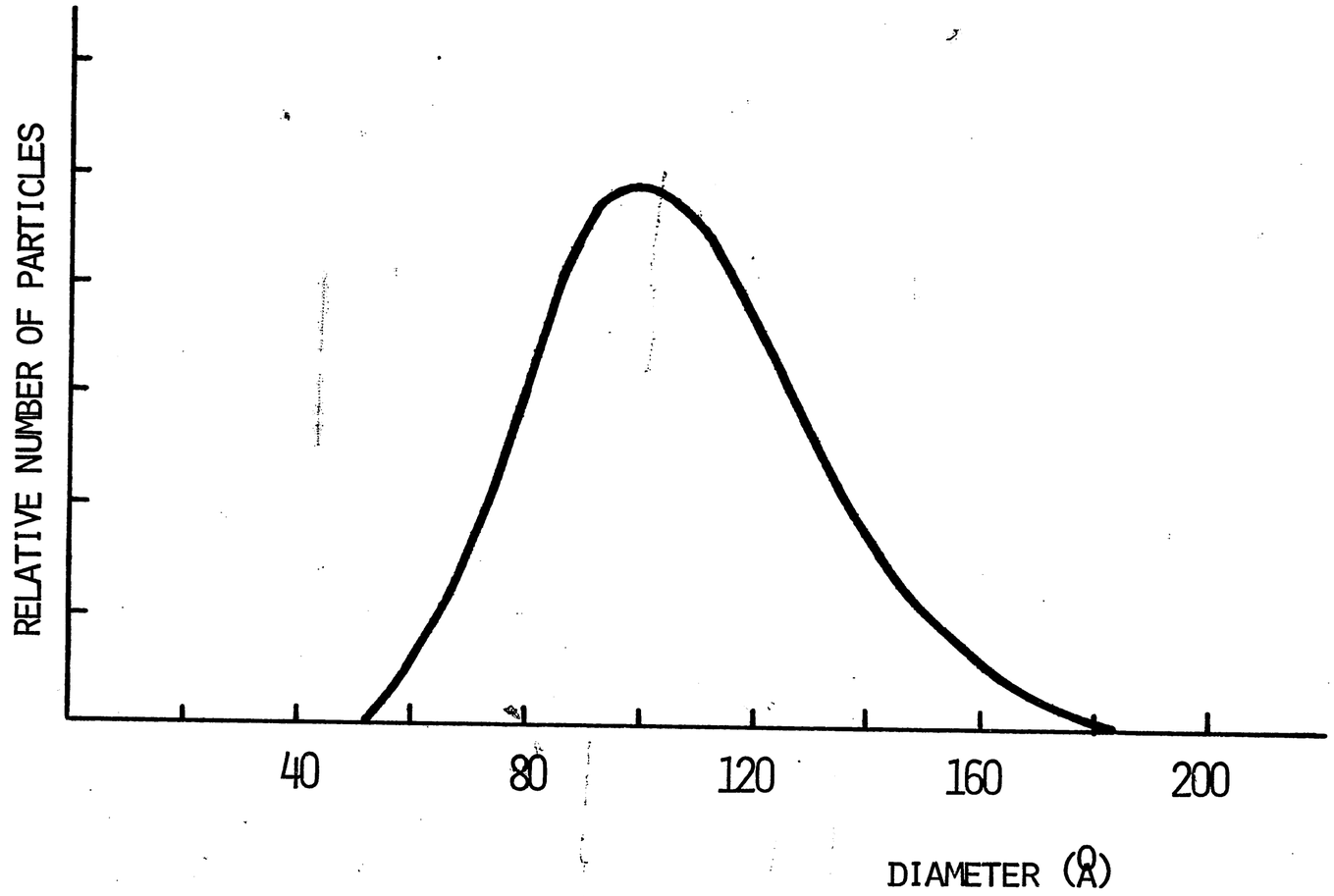

FIGURE 32 LOGNORMAL DISTRIBUTION USED TO TEST THE VARIOUS TECHNIQUES FOR DETERMINING SIZE DISTRIBUTIONS

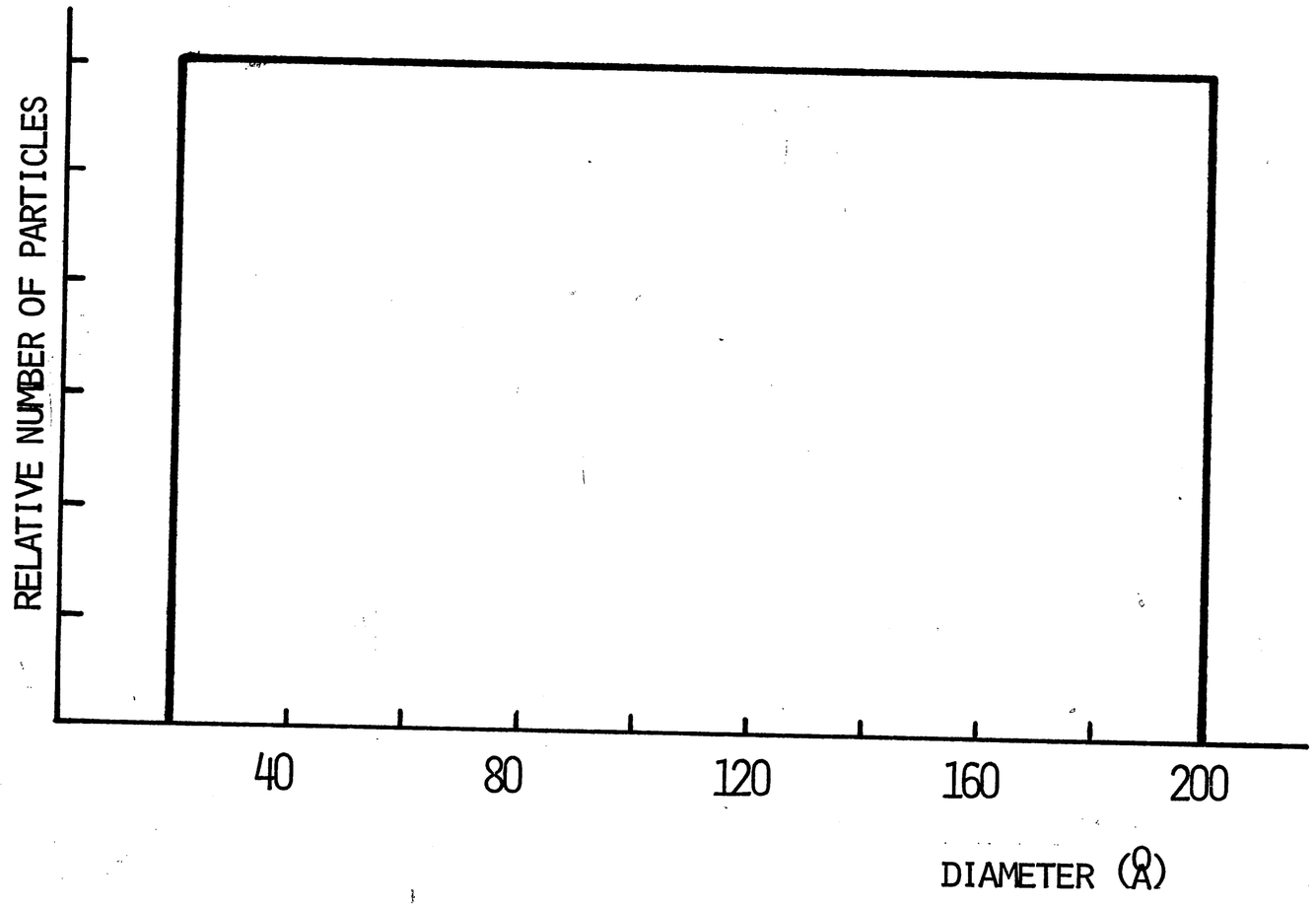

FIGURE 33 RECTANGULAR DISTRIBUTION USED TO TEST THE VARIOUS TECHNIQUES FOR DETERMINING SIZE DISTRIBUTIONS

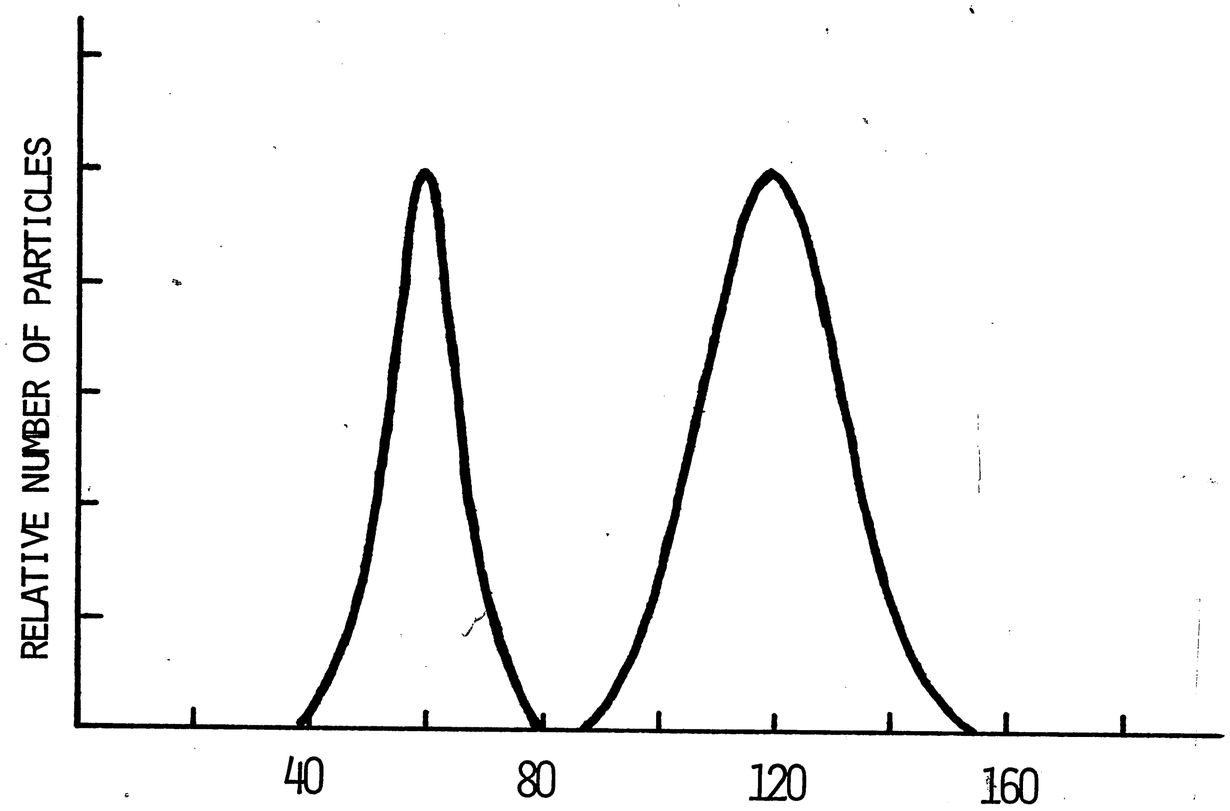

FIGURE 34 BIMODAL DISTRIBUTION USED TO TEST THE VARIOUS TECHNIQUES FOR DETERMINING SIZE DISTRIBUTIONS

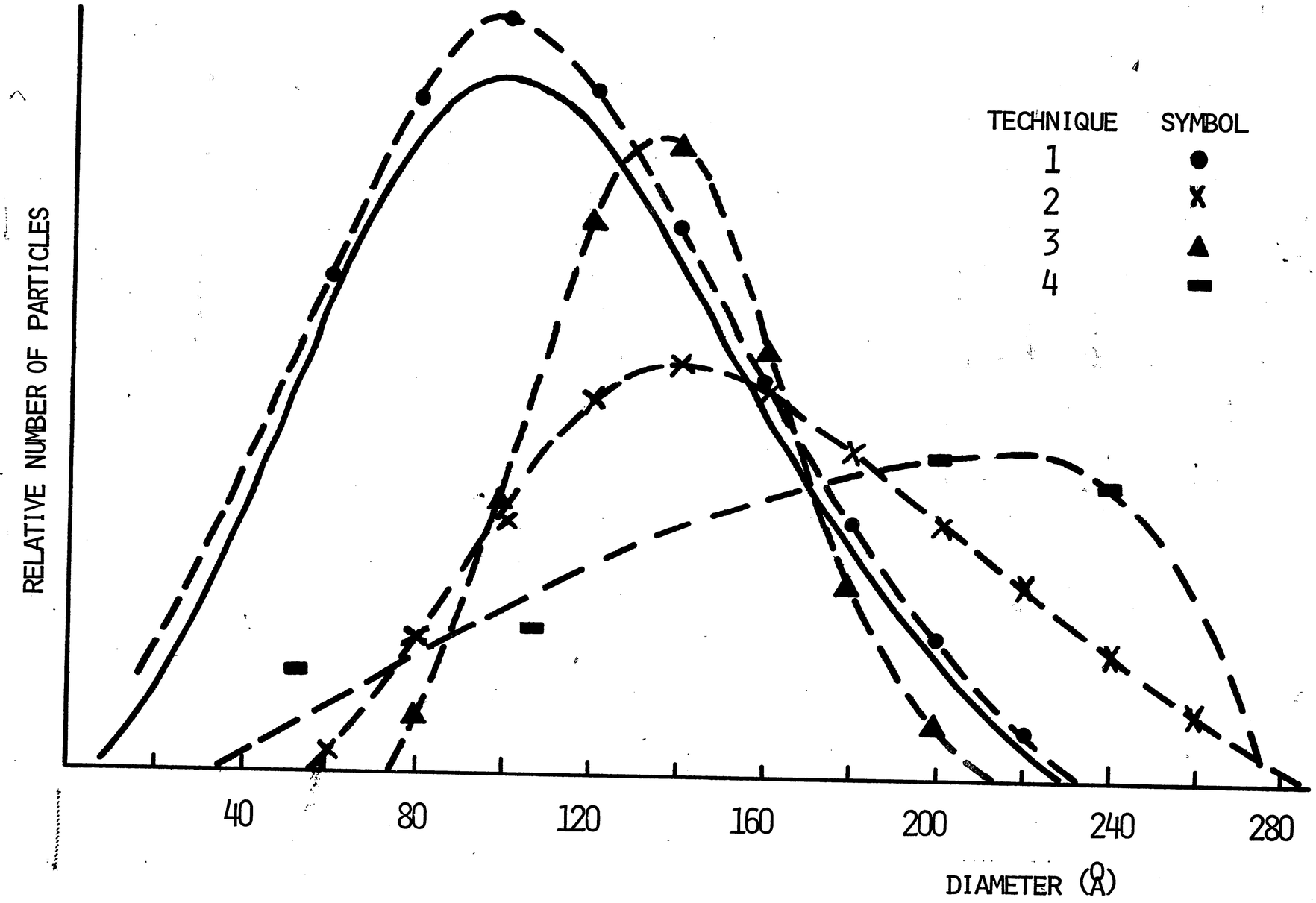

FIGURE 35 DIAMETER DISTRIBUTIONS DEDUCED BY APPLICATION OF THE VARIOUS TECHNIQUES

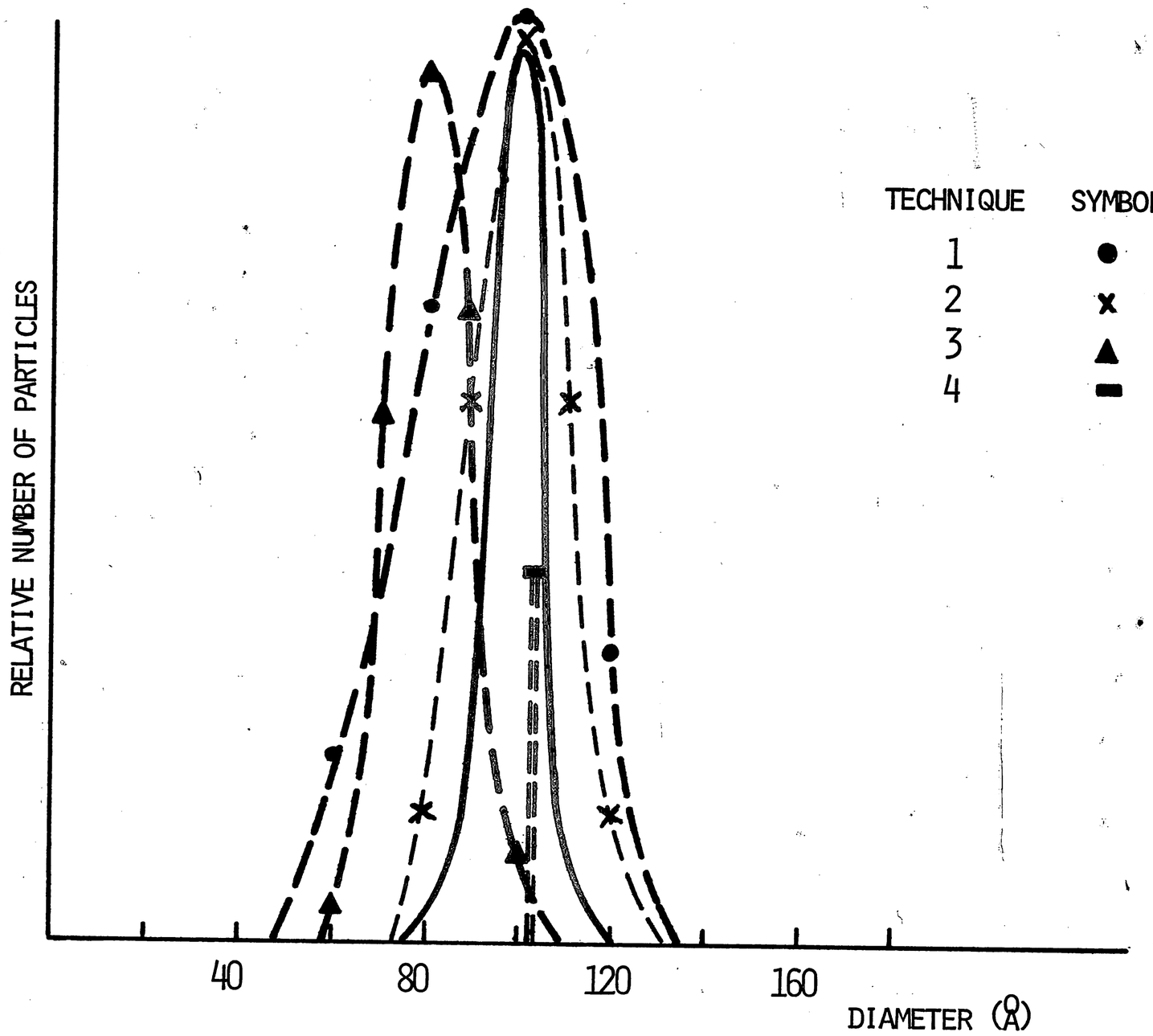

FIGURE 36 DIAMETER DISTRIBUTIONS DEDUCED BY APPLICATION OF THE VARIOUS TECHNIQUES

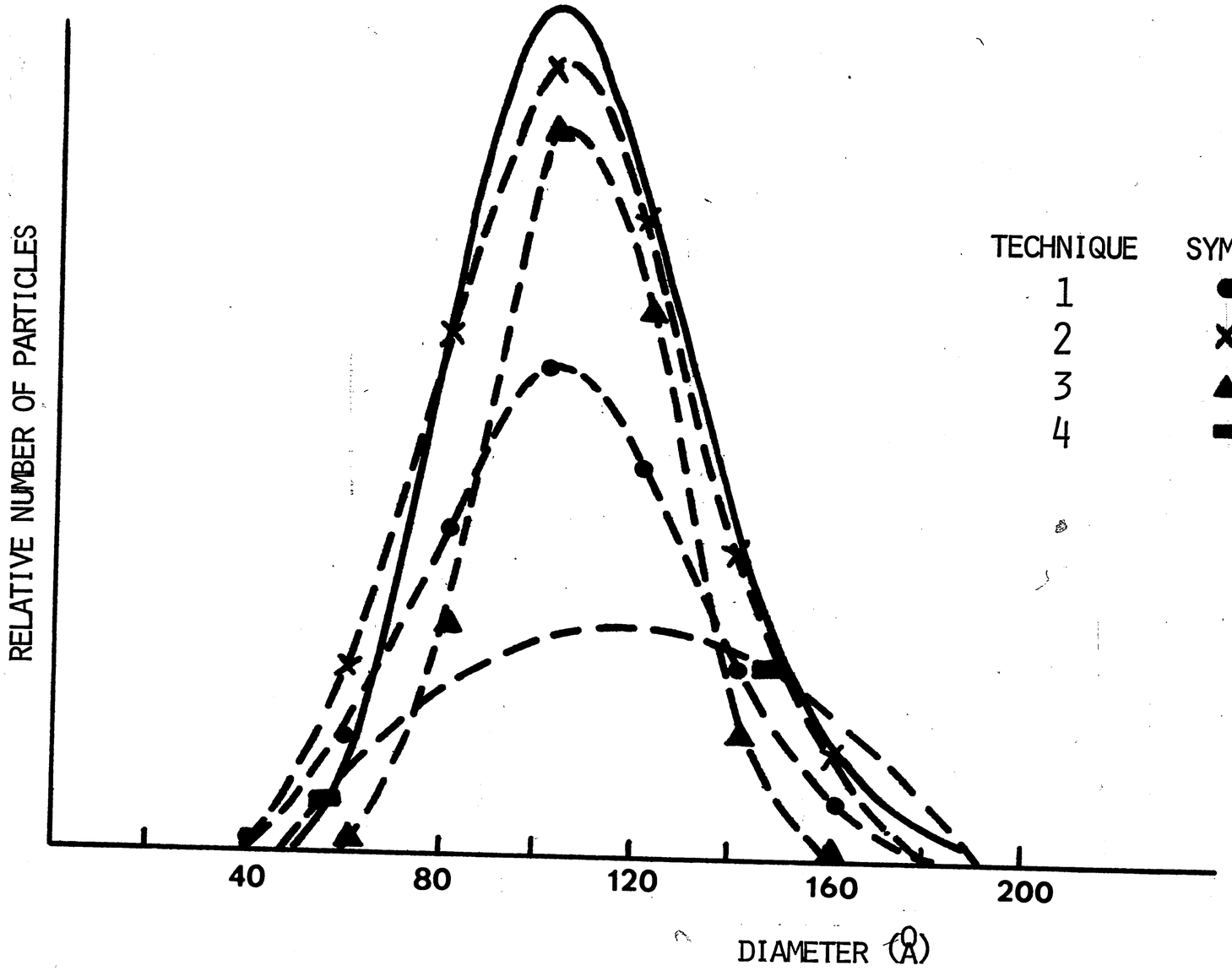

FIGURE 37 DIAMETER DISTRIBUTIONS DEDUCED BY APPLICATION OF THE VARIOUS TECHNIQUES

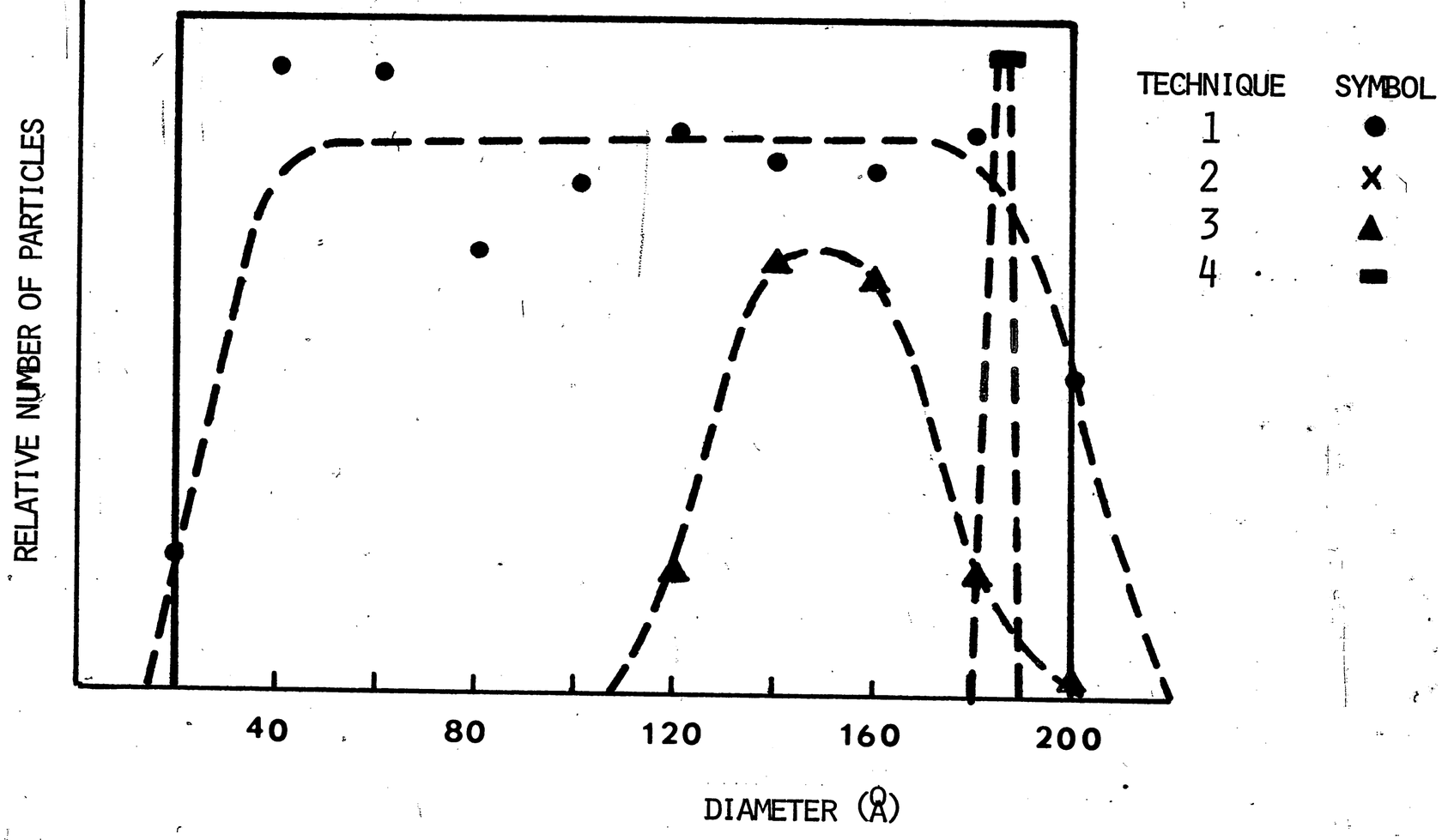

FIGURE 38 DIAMETER DISTRIBUTIONS DEDUCED BY APPLICATION OF THE VARIOUS TECHNIQUES

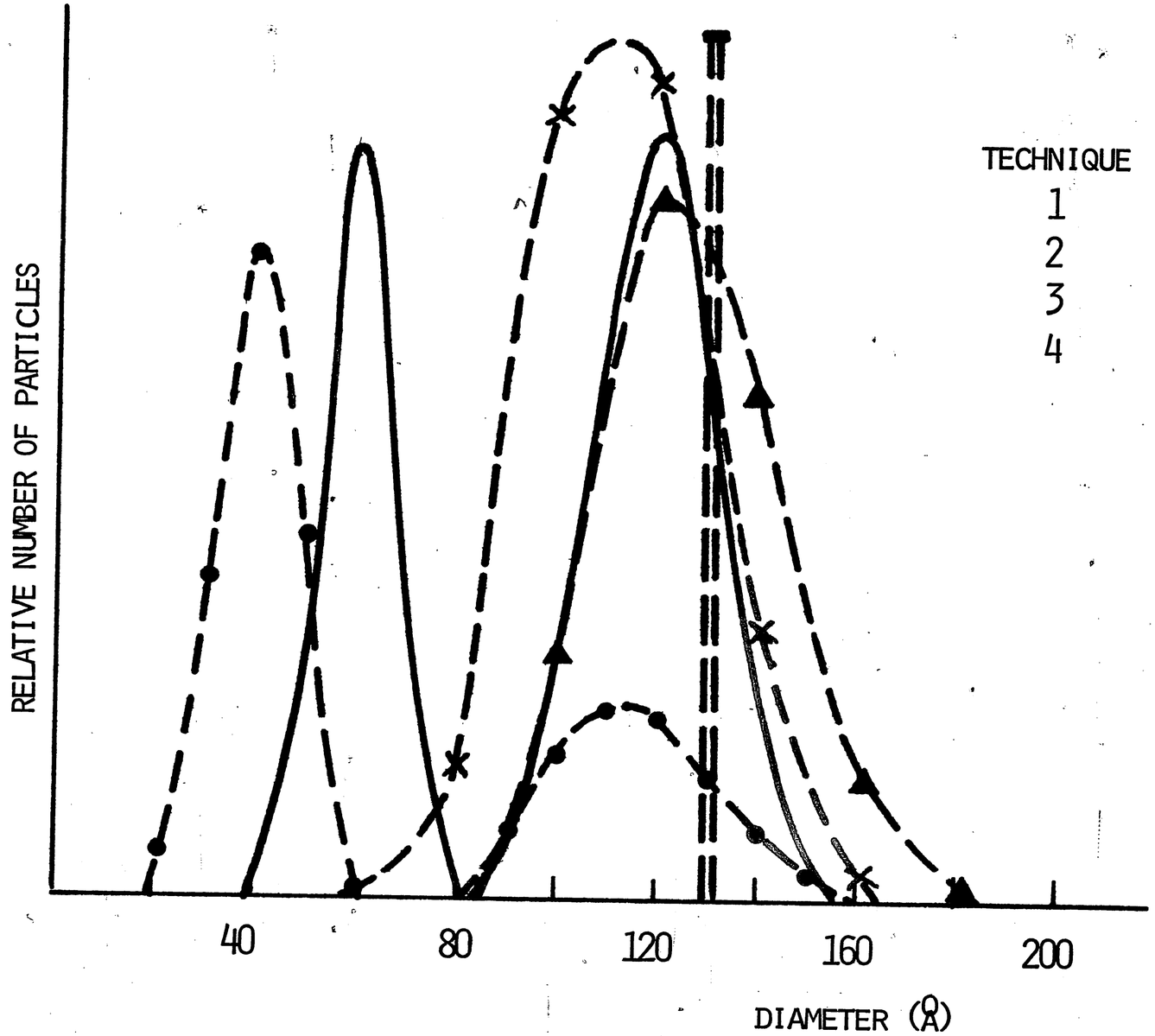

FIGURE 39 DIAMETER DISTRIBUTIONS DEDUCED BY APPLICATION OF THE VARIOUS TECHNIQUES

APPENDIX II

COLLIMATION SMEARING EFFECTS

In order to desmear, or correct an experimental curve for the effects of the collimation averaging effect, it is necessary to know the exact nature of the averaging process. Figure 40 is useful in describing the nature of this averaging. The scattered intensity which is registered at the nominal angle of the experiment, θ, is given as the six fold integral over the horizontal and vertical dimensions of the three reference planes of the scattering at angle ε.[32] The angle ε is determined by the coordinates in the three reference planes and will determine the range over which the averaging process occurs. Figure 41 shows vertical and horizontal cross sections of the schematic of Figure 40, and defines the geometric dependence of ε on the dimensions of the reference planes.

Hendricks and Schmidt[32] have shown that the six fold integration may be simplified to a double integral, one over the vertical dimensions, the other over the horizontal dimensions of the beam, with introduction of two functions known as weighting functions. The weighting functions essentially contain the results of the integrations over the first two reference planes of the schematic, and are of only qualitative interest here. In terms of the weighting functions, $W_l(\xi)$ and $W_w(\phi)$ ($W_w(\phi)$ is the weighting function

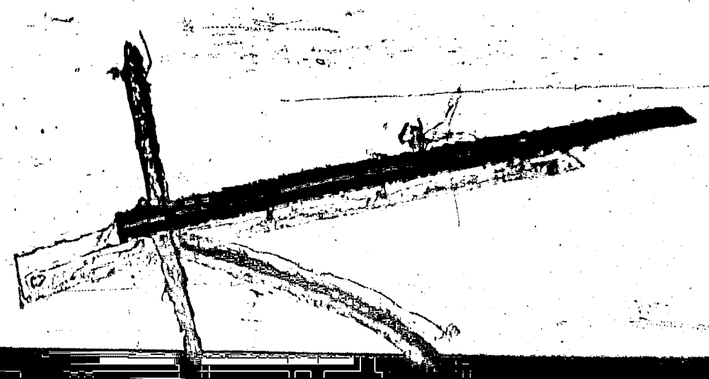

across the width of the beam, ϕ is the deviation from the nominal angle in the vertical sense, $W_1(\xi)$ is the weighting function across the length of the beam, and ξ is the angular deviation from nominal in the horizontal sense), the intensity actually recorded at θ is given by:

$$\tilde{I}(\theta) = \int_a^b W_w(\phi)\,d\phi \int_c^d I\left(\sqrt{(\theta+\phi)^2 + \xi^2}\right) W_1(\xi)\,d\xi \qquad (26)$$

Fortunately, the geometry of the Kratky camera makes certain simplification valid. If one dimension of the beam is very short with respect to the displacement of the goniometer screw, then the effects of the integral over the dimension is negligible.[9] That is the case in the Kratky camera, since the width of the beam ($\simeq$ 100 microns) is much less than the goniometer screw displacement ($\simeq$ 10 mm). Equation 26 then reduces to:

$$\tilde{I}(\theta) = \int_a^b I\left(\sqrt{\theta^2 + \xi^2}\right) W_1(\xi)\,d\xi \qquad (27)$$

A further simplification results if the remaining beam dimension is larger than the maximum angle of the experiment, and if the intensity is uniform over this dimension. Both of these requirements are satisfied for the Kratky camera, if properly aligned, so that equation (27) reduces to:[9]

$$\tilde{I}(\theta) = \int_0^\infty I\left(\sqrt{\theta^2 + \xi^2}\right) d\xi \qquad (28)$$

The weighting function, $W_1(\xi)$, drops out due to the uniformity of the beam intensity. The above conditions satisfy what is known as the infinite slit height approximation. Expression 28 may be manipulated to yield a direct expression for the true scattered intensity.[33]

$$I(\theta) = -C \int_0^\infty \frac{\tilde{I}'(t)}{(t^2-\theta^2)^{1/2}}\, dt \qquad (29)$$

Schmidt and various coworkers[34,35] have devised techniques for evaluating equation (29). Of primary concern is the increased random error associated with differentiating the experimental data. Schmidt performs the differentiation by fitting successive polynomials to the data in groups, and by differentiating these functions.

This technique has been tested under various circumstances,[36] and seems to yield consistently accurate results, and has been incorporated in a computer program written by Schmidt[35] but adapted for use here. All experimental curves will be desmeared using this computer program.

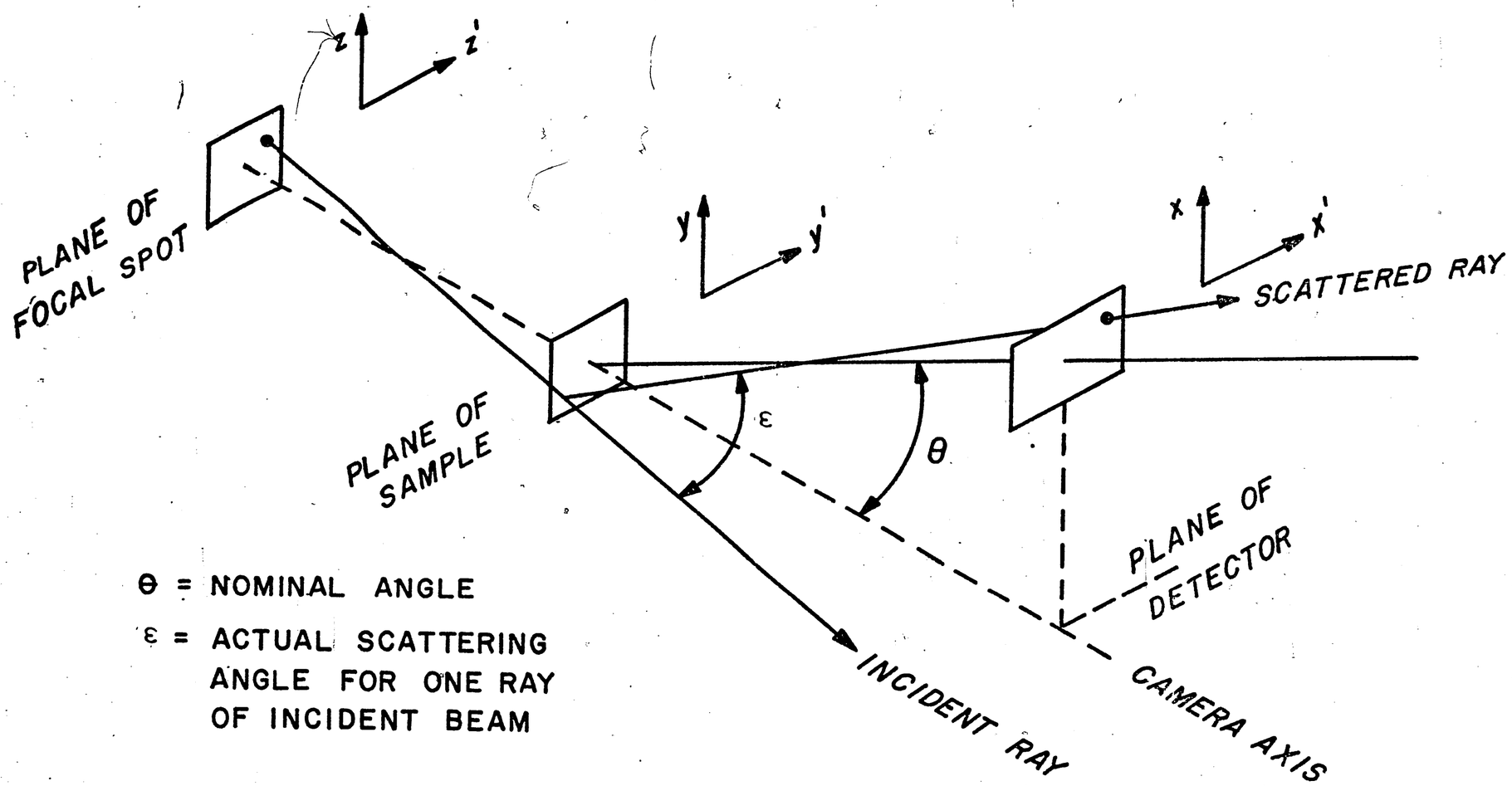

θ = NOMINAL ANGLE

ε = ACTUAL SCATTERING ANGLE FOR ONE RAY OF INCIDENT BEAM

FIGURE 40 SCHEMATIC OF ORIGIN OF COLLIMATION SMEARING. DUE TO FINITE DIMENSIONS OF SYSTEM, SCATTERING OCCURS IN AN ANGULAR RANGE OF θ.

TOP VIEW OF CAMERA

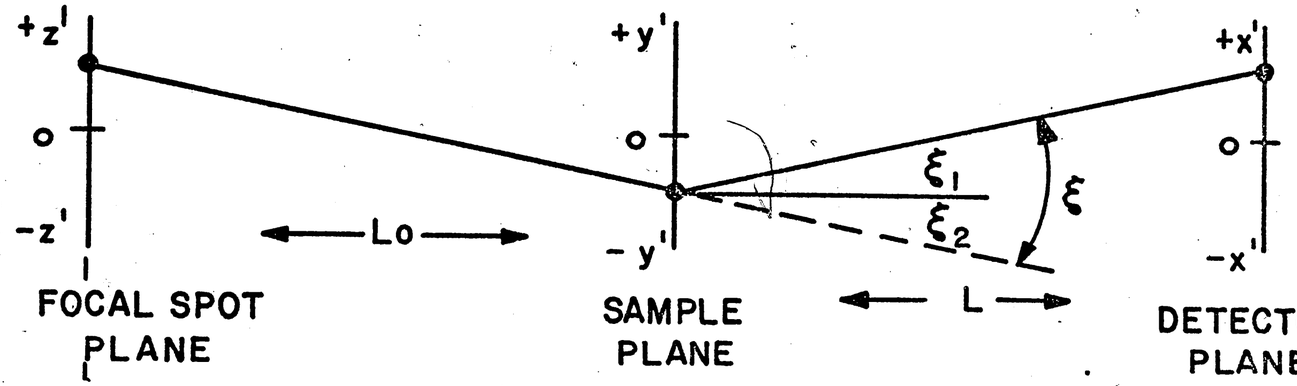

$\xi_1 = \frac{(x' - y')}{L}$

$\xi = \frac{z' - y'}{Lo}$

$\xi = \xi_1 + \xi_2$

$\phi_1 = (x - y)/L$

$\phi_2 = (z - y)/Lo$

$\phi = \phi_1 + \phi_2$

SIDE VIEW OF CAMERA ($\theta = 0°$)

SCATTERING ANGLE = $\epsilon = \sqrt{(\theta + \phi)^2 + \xi^2}$

FIGURE 41 SCHEMATIC OF ORIGIN OF COLLIMATION SMEARING. THE DEVIATIONS IN NOMINAL ANGLE, θ, DEPEND ON DIMENSIONS OF BEAM.

BIBLIOGRAPHY

1. Sharp, D. J., Plating, 58, 786, (1971).

2. D'Amico, J. F., et al, J. Electrochem. Soc., 118, 1695, (1971).

3. Sharp, D. J., Plating, 116, 143C, (1969).

4. Sharp, D. J., Plating, 116, 295C, (1969).

5. Sard, Plating, 117, 864, (1970).

6. Cohen, R. and West, K., J. Electrochem. Soc., 119, 433, (1972).

7. Orr, C., and Dalla Valle, J., Fine Particle Measurement, The MacMillan Company, N. Y., (1959).

8. Irani, R., and Callis, C., Particle Size Measurement, Interpretation and Application, John Wiley and Sons, N. Y., (1963).

9. Guinier, A., et al, Small Angle Scattering of X-Rays, John Wiley and Sons, N. Y., 1955.

10. Brill, O. L., Weil, C. G., and Schmidt, P. W., J. Colloid Int. Sci., 27, 3, (1968).

11. Letcher, J. H., and Schmidt, P. W., J. Appl. Phys., 37, 2, (1966).

12. Roess, L. C., J. Chem. Phys., 14, 11, (1946).

13. Riseman, J., Acta Cryst., 5, 193, (1952).

14. Brill, O. L., U. of Missouri, PhD Thesis, (1968).

15. Shull, C. G. and Roess, L. C., J. Appl. Phys., 18, 295, (1947).

16. Jellinek, M. H., Solomon, E., and Fankuchen, I., Ind. and Eng. Chem., 18, 3, (1946).

17. Kratky, O., Progress in Biophysics, Vol. 13, p1055ff, Pergammon Press, N. Y., (1963).

18. Schmidt, P. W., and Hight, R. W., Acta Cryst., 13, 6, (1960).

19. Schmidt, P. W., Acta Cryst., 13, 6, (1960).

20. Anderegg, J., Mardon, and Hendricks, R., ORNL-4476, (1970).

21. Koczak, M. J., and Herman, H., Rev. Sci. Instr., 41, 12, (1970).

22. Kratky Camera Users Manual, Anton Paar, Inc.

23. Cullity, B. D., Elements of X-ray Diffraction, Addison-Wesley, Reading, Mass., (1956).

24. Turkevich, J., Stevenson, P., and Hillier, J., Discussions Faraday Society, 11, 58, (1951).

25. Demchak, R. and Matijevic, E., J. Colloid Int. Sci., 31, 2, (1969).

26. Matijevic, E., et al., J. Colloid Int. Sci., 36, 2, (1971).

27. Kratohvil, S., and Matijevic, E., J. Colloid Int. Sci., 24, 47, (1967).

28. Hall, H., and Eyring, H., J. Am. Chem. Soc., 12, 782, (1950).

29. "Ludox Colloidal Silica", Product Data Sheet, E. I., DuPont De NeMours and Company.

30. Johnson, J. S., and Kraus, K. A., J. Phys. Chem., 63, (1959).

31. Cohen, R., and West, K., J. Electrochem. Soc., 119, 433 (1972).

32. Hendricks, R. W., and Schmidt, P. W., Acta Physica Austriaca, 26, (1967) p. 97.

33. Kratky, O., Porod G., and Kahovec, L., Z Electrochem., 55, 53, (1951).

34. Schmidt, P. W., and Hight, R. W., Acta Cryst., 13, 6, (1960).

35. Schmidt, P. W., Acta Cryst., 19, 6, (1965).

36. Weil, C. G., Schmidt, P. W., Janosi, A., Sekora, A., and Kratky, O., J. Appl. Cryst., 3, 90, (1970).

VITA

James M. Lamy was born on August 11, 1947, in Kansas City, Missouri, the son of Dr. and Mrs. John Lamy. He attended public schools in Sedalia, Missouri, and graduated from Smith-Cotton High School in June, 1965. Mr. Lamy then entered the University of Missouri, graduating in January, 1970, with a Bachelors degree in Electrical Engineering.

He then joined the Western Electric Company at the Kansas City Works as Product Engineer. He served in this capacity until June, 1971, when he was transferred to the Corporate Education Center in Princeton, New Jersey, in connection with the Western Electric Lehigh Masters Program.